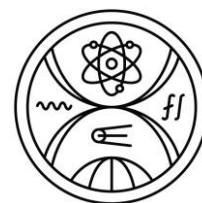




COMENIUS UNIVERSITY IN BRATISLAVA
FACULTY OF MATHEMATICS, PHYSICS AND INFORMATICS



Monte Carlo simulations of detectors background in underground laboratories
Dissertation Thesis

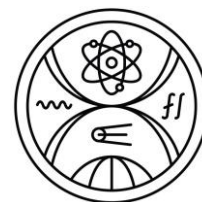
The Thesis worked-out in collaboration with CERN,
EUROPEAN ORGANISATION FOR NUCLEAR RESEARCH

2023

RNDr. Miloslava Bagínová



COMENIUS UNIVERSITY IN BRATISLAVA
FACULTY OF MATHEMATICS, PHYSICS AND INFORMATICS



Monte Carlo simulations of detectors background in underground laboratories
Dissertation Thesis

The Thesis worked-out in collaboration with CERN,
EUROPEAN ORGANISATION FOR NUCLEAR RESEARCH

Study programme: Nuclear and Subnuclear Physics
Field of study: 4.1.5. Nuclear and Subnuclear Physics
Supervisor: prof. Dr. Pavel Povinec, DrSc.
CERN Supervisor: Dr. Pavol Vojtyla, CSc.
Department of Nuclear Physics and Biophysics

Bratislava 2023

RNDr. Miloslava Bagínová

Zadanie záverečnej práce

Monte Carlo simulácie pozadia detektorov v podzemných laboratóriách

Dizertačná práca

RNDr. Miloslava Bagínová

Anotácia

Detektory jadrového žiarenia umiestnené v podzemných laboratóriách patria v súčasnosti medzi najcitlivejšie systémy na výskum zriedkavých jadrových premien a procesov. K nim patrí predovšetkým určenie klúdovej hmotnosti neutrína, ktoré umožní rozhodnúť či neutrína sú Majoranovské alebo Diracovské častice. Katedra jadrovej fyziky a biofyziky participuje na medzinárodnom experimente SuperNEMO, ktorý sa realizuje v najhlbšom podzemnom laboratóriu v Európe. Katedra pripravuje tiež výstavbu podzemného laboratória, ktorého súčasťou budú veľkoobjemové HPGe detektory. Dizertant v spolupráci s pracovníkmi Katedry, ako aj v spolupráci s viacerými zahraničnými pracoviskami sa bude podieľať na vývoji Monte Carlo simulačných metód na určenie pozadia detektorov v podzemných laboratóriách, a jeho porovnaní s experimentálnymi meraniami. Na vývoji Monte Carlo simulačného kódu sa využíva vývojové prostredie GEANT4, ktoré bolo vytvorené v CERNe. Súčasťou práce dizertanta budú aj zahraničné stáže na významných pracoviskách, využívajúcich nízkoenergia technológie, ako aj účasť v medzinárodnom projekte SuperNEMO.

Cieľ:

Cieľom je vyvinúť Monte Carlo simulačné programy pre analýzu pozadia detektorov v podzemných laboratóriách

Literatúra:

Povinec P.P.: New technologies in underground physics. J. Anal. Science and Technology, 2012;
Povinec et al.: APS 2008; GEANT4 Code, CERN; Nuclear Instr. and Methods in Phys. Res. A Proceedings; SuperNEMO publikácie

Kľúčové slová:

Monte Carlo simulácie, GEANT4, Ge detektory, SuperNEMO

Študijný program: Jadrová a subjadrová fyzika

Študijný odbor: 4.1.5. Jadrová a subjadrová fyzika

Školiteľ FMFI: prof. RNDr. Pavel Povinec, DrSc.

Školiteľ CERN: RNDr. Pavol Vojtyla, CSc.

Jazyk záverečnej práce: anglický

Katedra: Katedra jadrovej fyziky a biofyziky

Vedúci katedry: prof. RNDr. Stanislav Tokár, DrSc., prof. RNDr. Jozef Masarik, DrSc.

Dátum zadania: 17.02.2015

Dátum schválenia: 13.07.2015

Podpis garanta študijného programu: prof. RNDr. Jozef Masarik, DrSc.

Assignment of thesis

Monte Carlo simulations of detectors background in underground laboratories

Dissertation Thesis

Dr. Miloslava Bagínová

Annotation

Detectors of nuclear radiation located in underground laboratories are currently among the most sensitive systems for research of rare nuclear transformations and processes. These include, first of all, the determination of the neutrino's rest mass, which will allow us to decide whether neutrinos are Majorana or Dirac particles. The Department of Nuclear Physics and Biophysics participates in the international experiment SuperNEMO, which is being implemented in the deepest underground laboratory in Europe. The department is preparing the construction of an underground laboratory, which will host large sensitive volume HPGe detectors. The doctoral student, in cooperation with the staff of the Department, as well as in cooperation with reliable foreign institutes, will participate in the development of Monte Carlo simulation methods for determining the background of detectors in underground laboratories, and its comparison with experimental measurements. For development of the Monte Carlo simulation code, the GEANT4 simulation tool developed at CERN is used. Part of the doctoral work will also be foreign internships at prominent institutes using low-background technologies, as well as participation in the international SuperNEMO project.

Goal:

The goal is to develop Monte Carlo simulation codes for analysis of detectors background in underground laboratories

Literature:

Povinec P.P.: New technologies in underground physics. J. Anal. Science and Technology, 2012;
Povinec et al.: APS 2008; GEANT4 Code, CERN; Nuclear Instr. and Methods in Phys. Res. A Proceedings; SuperNEMO publikácie

Keywords:

Monte Carlo simulations, GEANT4, Ge detectors, SuperNEMO

Study programme: Nuclear and Subnuclear Physics

Field of study: 4.1.5. Nuclear and Subnuclear Physics

University Supervisor: prof. Dr. Pavel Povinec, DrSc.

CERN Supervisor: Dr. Pavol Vojtyla, CSc.

Language of thesis: English

Department: Department of Nuclear Physics and Biophysics

Department Chair: prof. Dr. Stanislav Tokár, DrSc., prof. Dr. Jozef Masarik, DrSc.

Date of assignment: 17.02.2015

Date of approval: 13.07.2015

Signature of the referee of the study programme: prof. Dr. Jozef Masarik, DrSc.

Acknowledgement

I would like to thank my supervisors, prof. Dr. Pavel Povinec, DrSc. and Dr. Pavol Vojtyla, CSc. for professional mentoring, lot of patience and their valuable help. I appreciate that. I am also thankful to CERN for granting my PhD fellowship and allowing me to use a laboratory with HPGe detectors and all necessary devices for my experiments, as well as the opportunity to publish my articles in open access. Special thanks to the staff of the Modane underground laboratory for information about the Obelix detector and provided data for background spectra.

Abstrakt

Dizertačná práca bola vypracovaná v rámci projektu APVV-15-576 *Zriedkavé jadrové procesy a vývoj metód na ich sledovanie*. Predmetom štúdie boli interakcie neutrónov s HPGe detektorom uskutočnené experimentálne, ako aj prostredníctvom Monte Carlo simulácií s použitím simulačného programu GEANT4. Pružný a nepružný rozptyl rýchlych neutrónov, rovnako ako aj neutrónový záchyt na Ge jadrách boli zreteľne pozorovateľné. V nameranom γ -spektre boli dobre viditeľné píky, ktoré boli vyvolané nepružným rozptylom neutrónov na ^{70}Ge , ^{72}Ge , ^{73}Ge , ^{74}Ge a ^{76}Ge . Detekované boli aj píky viditeľné v dôsledku nepružného rozptylu neutrónov na jadrách olova a medi, vrátane dobre známeho píku ^{208}Pb o energii 2614.51 keV. GEANT4 simulácie ukázali, že nasimulované spektrum bolo v dobrej zhode s experimentálnym. Pozorované rozdiely medzi nasimulovaným a nameraným spektrom boli spôsobené vyššou intenzitou γ -žiarenia neutrónového zdroja, implementovanou fyzikou v programe GEANT4 a kontamináciou ^{241}Am -Be neutrónového zdroja.

Ďalšia časť štúdie bola zameraná na pozadie detektora vyvolaného neutrónmi. Výskum sa uskutočnil prostredníctvom skúmania interakcií neutrónov pochádzajúcich z kozmického žiarenia s HPGe detektorom. Detektor bol umiestnený v kryte a nachádzal sa na prízemí 3-poschodovej budovy. Štúdium sa uskutočnilo experimentálne a prostredníctvom Monte Carlo simulácií s použitím GEANT4 simulačného nástroja. Podrobná analýza nameraného pozadového γ -spektra ukázala, že mnohé γ -čiary viditeľné v spektre boli vyvolané neutrónmi. Väčšina detegovaného γ -žiarenia pochádzala z germánia, medi, olova a cínu. Časti detektora vyrobené zo železa a hliníka patrili medzi menej dôležité zdroje pozadia. Nepružný rozptyl a neutrónový záchyt boli najčastejšie sa vyskytujúce procesy neutrónových interakcií s detektorom a jeho tienением. V pozadovom spektre bola prítomná aj kontaminácia spôsobená prírodnými rádionuklidmi, a to ^{214}Pb , ^{214}Bi , ^{40}K a ^{208}Tl . Avšak, približne 35% z ^{208}Tl píku o energii 2614.51 keV vzniklo v dôsledku nepružného rozptylu neutrónov na ^{208}Pb jadrách. Experimentálne získané pozadie bolo porovnané s GEANT4 simuláciami, ktoré boli vytvorené bez a vrátane tieniacej vrstvy budovy. Výsledná integrálna početnosť nameraného spektra v energetickom rozsahu od 50 keV do 2875 keV bola $1.26 \pm 0.07 \text{ s}^{-1}$ a nasimulovaného spektra $1.25 \pm 0.13 \text{ s}^{-1}$, čo naznačuje dobrú zhodu simulácie s experimentom.

Následne bolo skúmané pozadie HPGe detektora namerané v podzemnom laboratóriu, a to analyticky a prostredníctvom Monte Carlo simulácií, opäť s použitím simulačného nástroja GEANT4. Identifikované boli jednotlivé príspevky rôznych zdrojov pozadia k experimentálnemu spektru. Jednalo sa o kontamináciu materiálu v detektore a v jeho okolí, neutróny produkované v (α , n) reakciách prebiehajúcich kvôli prítomnosti alfa rádionuklidov v betónových stenách a skalách laboratória, ako aj v dôsledku spontánneho štiepenia ^{238}U , a kozmické žiarenie produkujúce neutróny. Simulácie zahrňujúce kontamináciu materiálu boli v dobrej zhode s experimentálnym spektrom. Zároveň boli nasimulované individuálne spektrá vyvolané neutrónmi a kozmickým žiarením. Kontaminácia častí detektora a stien laboratória členmi ^{238}U a ^{232}Th rozpadového radu, a ^{40}K tvorí takmer 94% kontinua experimentálneho spektra. V súlade so simuláciami je príspevok miónových interakcií k experimentálnemu γ -spektrom menší ako 1%, pričom sa potvrdilo, že pozadové spektrá vyvolané kozmickým žiarením sú o tri rády nižšie ako experimentálne spektrá. Porovnanie integrálnej početnosti experimentálneho spektra a nasimulovaného spektra vyvolaného neutrónmi ukázalo, že asi 6% kontinua nameraného pozadia je tvorených neutrónovými reakciami. Rýchle neutróny (asi 65%) prispievali k pozadiu viac ako termálne neutróny. Napriek tomu, že neutróny tvoria len asi 6% celkového pozadia, prispievajú hlavne k oblasti kontinua pod 250 keV, čo je región očakávaného výskytu interakcií slabo interagujúcich masívnych častíc (WIMP) temnej hmoty. Neutróny zároveň interagujú s detektorom a tienением nepružným rozptylom a vyvolávajú tak neželané γ -žiarenie. Neutrónový záchyt, ako aj pružný a nepružný rozptyl boli nasimulované samostatne. Ukázalo sa, že nepružný rozptyl je hlavným prispievateľom k spektru vyvolaného neutrónmi. Efekt neutrónov na pozadie HPGe detektora prevádzkovaného v podzemnom laboratóriu, ako je Obelix, sa prejavuje najmä príspevkom ku kontinuu do 1 MeV, a to obzvlášť v nižšej časti do

500 keV. Neutróny sú teda dôležitým pozad'ovým komponentom aj v hlbokých podzemných laboratóriách. Diskutovaná bola aj možná optimalizácia detektora.

Vzhľadom na zámer vybudovať na Slovensku podzemné laboratórium pre astrofyzikálne a environmentálne štúdium rádioaktivity, boli vypočítané miónové vertikálne spektrálne toky pre hĺbky 50 m w.e. a 1000 m w.e. Nasimulované bolo aj miónmi vyvolané pozadie HPGe detektora s relatívnou účinnosťou 100% v oboch hĺbkach. Kompletná geometria HPGe detektora bola zahrnutá do GEANT4 simulácie vrátane tienenia. Gamma čiary viditeľné v nasimulovanom pozad'ovom spektre, ktoré pochádzajú z neutrónových interakcií s detektorom a jeho tienením, boli analyzované a vyhodnotené. Ukázalo sa, že v pozad'ovom spektre nasimulovanom pre podzemné laboratórium v hĺbke 50 m w.e. prevládajú píky medi. V pozad'ovom spektre nasimulovanom pre podzemné laboratórium v hĺbke 1000 m w.e. prevládajú píky germánia do energie 1500 keV, a od 1500 keV dominujú opäť píky medi. Pozad'ové spektrá boli porovnané a zistilo sa, že hĺbka 1000 m w.e. je dostatočná nato, aby znížila pozadie od miónov o 5 rádov. Množstvo píkov v pozad'ovom spektre pochádzajúcich od neutrónových interakcií je väčšie v hĺbke 50 m w.e. než v hĺbke 1000 m w.e., tak ako sa očakávalo. Porovnali sa aj početnosti jednotlivých píkov v oboch spektrách. Na základe zistení sa použitie medi ako konštrukčného materiálu pre tienenie HPGe detektora umiestneného v podzemí neodporúča, z hľadiska pozadia vyvolaného kozmickým žiarením. Efekt prírodných rádionuklidov v plánovanom podzemnom laboratóriu na Slovensku bol odhadnutý. Príspevok prírodných rádionuklidov ku kontínuu pozad'ového spektra HPGe detektora s relatívnou účinnosťou 100% by tvoril približne 40% v hĺbke 1000 m w.e. a 10% v hĺbke 50 m w.e. Výber ultračistého materiálu pri výrobe detektora a tienenia je dôležitý faktor a odporúča sa s dôrazom na minimalizovanie vplyvu γ -žiarenia od prírodných rádionuklidov na pozadie detektora. Detekčný limit pre ^{137}Cs v hypotetickej vzorke bol stanovený pre obe uvažované hĺbky. V laboratóriu umiestnenom v hĺbke 50 m w.e. by bol detekčný limit 7.3 mBq a v hĺbke 1000 m w.e. by to bolo 0.54 mBq. Z uvedených hodnôt vyplýva, že umiestnením detektora v hĺbke 1000 m w.e. by sa dal detekčný limit znížiť najviac o jeden rád v porovnaní s hĺbkou 50 m w.e.

Abstract

The Thesis was worked-out within the project APVV-15-576 *Rare nuclear processes and development of methods for their investigations*. Interactions of neutrons with a high-purity germanium detector were studied experimentally and by simulations using the GEANT4 tool. Elastic and inelastic scattering of fast neutrons as well as neutron capture on Ge nuclei were observed. Peaks induced by inelastic scattering of neutrons on ^{70}Ge , ^{72}Ge , ^{73}Ge , ^{74}Ge and ^{76}Ge were well visible in the γ -ray spectra. In addition, peaks due to inelastic scattering of neutrons on copper and lead nuclei, including the well-known peak of ^{208}Pb at 2614.51 keV, were detected. The GEANT4 simulations showed that the simulated spectrum was in a good agreement with the experimental one. Differences between the simulated and the measured spectra were due to the high γ -ray intensity of the used neutron source, the physics implemented in GEANT4 and contamination of the ^{241}Am -Be neutron source.

Next, investigation of neutron-induced background was carried out by studying interactions of cosmic ray neutrons with an HPGe detector inside its shield placed on a ground floor of a 3-storey building. The study was conducted experimentally and by Monte Carlo simulations using GEANT4 simulation tool. Detailed analysis of measured background γ -ray spectra showed that many γ -lines visible in the spectra were induced by neutrons. The majority of detected γ -rays originated in germanium, copper, lead and tin. Iron and aluminium components were less important background sources. Inelastic scattering and neutron capture were the most often occurring processes of neutron interactions with the detector and its shielding. The contamination by natural radionuclides, particularly by ^{40}K , ^{214}Pb , ^{214}Bi and ^{208}Tl , was also present in the background spectra. Nevertheless, approximately 35% of the frequently observed ^{208}Tl peak at the energy of 2614.51 keV was produced by inelastic scattering of neutrons on ^{208}Pb nuclei. The experimental background was compared with GEANT4 simulations, which were carried out without and with the shielding layer of the building. The final integral count rates for the measured spectrum in the energy range from 50 keV to 2875 keV was $1.26 \pm 0.07 \text{ s}^{-1}$ and for the simulated one $1.25 \pm 0.13 \text{ s}^{-1}$, indicating a good agreement of simulation with the experiment and validating the tool.

Finally, the background of an HPGe detector measured in a deep underground laboratory was investigated analytically and by Monte Carlo simulations using the GEANT4 toolkit. Contributions of different background sources to the experimental γ -ray background were determined. Namely, contribution of radionuclides in the materials of the detector and around the detector, neutrons produced in (α, n) reactions due to presence of radionuclides in concrete and rock, by spontaneous fission of mainly ^{238}U , and finally, cosmic rays with neutron generation. The simulation, including radionuclides in the material, was in a good agreement with the experiment. At the same time, background spectra induced by neutrons and muons were simulated separately. The radiation coming from the presence of members of the ^{238}U , and ^{232}Th decay series, and ^{40}K in the detector parts and the laboratory walls contribute to the continuum of the experimental spectrum at the level of around 94%. According to simulations, the contribution of muon events to the experimental energy spectrum was below 1% and it was confirmed that muon induced spectra are about three orders of magnitude lower than the experimental one. The comparison of integral count rates of the experimental spectrum with the simulated spectrum induced by neutrons showed that about 6% of the measured background continuum originated from neutron reactions. Fast neutrons contributed more to the background (at around 65%) than thermal neutrons. Despite only a 6% share of neutron contributions in the total γ -ray background, they contributed mainly to the lower continuum of the spectrum up to 250 keV, which is a region of interest for potential low mass weakly interacting massive particle (WIMP) dark matter interactions. In addition, they interact with the detector and the shield by inelastic scattering and induce unwanted γ -rays. Neutron capture, elastic and inelastic scattering were simulated separately as well. It was found that inelastic scattering is the major contributor to the spectrum induced by neutrons. The effect of neutrons on the background of the HPGe detector operating underground, such as Obelix, is manifested mainly by their contribution to the continuum up to 1

MeV, especially in the lower part up to 500 keV. Thus, neutrons are an important background component in deep underground laboratories, too. Possible detector optimization is also discussed.

In order to build an underground laboratory in Slovakia for astrophysical and environmental radioactivity studies, calculations of the muon vertical energy spectrum in 1000 m w.e. and 50 m w.e. were carried out. The muon-induced backgrounds of a HPGe detector with a relative efficiency of 100% were simulated in both depths. The complete geometry of the HPGe detector was coded in GEANT4 including the low-level shield. Gamma lines coming from neutron interactions with the detector and its shield seen in the simulated background spectra were analysed and evaluated. It was found that in the background spectrum simulated in the 50 m w.e. shallow laboratory, the copper peaks are prevailing. In the background spectrum simulated in the 1000 m w.e. deep laboratory, the germanium peaks are prevailing up to 1500 keV, but above 1500 keV the copper peaks dominate. The simulated background spectra were compared and it was found that a depth of 1000 m w.e. is sufficient to reduce the cosmic-ray induced background by five orders of magnitude. The number of visible peaks coming from neutron interactions in the background spectrum simulated for the shallow laboratory in the depth of 50 m w.e. is higher than in the 1000 m w.e. deep laboratory, as expected. Comparison of count rates of individual peaks for both spectra were carried out as well. Use of copper in the detector shield for HPGe detectors located in underground laboratories is not recommended as far as background induction by cosmic rays is concerned. The effect of natural radioactivity in planned Slovak laboratory was estimated. The contribution of natural radionuclides to the total background continuum would be about 40% at the depth of 1000 m w.e. and 10% at 50 m w.e. using HPGe detector with relative efficiency of 100%. Selection of ultra-high purity materials for the detector and shield construction was recommended with the aim to minimize the contribution of γ -rays from natural radionuclides to the background spectrum. The detection limits for ^{137}Cs in a hypothetical sample was determined in both depths. It would be 7.3 mBq and 0.54 mBq in the 50 m w.e. and 1000 m w.e. laboratory, respectively. The detection limit would decrease by one order of magnitude at most if the laboratory would be built in the 1000 m w.e. depth compared to the depth of 50 m w.e.

Preface

This work was inspired by lack of information about neutron induced background, especially in underground laboratories, so important for experiments looking for rare processes. In deep underground laboratories, neutrons can be produced by natural radioactivity, via spontaneous fission or (α , n) reactions and by interactions of cosmic rays. Predicting all background components correctly is crucial for designing efficient shielding and applying appropriate event-rejection strategies, while neutron induced background was a poorly known background component.

The aim of this work was to investigate neutron-induced backgrounds and bring valuable information about it. The investigation was carried out by study of neutron interactions with shielding materials and HPGe detectors located in surface and deep underground laboratories. Within this investigation, also simulations of cosmic ray fluxes in surface and in deep underground laboratories using the GEANT4 simulation tool were carried out. All background sources of HPGe detectors were identified. Effects of cosmic rays, radioactive contamination of construction materials and from the natural radioactivity in the underground environment, such as ^{40}K , U and Th decay series, and neutrons on the background were studied. Simulations of contributions of all the above-mentioned sources to the detector background were carried out, too. Simulated results were compared with measurements in surface and deep underground laboratories. Obtained results should contribute to better understanding and improvement of low-background detector systems.

The main method used for investigations was Monte Carlo simulation. The Monte Carlo method is often used in complicated physics and mathematics processes where analytical solutions are very difficult or are not possible, such as background induction and optimization of a counting system considering its background characteristics. The GEANT4 simulation code developed at CERN was used for Monte Carlo simulations of interactions of neutrons with a Ge detector as well as for Ge detector backgrounds.

Several studies carried out in the past were dealing with neutron interactions with germanium detectors. The energy deposition process of the recoiling Ge nuclei has been studied, as well as elastic scattering of neutrons with Ge detectors. The study of neutron induced background of Ge detectors was focusing mainly on neutron interactions with Ge nuclei and on investigation of neutron fluxes from different underground sources.

As no study with complex information about neutron background has been available until now, interactions of neutrons with an HPGe detector were studied experimentally and by simulations using the GEANT4 simulation tool, as well as neutron-induced backgrounds in surface and deep underground laboratories. Contributions of different background sources to the experimental γ -ray background were determined and analysed. Simulations were compared with the experimental spectra and all results were in good agreement with measurements. The obtained results should be beneficial for underground experiments looking for rare nuclear processes.

Contents

Introduction	13
1. Dissertation goals	16
2. Monte Carlo simulations	17
2.1 Neutron interactions with Ge detectors	17
2.2 The background of HPGe detector operating in a surface laboratory	17
2.3 The background of HPGe detectors operating deep underground	18
2.4 Muon induced background in planned underground laboratory in Slovakia	19
3. Results	20
3.1 Investigation of neutron interactions with Ge detectors	20
3.1.1 ²⁴¹Am–Be source	20
3.1.2 Experimental setup	21
3.1.3 Evaluation of the experimental γ-ray spectrum	21
3.1.4 Comparison of experimental and simulated γ-spectra	22
3.2 The neutron component of background of an HPGe detector operating in a surface laboratory	22
3.2.1 Experimental setup	22
3.2.2 Evaluation of the experimental background γ-ray spectrum	23
3.2.3 Comparison of Monte Carlo simulations with the experiment	23
3.3 The effect of neutrons on the background of HPGe detectors operating deep underground	24
3.3.1 Modane underground laboratory	24
3.3.2 HPGe detector	25
3.3.3 Experimental background spectrum	26
3.3.4 Comparison of Monte Carlo simulations with experimental spectrum	26
3.3.5 Neutrons and their effect	28
3.4 Simulation of muon induced background in a proposed underground laboratory in Slovakia 28	
3.4.1 Design of underground laboratories	28
3.4.2 Peak analysis	29
3.4.3 Evaluation of the simulated results	30
4. Effect of the natural radioactivity	35
Conclusions	42
References	45
Attachments	47
List of conferences	47

List of publications	47
Author's Publications	47
Investigation of neutron interactions with Ge detectors	48
The neutron component of background of an HPGe detector operating in a surface laboratory .	58
Effect of neutrons on background of HPGe detectors operating deep underground.....	73

Introduction

High-purity germanium detectors are semiconductor detectors primarily used for γ -ray spectrometry. The sensitive part of the detector is formed by a germanium crystal, which is fabricated from ultrapure material with a purity of at least of 99.999%. The dimensions of the crystal can reach several centimetres, what together with the fact that germanium has a very high photoelectric cross section leads to the total absorption of γ -rays up to a few MeV. The high detection efficiency and the high resolution are the main advantages of HPGe detectors in comparison with other types of semiconductor detectors. The band gap in germanium is small, therefore the detectors are cooled by liquid-nitrogen to a temperature of 77 K to reduce the thermal generation of charge carriers. Depending on contacts on the surface of the crystal 2 types of the HPGe detectors are known, p-type and n-type, while based on the shape of the crystal the detectors are classed into 3 categories: planar, coaxial and well. Every type of HPGe detector has specific geometry and performance characteristics.

Background of high-purity germanium detectors induced by neutrons is a poorly understood component in low-level γ -spectrometry systems. In surface laboratories with passive shielding, as well as in underground laboratories, neutrons can be produced in interactions of high energy cosmic rays and by natural radionuclides in spontaneous fission and in (α, n) reactions. Predicting all background components correctly is crucial for designing efficient shielding and applying appropriate event-rejection strategies.

The suppression and rejection of background is one of the key issues in experiments looking for rare nuclear events, such as neutrinoless $\beta\beta$ decay experiments, dark matter searches or experiments with low-energy neutrinos. Monte Carlo simulations of neutron background play a crucial role in evaluation of the total background and in optimization of rejection strategies (e.g. [1, 2]).

No study with complex information about neutron background has been available until now, however, several studies were dealing with neutron interactions with germanium detectors. The knowledge of germanium peak shapes is important because they could cause systematic errors. Past measurements of neutron interactions with Ge detectors were carried out using ^{252}Cf neutron sources and environmental neutrons (e.g. [3, 4]). A comparison of the results showed that there is no substantial difference between Ge experimental peaks in a wide spectrum of neutron energies. The broader germanium peaks were observed for high energy neutrons [4].

The energy deposition process of the recoiling Ge nuclei has been studied, as well as elastic scattering of neutrons with Ge detectors [4, 5]. Monte Carlo simulations of ^{252}Cf induced γ -ray spectra in Ge detectors were also carried out, and a good agreement of simulated spectra with experimental ones was found, especially for the region of elastic neutron scattering up to 50 keV. However, no detailed analysis of experimental γ -ray spectra was carried out until now. As such investigations are crucial for determination of all Ge background components (especially in underground laboratories), we decided to carry out analysis of ^{241}Am -Be neutron induced γ -ray spectra both experimentally and by Monte Carlo simulations.

High-purity germanium detectors have been very often used for analysis of radionuclides at very low levels, as well as in experiments looking for rare events, especially those operating in deep underground laboratories. Success of such experiments depends mainly on the detector background that can overlap the useful signal coming from the detector. For this reason, it is very important to know all sources of background of HPGe detectors and minimize or eliminate their influence on the searched signals. A significant source of the Ge detector background has been due to neutrons. Neutrons interacting with HPGe detector materials and the shield produce many γ -rays that can hide or imitate the searched signal [6]. Neutrons are present not only in surface laboratories but also in deep underground laboratories, either as a result of spontaneous fission of natural long-lived radionuclides, (α, n) reactions, or muon interactions with surrounding rocks and detector materials [7].

Reliable identification and investigation of neutron-induced background is a challenge due to diversity of neutron interactions with detectors and shielding materials. There are several studies dealing with neutron induced background of Ge detectors focusing mainly on neutron interactions with Ge nuclei (e.g.[8,9]). Neutrons interacting with Ge crystals produce several γ -lines resulting from capture of thermal neutrons and inelastic scattering of fast neutrons on individual Ge nuclei. These γ -lines can be used for estimation of the flux of thermal and fast neutrons around a detector. Different types of Ge detectors and various shielding materials were used for background measurements. It has been found that the production of neutrons induced by cosmic muons significantly depends on the atomic number Z of the shielding material, as it increases with rising Z . Therefore, a shield with high Z , which is commonly used for reduction of γ -rays coming from natural radionuclides and from interactions of cosmic rays is a source of neutrons, too [8]. This has to be taken into account especially when building large shields for surface laboratories, compromising the composition and thickness of the shield.

Germanium γ -ray peaks were used for identification of neutron sources in the Ge detector environments, as well as for calculation of their contribution to detector background. It was found that the germanium crystal itself is one of the most intensive sources of neutron-induced γ -rays in an HPGe detector [9].

However, a study providing complex information on the neutron induced background in Ge spectrometers is still missing. In order to bring additional information about the neutron-induced background and to contribute to better understanding of low-background detector systems, γ -ray background of an HPGe detector operating in a surface laboratory was measured and compared with Monte Carlo simulations in the present study.

Underground experiments looking for rare events such as searching for dark matter interactions, rare α and β decays or detection of low energy neutrino interactions are important experiments of today. These experiments are based on the detection of rare signals therefore the main research tools are detectors with large sensitive volumes, e.g. HPGe detectors with big germanium crystals. These detectors are used also for material screening. Shielding against particles coming from muon interactions and γ -rays coming from decay of natural radionuclides is a key issue for such detectors. Signals produced by neutrons interacting in a low-background experiment are particularly troublesome as they may imitate or mask the very signals that are being searched for [6]. In deep underground laboratories cosmic rays are represented only by their hard component, thus only cosmic-ray muons and neutrinos are present here, as only they are able to penetrate to such depths. Neutrons are produced in interactions of muons with the experimental setup and the surroundings, and they may contribute to the background. Another source of neutrons deep underground is spontaneous fission of natural radionuclides (such as ^{232}Th and ^{238}U) and (α, n) reactions [7]. Therefore, the investigation of neutron induced backgrounds in deep underground laboratories is crucial for low background experiments.

Existing background studies in underground experiments deal therefore also with the neutron influence on the expected results. They are mainly focused on investigation of neutron fluxes from different underground sources and on the neutron energy spectra, when neutrons are originating from natural radioactivity (e.g. [8, 9]). An important part of the low energy neutron background comes from natural radioactivity. The main contributors are uranium and thorium decay chains via (α, n) reactions and, to a smaller extent, spontaneous fission. The background from fast neutrons is induced by interactions of cosmic-ray muons with detectors and their shielding. The neutron induced spectrum formed by muon interactions in deep underground laboratories can range up to several GeV [8]. Several Monte Carlo simulations of neutron energy spectra caused by uranium and thorium decay chains were carried out in materials considered as potential neutron sources, with the aim to estimate the event rate invoked by neutrons. Contributions of spontaneous fission and (α, n) reactions were estimated in [9].

A thorough analysis of background spectra measured in a deep underground laboratory can bring valuable information about the neutron induced background of HPGe detectors and help to identify

all background components. Such a study would be beneficial for underground experiments looking for rare nuclear processes.

The aim of this study was to investigate the neutron background in the Obelix HPGe detector operating in the Modane deep underground laboratory. The measured background energy spectrum of the HPGe detector was studied and compared with Monte Carlo simulations carried out by the GEANT4 simulation code for better understanding of neutron contributions to the detector background.

Slovak scientific community is a part of several low-background experiment collaborations, such as SuperNEMO or Cobra. These experiments are located in underground laboratories with the aim to minimize the detector background that can interfere the searched signal. There is no underground laboratory in Slovakia yet and building of such laboratory with a large low-level HPGe detector has been considered. Calculations of muon energy spectra and investigation of muon induced background spectra were carried out for two localities, at a 50 m w.e. depth and at a 1000 m w.e. depth to recommend design principles. The muon induced background energy spectra of an HPGe detector were simulated by using the GEANT4 simulation code. The effect of natural radioactivity in planned Slovak laboratory was estimated and the detection limits for ^{137}Cs in a hypothetical sample was determined in both depths.

1. Dissertation goals

- Design and application of suitable software modules for generators of cosmic-ray fluxes in surface and in deep underground laboratories.
- Evaluation of effects of neutrons, cosmic rays, radioactive contamination of construction materials and the detector environment in the underground laboratories.
- Simulations of contribution of the above-mentioned sources to the detector background, especially for detectors operating deep underground.
- Comparison of the results with measurements in surface and deep underground laboratories with the aim of better understanding and improvement of low-background detector systems.
- Design principles for construction of an underground laboratory in Slovakia for astrophysical and environmental radioactivity studies.

2. Monte Carlo simulations

A Monte Carlo simulation is a set of computer algorithms based on random sampling in order to reach relevant results. Input variables are processed by different probability distributions. Monte Carlo method is often used in complicated physics and mathematics processes where analytical solutions are very difficult or are not possible, such as background induction and optimization of counting system considering its background characteristics. Except the possible outcome, it predicts also the probability of the outcome occurrence.

The GEANT4 simulation code developed at CERN was used for Monte Carlo simulations of interactions of neutrons with a Ge detector and for Ge detector background spectra. GEANT4 is an object-oriented simulation toolkit based on C++ programming language, which provides an extensive set of software components for simulation of particle interactions with matter in a wide energy range. It is equally suitable for simulations at high energies as at low energies. The code includes all aspects of the simulation process, such as the geometry, materials, particles, the tracking, physics processes, and the detector response. The software is capable to generate and store events and tracks, to visualize the detector and particle trajectories, and to record the simulation data, energy deposition included. GEANT4 disposes with extensive databases of cross sections, which are stored in individual data files for specific processes [10, 11, 12, 13].

2.1 Neutron interactions with Ge detectors

For γ -ray interactions the G4EMLOW 6.5 and for neutron interactions the G4NDL 4.5 data files were used, respectively. The experimental neutron spectrum of the ^{241}Am -Be source was taken from [14]. The spectrum was digitized and used as the input source for GEANT4 simulations, together with γ -rays emitted by ^{241}Am and those generated in nuclear reactions inside the source. Gaussian energy distribution was used for γ -rays of ^{241}Am and γ -rays from $^9\text{Be}(\alpha, n)^{12}\text{C}$ reaction with mean energies of 59.54 keV and 4438.91 keV, with standard deviations of 0.24 keV and 1.55 keV, respectively. Values of mean energies were taken from NuDat 2.6 database [15], and values of standard deviations were taken from the energy resolution of the Ge detector, which was measured using radioactive standards. The resolution curve was calculated using the least square method and approximated up to 5 MeV. The aim was to simulate the instrumental spectrum of the detector used in the experiment.

Real conditions were implemented into the Monte Carlo simulation. The simulated source matches the shape and dimensions of the real source and it emits particles isotropically.

The precise geometry setup was coded including individual material compositions. Special attention was paid to impurities in different materials. Investigation of impurities was carried out and every known material impurity was incorporated into simulation. The physics list SHIELDING 2.1, developed for neutron penetration studies and ion-ion collisions, was used in the simulations. It contains the best selection of electromagnetic and hadronic physics processes required to solve shielding problems including low background experiments. During simulation, every particle and process were tracked including particle's kinematics. The deposited energy was recorded each time a particle hit the detector.

2.2 The background of HPGe detector operating in a surface laboratory

For background simulations in a surface laboratory, the detector and the shield geometry were coded in GEANT4, including composition of shielding materials and impurities. Detailed drawings of the detector setup were provided by Mirion Technologies / Canberra for the study. Gamma rays of ^{241}Am in a wide energy range were simulated and compared with experimental ones so that the simulated detector response could be validated.

The setup was placed into a box with dimensions of $7 \times 4 \times 3 \text{ m}^3$ representing the laboratory with concrete walls of 32 cm thickness. The laboratory with the HPGe detector is located in a basement of a building and the cosmic rays from an open area pass through masonry structures of the building. The detailed structure of the overhead material layers was not known but its concrete equivalent was estimated to be 1 meter, arranged as a ceiling equivalent to a roof and two floors. Good results were obtained with this realistic assumption while the equivalent thickness was not a free parameter of the model. We expect that the nucleonic and soft components of cosmic rays were reduced approximately by a factor of 4 [16].

The cosmic rays at sea level were used as source of particles impinging on the setup, without and with the concrete overhead shielding. The source consisted of muons, neutrons, electrons, positrons, γ -rays, protons, and pions. The measured energy spectra of individual cosmic ray particles taken from [17] were implemented into GEANT4 simulation. The intensity of particles was coded based on their abundances in cosmic rays at sea level as indicated in [18]. The assumed relative abundances of different particle types were muons (63%), neutrons (21%), electrons and positrons (7.5%), γ -rays (7.5%), and protons and pions (1%). The fluxes of positive and negative muons, positive and negative pions, as well as electrons and positrons were calculated from charge ratios reported in [17]. The cosmic-ray particle source was modelled as a plane ($10 \times 10 \text{ m}^2$) placed above the laboratory. See [17] for detail information on spectral fluxes of the different cosmic-ray particle types.

SHIELDING 2.1 was selected as the most suitable GEANT physics list. The G4NDL 4.5 and G4NEUTRONXS 1.4 data files were used for neutron processes and G4EMLOW 6.5 data file for γ -ray interactions. G4NEUTRONXS 1.4 is suitable for elements with natural composition, and G4NDL 4.5 is used especially for thermal neutron cross sections. The correct coding of the given detector and shield to GEANT4 and the software setup with the selection of the physics data files were validated in the work [7].

2.3 The background of HPGe detectors operating deep underground

For simulation of the Obelix detector background, the complete geometry of the Obelix detector was coded in GEANT4 including the massive lead shield. The detector was placed into a box with dimensions of $14 \times 5 \times 3 \text{ m}^3$ representing the detector hall in the Modane underground laboratory (LSM) and the rock and concrete around were modelled as layers 60 cm and 10 cm thick, respectively. The thickness of walls was considered as sufficient, because already 30 cm of the Fréjus rock decreases the neutron energy below 1 MeV, below which the probability to emerge from the wall is negligible [19]. The compositions of rock and concrete were taken from [19], except the density of the Fréjus rock, which was taken from [17]. The rock density of 2.65 g cm^{-3} reported in [19] is typical for standard rock, while the real density of the Fréjus rock is higher.

The cosmic rays deep underground are represented by muons. The muon vertical energy spectrum in LSM was calculated from the equation (4.25) reported in [17]. The fluxes of positive and negative muons were calculated from the charge ratio reported in [20]. The values of the energy loss parameters ($a = 0.217 \text{ GeV m.w.e.}^{-1}$, $b = 4.24 \times 10^{-4} \text{ m.w.e.}^{-1}$) in the Fréjus rock were taken from [17]. The spectral index γ of muon flux at sea level and the normalization constant A were taken from [21]. The average muon energy ($E_{ave} = 250 \text{ GeV}$) was calculated from the equation (4.26) reported in [17]. The total muon flux of $4.73 \text{ m}^{-2}\text{d}^{-1}$ as measured in the laboratory was taken into account. This flux does not include muon multiplicities. The cosmic-ray particle source was modelled as a plane ($14 \times 5 \text{ m}^2$) placed above the laboratory.

The contamination of the detector parts and walls was also coded to GEANT4. The RadioactiveDecay 4.3.2 data file was used for simulation of decay modes and individual decays of radionuclides in selected volumes were processed by the grdm command.

Neutron processes were treated by G4NEUTRONXS 1.4 and G4NDL 4.5 data files, and γ -ray processes by G4EMLOW 6.5 data file. SHIELDING 2.1. physics list was used for simulation of particle interactions with the Obelix detector.

2.4 Muon induced background in planned underground laboratory in Slovakia

For simulation of the HPGe detector background induced by muons, the complete geometry of the HPGe detector with relative efficiency of 100 % was coded in GEANT4 including the low-level shield. The main hall of the laboratory was coded as a box with dimensions of $14 \times 5 \times 3 \text{ m}^3$ and walls with 60 cm layer of standard rock and 10 cm of concrete. The standard-rock density of 2.65 g cm^{-3} and the concrete density of 2.40 g cm^{-3} were assumed. The muon vertical energy spectrum at the 50 m w.e. and 1000 m w.e. depths (Fig. 1) were calculated from the equation (4.25) reported in [17] taking into account the muon total energy loss given in the equation (4.1) in the same reference. The fluxes of positive and negative muons were calculated from the charge ratios reported in [17]. The values of the energy loss parameters $a = 0.217 \text{ GeV (m w.e.)}^{-1}$ and $b = 4.5 \times 10^{-4} \text{ (m w.e.)}^{-1}$ in standard rock were taken from [17]. The spectral index γ of the muon flux at the sea level and the normalization constant A were taken from [21]. The calculated total muon fluxes are $3.5 \times 10^8 \text{ m}^{-2} \text{ d}^{-1}$ (50 m w.e.) and $3456 \text{ m}^{-2} \text{ d}^{-1}$ (1000 m w.e.). These values are in good agreement with the measured muon fluxes in such depths reported in [17, 38]. The average muon energies at 50 m w.e. ($E_{\text{ave}} = 6 \text{ GeV}$) and at 1000 m w.e. ($E_{\text{ave}} = 98 \text{ GeV}$) were calculated from the equation (4.26) in [17]. Fig. 2 illustrates the muon flux attenuation curve while passing through the rock from the depth of 50 m w.e. to the depth of 1000 m w.e. The muon source was modelled as a plane ($14 \times 5 \text{ m}^2$) placed above the laboratory. Simulation of muon backgrounds were carried out for an equivalent live time of 30 days. However, the simulation of background spectrum in the 50 m w.e. laboratory was terminated sooner because of long computing time caused by a high muon flux in this depth. G4NEUTRONXS 1.4 and G4NDL 4.5 data files were used for the neutron processes, and G4EMLOW 6.5 data file for γ -ray processes. SHIELDING 2.1. physics list was used for simulation of underground experiments as in the previous works.

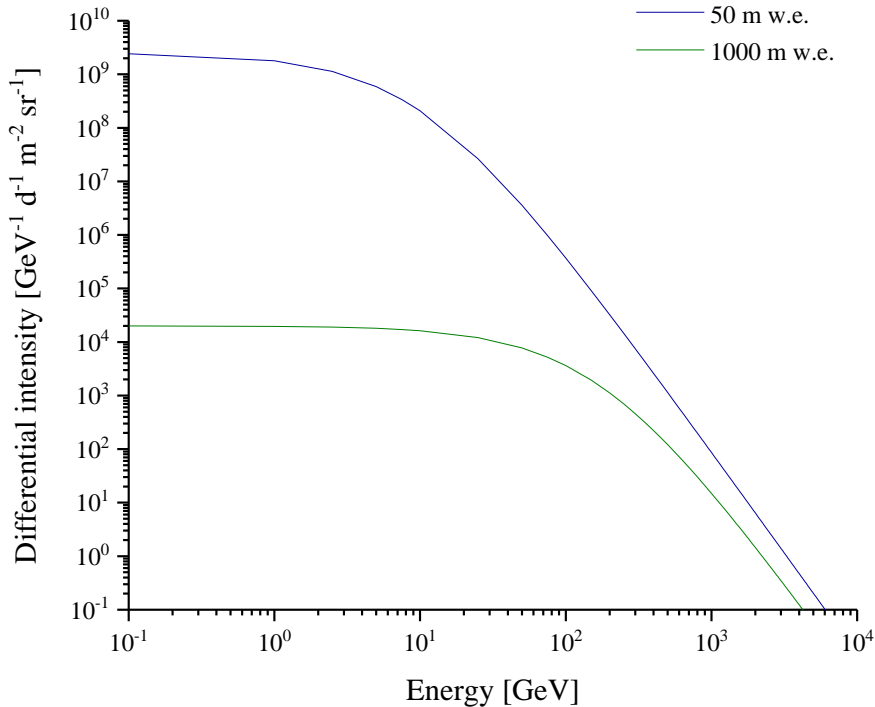


Fig. 1. Calculated muon energy spectra in depths 50 m w.e. and 1000 m w.e.

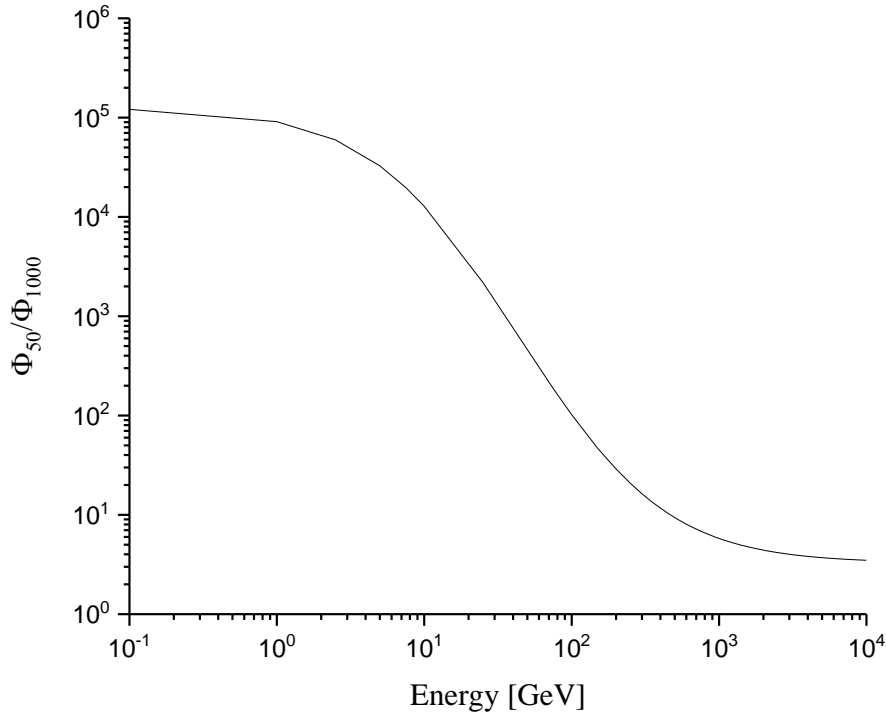


Fig. 2. Attenuation of the muon flux depending on the muon energy from the depth of 50 m w.e. to the depth of 1000 m w.e.

3. Results

First, interaction of neutrons from a ^{241}Am -Be source with an HPGe detector were studied experimentally and by simulations using the GEANT4 simulation tool. Besides the information about neutron interactions, this work stage enabled us to develop and validate the methodology. Second, a cosmic ray induced backgrounds of an HPGe detector placed in a surface laboratory were measured, simulated, and compared. Third, a background spectrum of an HPGe detector (Obelix) in a deep underground laboratory at 4800 m w.e. was simulated and relevant induction processes were explored. Fourth, two laboratories in intermediary depths of 50 and 1000 m w.e. were considered as candidates for a Slovak underground laboratory.

3.1 Investigation of neutron interactions with Ge detectors

3.1.1 ^{241}Am -Be source

The ^{241}Am -Be source with a nominal activity of 370 MBq was used as a neutron source in the experiment. The source was produced in 2009 and its working life is 15 years. It contained compacted mixture of powders of ^{241}Am oxide and ^9Be . The neutron intensity in 2016 was about 23 000 neutrons s^{-1} . The standard neutron spectrum has the average and the maximal neutron energies of 4.2 and 11 MeV, respectively. Neutrons are produced in $^9\text{Be}(\alpha, n)^{12}\text{C}$ reactions, which are accompanied by emission of 4.44 MeV γ -rays from excited ^{12}C daughter nuclei. The shape of the neutron source is a cylinder with a diameter of 14 mm and a length of 12 mm. The active part was encapsulated in a case made of stainless steel and an aluminium shell.

3.1.2 Experimental setup

The experimental setup consisted of an ^{241}Am –Be source placed coaxially 161.2 mm above a Canberra coaxial p-type Ge detector with a relative efficiency of 50%. The germanium crystal with a diameter of 66 mm and a height of 59 mm was enclosed in a thermoplastic foil and in an aluminium cryostat with a copper crystal holder. The cavity inside the crystal was 10 mm in diameter and 45 mm in height. The energy resolution of the detector was 2.07 keV for 1332.40 keV γ -rays of ^{60}Co . The energy calibration of the detector was done with a ^{60}Co source. The detector efficiency calculation was done using LabSOCS software from Canberra. Two circular iron absorbers were placed above the detector to absorb abundant but low-energy γ -rays of ^{241}Am with the aim to reduce the dead time of the detector. A plastic beaker was used to place the source at a certain distance from the detector to further reduce the dead time and to minimize the energy summation effect. In this way, a dead time correction of only about 12.6% could be reached. The source–detector setup was placed in a shield consisting of 9.5 mm of carbon steel, 102 mm of lead, 1 mm of tin foil and 1.5 mm of copper cladding (from outside to inside). The outer shield dimensions were 508 mm in diameter and 635 mm in height. The γ -energy spectrum ranged from 10 to 3000 keV. Typical measuring time was 25 h. The background γ -spectrum (without ^{241}Am –Be source) was measured as well, and it was subtracted from measured neutron induced spectra. A low nominal activity of the neutron source and short measuring time did not produce any neutron damage of the detector.

3.1.3 Evaluation of the experimental γ -ray spectrum

A detailed analysis of the experimental spectrum was carried out. Almost all peaks in the spectra were identified and explained. A typical feature of neutron interactions with a Ge detector are triangular γ -ray peaks. When a germanium detector is exposed to neutrons at energies of 1 MeV or more, triangular peaks may result from summation of the recoil energy of a Ge nucleus deposited within the detector itself and the energy of a photon emitted during de-excitation of the nucleus previously excited during inelastic scattering [4]. In the experiment, such peaks were observed at the energies of 68.80 keV, 562.93 keV, 595.84 keV, 689.60 keV, 834.01 keV, 1039.51 keV, 1108.41 keV, 1204.20 keV and 1463.75 keV.

In the case of the 691.43 keV peak, the induction mechanism is slightly different. The excited nucleus of ^{72}Ge de-excites by an E0 transition, which is an internal conversion process for this nuclide: $^{72}\text{Ge}(n, n'e)^{72}\text{Ge}^*$. The total detectable energy of ^{72}Ge includes the energy from the X-ray and it is summed with the recoil energy of the ^{72}Ge nucleus to form a triangular shape [22]. The shapes of the triangular peaks are sharp at lower energies but lose their sharpness with increasing energy. The reason is the difference between angular distributions of the neutron scattering on given Ge isotopes at different impacting neutron energy and cross section [4].

A large number of other peaks were observed in the spectra, which are caused by neutron interactions with other materials in the setup, and particularly with impurities. Most of the peaks, which clearly dominate in the spectra are from lead and copper, the most abundant materials around the Ge crystal. They originate from inelastic scattering of neutrons on copper and lead nuclei. Although various impurities are present in small amounts in the setup, they may be important due to large neutron cross-sections for certain isotopes.

The presence of copper and lead influences the γ -spectrum strongly. Interactions of neutrons with these materials produce many γ -lines visible in the spectrum, which can hide or imitate the searched signals. This is an unwanted effect, especially in experiments looking for rare nuclear processes. For example, γ -rays resulting from neutron inelastic scattering or neutron capture reactions may imitate signatures of the neutrinoless $\beta\beta$ decay [6]. Possible replacement of copper and lead as shielding materials in underground experiments would require, however, further investigations.

Aluminium causes only a few strong γ -lines in the spectrum, and they form a significant background component. To avoid its contribution is, however, very difficult, because aluminium is the most commonly used material for cryostats and entrance windows. Nevertheless, the problem can be solved by elaboration of appropriate event-rejection strategy.

Similarly, γ -lines from tin parts of the setup are important potential sources of background. However, tin layers are usually not present in shields of Ge detectors located deep underground. As it was shown previously, descending-Z shields consisting of lead, tin and copper are superior as far as the muon background is concerned [23]. Once it is suppressed, passively and/or actively, other materials remain for consideration.

To minimize the background induced by neutron interactions with impurities in the materials, it is necessary to use ultra-pure materials for experimental setups, and to know the identity and the amount of the residual elements.

In shallow as well as in deep underground laboratories fast neutrons are always present. They are produced by cosmic-ray interactions generating hadron showers as well as by capture of negative muons, predominantly on heavy nuclei like lead. Hence, inelastic scattering will always contribute to the background of Ge detectors in the energy region of interest manifesting itself by Ge peaks observed experimentally. If the spectrum statistics is sufficient to recognise such peaks, the contribution of neutrons to the total background can be unfolded. However, validated Monte Carlo simulations should be always carried out for estimation of the neutron background component.

3.1.4 Comparison of experimental and simulated γ -spectra

The experimental spectrum was compared with the GEANT4 simulation of neutron and γ -ray interactions with the detector and the shield. The simulated spectrum reproduces the main features of the measured spectrum fairly well considering the complexity of the interactions. Integral count rates were compared for the experimental and the simulated spectra for the energy region from 115 keV to 2880 keV. This energy range was chosen due to a difference between experimental and simulated data for a lower continuum below 115 keV due to a higher γ -ray intensity of the neutron source, and the end of the measured spectrum at 2880 keV. The integral count rate of the measured spectrum ($378 \pm 3 \text{ s}^{-1}$) was in reasonable agreement with the calculated one ($369 \pm 11 \text{ s}^{-1}$). For detailed information including all figures, see Chapter *Author's publications*, the article *Investigation of neutron interactions with Ge detectors*.

3.2 The neutron component of background of an HPGe detector operating in a surface laboratory

3.2.1 Experimental setup

A Mirion Technologies (Canberra) coaxial low-level p-type HPGe detector GC-5019 with a relative efficiency of 50% was used for background measurement. The germanium crystal was a cylinder with a cavity inside the crystal. The dimensions of the crystal were 66 mm in diameter and 59 mm in height. The cavity was 10 mm in diameter and 45 mm in height. The crystal was placed in a thermoplastic foil and in a copper crystal holder, which was enclosed in an aluminium “swan-neck” cryostat. The detector was placed in a low-level shield consisting of (from outside to inside) 9.5 mm of carbon steel, 92 mm of common lead, 10 mm of old low-activity lead, 1 mm of tin foil, and 1.5 mm of copper cladding. The outer dimensions of the shield were 508 mm in diameter and 635 mm in height. The preamplifier was placed outside the shield. The “swan-neck” prevented a direct sight of the crystal on a Dewar vessel and the floor below. The energy resolution of the detector was 2.07 keV for 1332.40 keV γ -rays of ^{60}Co . The Canberra GENIE 2000 software was used for γ -ray spectrum analysis. The spectrum was acquired in the energy range from 10 to 3000 keV during 84 h of live time. The measurement was carried out after an experiment with an Am–Be neutron source [7], in

which two circular iron absorbers and one plastic beaker were placed above the detector with the aim of reducing the dead time by increasing the source-detector distance and absorbing the ^{241}Am gamma rays. As the same background spectrum was used in this work, the iron absorbers and the plastic beaker were left inside the shield.

3.2.2 Evaluation of the experimental background γ -ray spectrum

The measured background γ -spectrum of the HPGe detector was analysed and evaluated in detail. Many peaks were identified and explained also using information from the previous experiment with Am-Be neutron source [7]. Triangular γ -ray peaks, which are typical for interactions of fast neutrons with individual Ge nuclei, are present in the spectra.

The experimental γ -spectra also contain many other peaks produced by neutron interactions with materials used in the setup, especially with shielding materials. The majority belongs to copper and lead peaks, as both materials with large neutron cross sections are the most abundant in the setup. Several well visible peaks originating in natural radioactivity are present in the spectra. They come from contamination of the detector, the shield and the surrounding materials, such as the laboratory walls and objects.

3.2.3 Comparison of Monte Carlo simulations with the experiment

Two simulations of the background spectrum were carried out without considering the contamination by natural radionuclides. First, a simulation without the concrete building was carried out and the resulting spectrum was compared with the measured background. There is a significant difference between the experimental and simulated spectra in the continuum below 500 keV. The main reason is that penetration of cosmic rays through the building was not in this case taken into account. Next, contamination lines visible in the experimental spectrum and stemming from natural contamination by ^{40}K , ^{208}Tl , ^{214}Pb , and ^{214}Bi were not coded, so Compton continuum from the corresponding peaks did not contribute to count rates up to 500 keV. Several other differences were observed. The γ -ray emission for a few peaks in the energy range from 450 keV to 1 MeV is higher than in the experimental background spectrum. This effect is visible due to missing concrete layer of the building. Absorption in the concrete layer reduces the γ -ray intensity in this energy range.

The triangular shape of Ge peaks coming from summation of the recoil energy in Ge nucleus and the energy of emitted γ -rays, is not simulated correctly by GEANT4, as they are lower, less sharp, and their tails do not fit the real ones. The peak at the energy of 477.61 keV coming from $^{10}\text{B}(n, \alpha)^7\text{Li}$ reaction is overestimated. The count rate of the simulated peak was approximately 5-times higher than the experimental one. The main reason is that the boron content in the doped Ge dead layer was not known exactly. As the cross section for boron for this reaction is very high, the simulation could be affected considerably.

Special attention was paid to the lead γ -rays in the simulated spectrum. The ^{208}Pb peaks known as originating in β -decay of ^{208}Tl , usually present in detector systems as a contaminant, are clearly visible also in the simulated spectrum, although no contamination was assumed. The γ -lines come from the inelastic scattering of neutrons on ^{208}Pb nuclei. The count rates of the main ^{208}Pb peak (2614.51 keV) were compared. It is $0.00048 \pm 0.00014 \text{ s}^{-1}$ for the experimental peak and $0.00024 \pm 0.00007 \text{ s}^{-1}$ for the simulated one. The count rate is higher in the measured than in the simulated background, indicating that there is also a direct contribution from ^{208}Tl decay, as expected. It can be concluded that, approximately 50% of the peak in the measured background spectrum is formed by neutron interactions with ^{208}Pb nuclei. Therefore, as long as lead will be present in the experimental setup, these peaks will be present in the background spectrum, even if the contamination with ^{208}Tl would be eliminated.

The experimental and the simulated spectra were compared by integral count rates for the energy range from 500 keV to 2875 keV where the spectra match each other. The integral count rate

measured in the experiment $0.56 \pm 0.03 \text{ s}^{-1}$ was in a very good agreement with the calculated value $0.53 \pm 0.05 \text{ s}^{-1}$. However, omission of the roof shielding in the simulation results in a considerable difference between the measured and simulated spectra below 500 keV.

Another simulation of background γ -ray spectrum was carried out, this time considering the building. The shape of the simulated spectrum replicates the experimental one much better than when the building effect was omitted. The typical wide hump in the continuum around 200 keV is predicted well. However, there is still a slight difference in the continuum heights up to 350 keV, probably caused by omission of radionuclide contamination of construction materials in the simulations. The simulated continuum is slightly lower, especially in the part below the ^{214}Bi peaks. The simulated peak of ^7Li at the energy of 477.61 keV is again overestimated, but the count rate of the simulated peak decreased by about a factor of two. The count rates of the ^{208}Pb peaks at the energy of 2614.51 keV were compared again. The experimental one is $0.00048 \pm 0.00014 \text{ s}^{-1}$, while the simulated one is $0.00017 \pm 0.00005 \text{ s}^{-1}$, what means that approximately 35% of the experimental peak originate in inelastic scattering of neutrons on lead nuclei. The count rate of the simulated peak is lower than in the previous simulation (without the concrete) by 30%, what can be explained by changed neutron spectral fluxes after passing the concrete layer. Due to the same reason, the triangular shape of Ge peaks is less visible as it was in the simulation without the concrete layer.

Integral count rates of the experimental and simulated spectra were compared for the energy region from 50 to 2875 keV taking into account the concrete shielding. Below the energy of 50 keV, the count rate is strongly influenced even by small changes in the thicknesses and material composition of various layers. Therefore, it is difficult to achieve a quantitative agreement of count rates below this energy. The integral count rate of the measured spectrum of $1.26 \pm 0.07 \text{ s}^{-1}$ matches the simulated one of $1.25 \pm 0.13 \text{ s}^{-1}$, indicating a very satisfactory agreement. The numerical difference of less than 1% is rather a random coincidence than a precise result match. It may seem that, in the region above 2000 keV, the simulated count rate is higher than the measured one. Therefore, the integral count rates (continuum and peaks) were calculated for both spectra in the energy range from 2000 keV to the end of the measured spectrum at 2875 keV. The obtained count rates were $0.07 \pm 0.005 \text{ s}^{-1}$ for the experimental spectrum and $0.08 \pm 0.009 \text{ s}^{-1}$ for the simulated one (only statistical uncertainties at the 1σ level). The experimental spectrum shows greater statistical fluctuations, which are more pronounced at lower values in the logarithmic y scale.

The continuum in the HPGe background spectrum is formed mainly by muon and neutron interactions. Neutrons interacting with the detector materials, especially with lead, produce many photons contributing to the continuum, while muons contribute via bremsstrahlung of delta electrons. A continuum is, however, not induced only by cosmic ray particles. A part of it is formed by radioactive contaminants present in the system. Further contributors are, therefore, β -rays originating from decaying radionuclides and Compton scattering coming from interactions of high-energy photons [25]. In particular, commercial lead used for shielding of HPGe detectors is contaminated with ^{210}Pb . In surface laboratories, this background component is not distinguishable from the low-energy part of continuum induced mainly by muons [26].

For detailed information including all figures, see Chapter *Author's publications*, the article *The neutron component of background of an HPGe detector operating in a surface laboratory*.

3.3 The effect of neutrons on the background of HPGe detectors operating deep underground

3.3.1 Modane underground laboratory

The deepest European underground laboratory hosting experiments related to rare nuclear processes and decays is the Modane underground laboratory (Laboratoire Souterrain de Modane, LSM). It hosts experiments such as EDELWEISS for direct detection of dark matter particles and SuperNEMO for neutrinoless double-beta decay. The laboratory is located in Auvergne-Rhône-Alpes region under the Cottian Alpes mountains. It is situated in the middle of the 12.6 km long Fréjus road

tunnel connecting France and Italy at 1700 m under the Fréjus Peak, equivalent to a depth of 4800 m w.e. Thanks to this depth, LSM is very well shielded against cosmic rays, therefore the muon flux there is very low (4.73 ± 0.09) $\text{m}^{-2}\text{d}^{-1}$ [27]. The flux was measured through a horizontal plane [28]. Natural radionuclides such as ^{40}K and members of the ^{238}U and ^{232}Th decay series are present in the laboratory walls consisting of Fréjus rock and concrete, in surrounding materials and, in construction parts of the detectors. The concentrations of ^{238}U in the rock and in the concrete are (11.8 ± 6) Bq kg^{-1} and (10.2 ± 5) Bq kg^{-1} . The concentrations of ^{232}Th in the rock and in the concrete are (22.8 ± 7) Bq kg^{-1} and (6.7 ± 2) Bq kg^{-1} , respectively. The concentration of ^{40}K is (182 ± 4) Bq kg^{-1} in rock and (91 ± 3) Bq kg^{-1} in concrete [8]. Further, the LSM operates a ventilation system removing the inert and noble gases Radon (^{222}Rn) and Thoron (^{220}Rn), and so reduces also their progenies in the ambient air to negligible levels. The γ -ray flux in LSM is relatively very high $(5.4 \pm 0.4) \times 10^8$ $\text{m}^{-2}\text{d}^{-1}$ (measured in the power supply room) when compared with the muon flux, and therefore it significantly contributes to the background. However, most of the detectors operating in LSM are located in the detector hall, where the count rate of measured γ -rays is higher almost by about a factor of 3 than in the mentioned power supply room [30].

Another source of background in the LSM laboratory is due to neutrons. The measured neutron flux in LSM is (1381 ± 860) $\text{m}^{-2}\text{d}^{-1}$ for neutron energies above 2 MeV [31] and (1382 ± 864) $\text{m}^{-2}\text{d}^{-1}$ for thermal neutrons [32] measured before the installation of large experiments. After these installations, the flux of thermal neutrons was measured again and it was found that it increased to (3084 ± 280) $\text{m}^{-2}\text{d}^{-1}$ [33]. However, the flux of thermal neutrons may vary as much as by a factor of 3, depending on the location. A table of thermal neutron fluxes for different locations at LSM is given in [34]. The flux of thermal neutrons in the detector hall is (3888 ± 432) $\text{m}^{-2}\text{d}^{-1}$. Fast neutrons in LSM are produced by (α, n) reactions of alpha particles emitted by members of the ^{238}U and ^{232}Th decay series on light elements such as C, O, Mg, Na, Al, Si and Fe, present mainly in the walls, and by spontaneous fission of natural radionuclides, present mostly in the walls, especially of ^{238}U . The (α, n) reactions contribute to the fast neutron flux by 1930 $\text{y}^{-1}\text{kg}^{-1}$, while spontaneous fission adds 470 $\text{y}^{-1}\text{kg}^{-1}$ [32]. Neutrons originating in muon interactions with walls contribute to fast neutron flux by $(2.3 \pm 0.5) \times 10^{-5}$ $\text{y}^{-1}\text{kg}^{-1}$, while neutrons resulting from muon interactions with the lead shield of the detector by $(3.2 \pm 0.2) \times 10^{-4}$ $\text{y}^{-1}\text{kg}^{-1}$ [32]. We can conclude that, neutrons from (α, n) reactions are the major contributor to the total fast neutron flux in LSM, while the contribution from muon-induced neutrons is minimal.

3.3.2 HPGe detector

Several HPGe detectors with large germanium crystals are located in the detector hall in LSM. One of them is the detector called Obelix, primarily used for radiopurity measurements and for investigations of rare decays [29]. Obelix is a p-type coaxial HPGe detector (Canberra) with a relative efficiency of 160%, which is the efficiency relative to a ^{60}Co source (using the 1332 keV peak) measured with a NaI(Tl) detector at a distance of 25 cm from the detector. The volume of the crystal is 600 cm^3 , which corresponds to about 3 kg of ultra-pure germanium. The crystal is placed in a thermoplastic foil, embedded in the crystal holder made of an Al-Si alloy (4% of Si) and enclosed in aluminium U-type cryostat made of the same alloy. The cryostat is connected with a cooled Field Effect Transistor (FET). The entrance window of the end-cap is made of the same material as the crystal holder. The thickness of the entrance window is 1.6 mm. The distance between the entrance window and the crystal is 4 mm. The end cap is fixed to the bottom part of the cryostat by an O-ring made of synthetic rubber. The detector is placed in ultra-low level shield consisting of (from outside to inside) radiopure normal lead with a thickness of 20 cm and a roman low-activity lead with a thickness of 12 cm. The lead shield is secured by a stainless steel frame. All screws in the detector are made from leadless brass. The energy resolution of the detector is 1.2 keV at 122.06 keV γ -rays of ^{57}Co and 2 keV at 1332.40 keV γ -rays of ^{60}Co . The detector can be operated either with 8192 channels or 16384 channels ADCs.

The detector parts were produced from ultra-pure materials with the aim to reduce the concentration of natural radionuclides to a minimum. Al-Si alloy contains cosmogenic ^{26}Al and it also contains ^{226}Ra , ^{228}Ra , ^{228}Th and ^{40}K . Radionuclides ^{226}Ra , ^{228}Ra , ^{228}Th and ^{40}K are present in other construction parts of the detector, such as leadless brass, O-ring and FET, as well. Even if the brass is classified as leadless, it still contains ^{210}Pb at measurable levels. The concentration of these radionuclides in the O-ring is high, but the O-ring is small and it is placed far enough from the crystal. The FET is one of the most radioactive parts of the detector and it contributes to the detector background. In order, to reduce the background from the FET, a disk made of roman lead with a thickness of 10 mm is placed at the bottom part of the crystal holder. The radioactivity concentration in this lead is minimal. Normal lead contains a high concentration of ^{210}Pb in comparison with roman lead. Besides ^{210}Pb , roman lead contains also ^{226}Ra and ^{228}Ra . All values of the various radionuclide concentrations were taken from [29].

3.3.3 Experimental background spectrum

In order to determine neutron contributions to the Obelix background energy spectrum measured in the Modane underground laboratory, investigations of impacts of cosmic ray interactions with the HPGe detector materials, as well as the influence of present radionuclides on the resulting background were carried out. The experimental background spectrum was analysed and reproduced using a Monte Carlo simulation. The spectrum of 34.2 days shown in [29] was used for analysis.

Gamma lines in the background spectrum measured deep underground were analysed. Contribution of radionuclides dominates in the energy spectrum, as seen by the presence of peaks from the daughter isotopes of ^{238}U , ^{232}Th decay series and by ^{40}K . Natural radionuclides are present in the detector construction materials, in the shield and its surroundings, especially in the walls.

The Monte Carlo simulation of the experimental background energy spectrum was carried out including the concentration of radionuclides in the detector parts and the laboratory walls, reported in [27]. Specific activities of 12 Bq kg^{-1} of ^{238}U , 12 Bq kg^{-1} of ^{232}Th and 182 Bq kg^{-1} of ^{40}K were coded into the Fréjus rock. The concentration of these contaminants in concrete was 10 Bq kg^{-1} , 23 Bq kg^{-1} and 91 Bq kg^{-1} , respectively. Into crystal holder, cryostat and entrance window, 0.4 mBq kg^{-1} of ^{26}Al was coded, as well as 0.3 mBq kg^{-1} of ^{226}Ra , 0.1 mBq kg^{-1} of ^{228}Ra , 1.4 mBq kg^{-1} of ^{228}Th and 1.1 mBq kg^{-1} of ^{40}K . O-ring contamination was included, too. The concentration of 910 mBq kg^{-1} of ^{226}Ra , 320 mBq kg^{-1} of ^{228}Ra , 350 mBq kg^{-1} of ^{228}Th and 1360 mBq kg^{-1} of ^{40}K was coded in GEANT4 simulation. Contamination of FET was involved per unit, specifically 1.6 mBq of ^{226}Ra , 2.9 mBq of ^{228}Ra , 0.4 mBq of ^{228}Th , 4.9 mBq of ^{40}K and 1.7 mBq of ^{207}Bi . Lead shield is contaminated as well, therefore 20 Bq kg^{-1} of ^{210}Pb was coded into normal lead and 60 mBq kg^{-1} of the same radionuclide into roman lead. Additional amount of 0.2 mBq kg^{-1} of ^{226}Ra and 0.2 mBq kg^{-1} of ^{228}Ra was added to the roman lead. The concentration level of cosmogenic radionuclides (except of ^{26}Al) was not known therefore it was not coded into the simulation (i.e. ^{22}Na , ^{54}Mn , ^{57}Co and ^{65}Zn).

3.3.4 Comparison of Monte Carlo simulations with experimental spectrum

The experimental spectrum was compared with the simulated one. Integral count rates were calculated in the energy range from 40 keV to 3000 keV. The value of the integral count rate for the experimental spectrum was $345 \pm 18 \text{ d}^{-1}$ and $320 \pm 31 \text{ d}^{-1}$ for the simulated one. The simulation reproduces the main features of the measured spectrum fairly well, considering the poor statistics of the experimental spectrum and missing peaks from the cosmogenic radionuclides. We can conclude, that the simulation is in a good agreement with the experiment. The count rates of individual peaks were compared, too. The count rates of the simulated peaks agree with the experimental ones well, except for the 84.21 keV peak of double origin. However, the difference is still within a factor of two.

Muons are survivors of cosmic-rays passing underground, therefore background spectra induced only by muons were simulated. The muon flux in LSM is very low, therefore muons only make a small contribution to the detector background. Simulation of muon background with a live time of 34.2 days was carried out and subsequently, the contribution of muon events to the experimental spectrum was calculated. It was found, that only $0.20 \pm 0.02 \text{ d}^{-1}$ of them deposited energy in the detector, which is much less than 1% of the total count rate $345 \pm 18 \text{ d}^{-1}$. Therefore, the role of muons in the background energy spectrum of the HPGe detector measured underground is negligible. Nevertheless, if the background induced by radionuclides would be suppressed, then it would gain significance, especially for experiments looking for rare processes. In order to investigate and demonstrate the contribution of muons to the long-time measured spectrum, the next simulation of background induced by muons were carried out with the number of events corresponding to measuring time of 220 years. The long measuring time was chosen in order to show a relevant energy spectrum induced by muon interactions with a sufficient number of counts due to the very low muon flux. The simulated spectrum was analysed and it was found, that besides the annihilation peak, also neutron induced peaks are rising from the continuum. Peaks were identified and explained also using information from the previously measured background energy spectrum [35]. Although the statistics are still very low, these peaks indicate, that muon induced neutrons indeed contribute to the spectrum. We can see rising ^{208}Pb peaks at energies of 583.19 keV and 2614.51 keV, as well as indication of ^{74}Ge and ^{72}Ge peaks at energies of 595.84 keV and 691.43 keV, respectively. It means, that neutron induced peaks from cosmic-rays contribute to the total background but might be visible only in spectra measured over a long time. Hence, peaks originating in neutron interactions with the lead shield also contribute to the total count rate of ^{208}Pb peaks coming from ^{208}Tl decay. The measured spectrum was compared with the simulated muon-induced spectrum. It was confirmed, that the simulated spectrum is about three orders of magnitude lower than the experimental one as it was stated in [36].

Since neutrons from (α, n) reactions and spontaneous fission form a critical background source in underground laboratories, their effect on the Obelix detector was simulated as the next step. Neutron fluxes in LSM reported in [31] and [32] were used for the simulations. A total energy spectrum induced by neutrons was simulated, as well as individual contributions from thermal and fast neutrons for measuring times 34.2 and 900 days. The integral count rate of the total spectrum induced by neutrons with a live time of 34.2 days was compared with the count rate of the experimental spectrum. The simulated one was $19 \pm 2 \text{ d}^{-1}$ and the experimental one of $345 \pm 18 \text{ d}^{-1}$, which indicates, that about 6% of the measured background continuum is formed by neutron interactions. A comparison of the integral count rates of the spectra induced by thermal and fast neutrons with the total spectrum showed that fast neutrons contribute to the total spectrum of neutrons more than thermal neutrons. The integral count rate of the spectrum induced by fast neutrons was $12.5 \pm 1.3 \text{ d}^{-1}$, indicating that about 65% of the total spectrum ($19 \pm 2 \text{ d}^{-1}$) was invoked by fast neutrons. Thermal neutrons typically give rise to a boron peak at the energy of 477.61 keV coming from $^{10}\text{B}(n, \alpha)^7\text{Li}$ reaction due to boron present in the contact layer of the crystal, while fast neutrons significantly contribute to the continuum up to 250 keV, and induce lead and germanium peaks coming from inelastic scattering of neutrons on Pb and Ge nuclei. Rising ^{206}Pb , ^{207}Pb and ^{208}Pb peaks are visible in the spectrum induced by fast neutrons at the energies of 803.06 keV, 569.70 and 1770.23 keV, and 2614.51 keV, respectively. A peak of ^{72}Ge at the energy of 691.43 keV is indicated as well. The contribution of fast neutrons up to 250 keV energy region is important for dark matter particle search in the low mass range of WIMPs ($<1 \text{ GeV}$), and γ -rays resulting from neutron interactions can imitate signatures of such events [6]. The boron peak clearly dominates in the spectra induced by thermal neutrons. The inner electrode of the detector is made of boron and the ^{10}B cross section for thermal neutrons is very high, especially for (n, α) reaction, therefore the boron peak is well visible in these spectra. Similarly, ^{10}B , ^{72}Ge and ^{208}Pb peaks are also visible in the total spectra induced by neutrons. In addition, a peak due to inelastic scattering of neutrons on ^{74}Ge nuclei is seen there as well. The statistics are again very low, therefore only the boron peak is identified reliably. The rest of the peaks were predicted based on the

information from the measured energy spectrum induced by a neutron source [7]. All neutron induced peaks contribute to the total measured background, too. Nevertheless, the contribution of neutron induced γ -rays to the total count rate of these peaks is only about 2%.

3.3.5 Neutrons and their effect

The continuum of background spectrum obtained underground with the Obelix γ -ray spectrometer is formed mainly by contribution of radionuclides and only a small part can be assigned to neutron interactions. Concentration of the natural radionuclides in the detector parts and the laboratory walls forms almost 94% of the continuum, which raises a question of the importance of radiopure material usage. The contribution from muons is much less than 1% and is therefore negligible. Nevertheless, neutrons are still an important background component even if their contribution to the continuum is only about 6%. In order to further investigate the effect of neutrons on the background spectrum of the Obelix detector, simulations of individual physics processes of neutron interactions were carried out. Neutron capture, elastic and inelastic scattering were simulated separately. Simulations were carried out for a measuring time of 900 days, as the total neutron induced spectrum. It was found that inelastic scattering is the major contributor to the spectrum induced by neutrons. The second most frequent process was neutron capture. Elastic scattering occurred infrequently. In comparison with inelastic scattering, it is about 70% less. Neutron capture is about 30% less occurring than inelastic scattering. Inelastic scattering significantly contributes to the lower continuum of the spectrum induced by neutrons up to 500 keV and contributes less to the part up to 1 MeV. Neutron capture contributes to the total neutron induced energy spectrum almost evenly. Elastic scattering contributes only to the first part of the total neutron induced energy spectrum up to 300 keV. We can conclude that the effect of neutrons on the background of the HPGe detector operating underground, such as the Obelix, is manifested mainly by their contribution to the continuum up to 1 MeV, and especially below 500 keV.

Investigation of neutron production in the lead shield was carried out as well. Simulations of neutron interactions with the lead shield were carried out with the generation of secondary particles in the shield and without. Simulations showed that particles generated in the shield contribute only about 1% to the total count rate of the resulting spectrum. It indicates that neutrons coming from outside of the detector are more important than neutrons generated inside the lead shield. For detailed information including all figures, see Chapter *Author's publications*, the article *The effect of neutrons on the background of HPGe detectors operating deep underground*.

3.4 Simulation of muon induced background in a proposed underground laboratory in Slovakia

3.4.1 Design of underground laboratories

A shallow laboratory at a depth of 50 m w.e. and a deep underground laboratory at a depth of 1000 m w.e. have been considered for environmental radioactivity and astrophysical studies. Several halls for experiments including the main hall where an HPGe detector should be located have been foreseen. The main hall for operation of the HPGe detector was modelled as a box with dimensions of $14 \times 5 \times 3$ m³. Standard rock and concrete were considered as potential construction materials of the walls. The rock and concrete were modelled as 60 cm and 10 cm thick layers. The detector was placed in the middle of the hall and approximately 80 cm from the rear wall. Only this one detector was considered to be present in the hall for the purpose of simulations. The same laboratory design was used for both the depths. The calculated muon vertical energy spectra at the 50 m w.e. and 1000 m w.e. depths are shown in Fig. 3.

The detector selected for low-background experiments is a p-type coaxial HPGe detector with a relative efficiency of 100%. The volume of the crystal is 375 cm³, which corresponds to about 2 kg of ultra-pure germanium. The crystal is placed in a thermoplastic foil, embedded in the crystal holder

made of an Al-Si alloy (4% of Si) and enclosed in aluminium cryostat made of the same material as the crystal holder. The entrance window of the end-cap is made of the same material as the crystal holder. The detector is placed in a low-level shield consisting of (from outside to inside) radiopure normal lead with a thickness of 15 cm, carbon steel with a thickness of 30 cm and copper with a thickness of 1 cm. The energy resolution of the detector is expected to be 2 keV at 1332.40 keV γ -rays of ^{60}Co .

3.4.2 Peak analysis

Gamma lines in the simulated background spectra were analysed (Fig. 4) and their count rates were evaluated. In the case of the 1000 m w.e. laboratory, some peaks are hardly distinguishable from the continuum. Very short-lived radionuclides (half-lives of less than 1 ms), usually excited states, are marked with the asterisk character. Nuclear data were taken from NuDat 3.0. Several peaks coming from neutron interactions with the detector and its shield are visible in the simulated spectra. These neutrons are produced mostly in capture of negative muons by heavier nuclei.

Shallow laboratory – 50 m w.e.

In the background spectrum simulated in the 50 m w.e. shallow laboratory, the copper peaks are prevailing. Copper is used as the inner part of the shield and such peaks are resulting from neutron capture or inelastic scattering of neutrons on copper nuclei. Peaks induced by neutron capture on ^{63}Cu nuclei resulting in a compound nucleus ^{64}Cu are visible at the energies of 212.39 keV, 259.30 keV, 343.94 keV, 711.94 keV, 1232.13 keV, 1293.92 keV and 2291.42 keV. Similarly, peaks of ^{66}Cu originating in neutron capture on ^{65}Cu nuclei were found at the energies of 315.71 keV, 385.78 keV, 622.69 keV, 2144.22 keV and 2448.70 keV. Peaks corresponding to inelastic scattering of neutrons on ^{63}Cu are observable at energies of 955.0 keV, 1668.90 keV, 1861.30 keV, 2512.0 keV and 2562.0 keV. The same reaction on ^{65}Cu generates peaks at energies of 924.5 keV and 1724.92 keV.

The middle part of the shield is made of carbon steel with a thickness of 30 cm, and inelastic scattering of neutrons on the iron nuclei on iron nuclei takes place. The scattering on ^{56}Fe gives rise to γ -lines at the energies of 846.76 keV and 2763.0 keV. Also γ -lines at the energies of 1153.10 keV, 1408.10 keV and 1936.50 keV belonging to ^{54}Fe were found in the spectrum. The 2922.50 keV γ -line of ^{57}Fe originates in neutron capture on ^{56}Fe .

Gamma lines resulting from inelastic scattering of neutrons on lead nuclei were observed at the energies of 583.19 keV, 1380.89 keV, 2614.51 keV and 2720.57 keV for ^{208}Pb , at the energies of 1063.66 keV and 1770.23 keV for ^{207}Pb , and at the energy of 683.50 keV for ^{204}Pb .

As far as the HPGe detector is concerned, inelastic scattering of neutrons on ^{76}Ge gives rise to the peak at 431.0 keV. Neutron capture on ^{70}Ge and ^{76}Ge induces peaks at 174.96 keV and 1457.84 keV. The crystal holder and the cryostat are made of aluminium and silicon. The 2108.24 keV ^{28}Al peak originates in neutron capture on ^{27}Al . Two ^{30}Si peaks induced by the same reaction on ^{29}Si are seen at the energies of 1534.12 keV and 2235.23 keV.

The 477.61 keV peak of ^7Li is coming from the $^{10}\text{B}(n, \alpha)^7\text{Li}$ reaction that has a high cross section for thermal neutrons. The inner electrode of the crystal contains boron as a semiconductor dopant.

Deep laboratory – 1000 m w.e.

In the background spectrum simulated in 1000 m w.e. deep laboratory, the germanium peaks are prevailing up to 1500 keV, from 1500 keV the copper peaks dominate. Germanium peaks at the energies of 297.30 keV and 430.30 keV are induced by the neutron capture on ^{72}Ge . The inelastic scattering of neutrons on ^{74}Ge results in peaks at 595.85 keV, 1105.56 keV, 1489.35 keV, and 2260.0 keV. The 691.43 keV peak of ^{72}Ge is induced by the internal conversion process.

Peaks due to the neutron capture on ^{63}Cu are at 343.94 keV, 1799.48 keV, 1852.40 keV, while this reaction on ^{65}Cu generates peaks at 1212.52 keV, 1944.97 keV, 2448.70 keV, 2457.66 keV and

2952.64 keV. Peaks originating in inelastic scattering of neutrons were identified as well: ^{63}Cu 962.06 keV and 2857.60 keV; ^{65}Cu : 550.0 keV and 1724.92 keV.

Lead peaks are coming only from inelastic scattering of neutrons on ^{208}Pb (722.25 keV, 860.56 keV and 1380.89 keV) and ^{204}Pb (2666.2 keV).

There is only one γ -line resulting from neutron capture on ^{54}Fe at the energy of 1640.40 keV. Two γ -line originate in inelastic scattering on ^{56}Fe : 1303.40 keV and 2034.79 keV.

In this spectrum the peak coming from the $^{10}\text{B}(n, \alpha)^7\text{Li}$ reaction at the energy of 477.61 keV is visible as well.

The peak at 511 keV results from annihilation of electron–positron pairs generated by photon interactions with the detector and shield material and the summation peak at 1022 keV can be also observed. The annihilation can be summed with 510.74 keV γ -rays of ^{208}Pb emitted after inelastic scattering of neutrons on ^{208}Pb .

3.4.3 Evaluation of the simulated results

The simulated background spectra are compared in Fig. 5. It was found that the spectrum simulated for the underground laboratory in the depth of 1000 m w.e. is about five orders of magnitude lower than the one simulated for the shallow laboratory. The background spectrum simulated in the shallow laboratory reflects the neutron production in such depth. The interactions of neutrons with the detector and the shield are more often occurring there than in 1000 m w.e. deep laboratory, therefore the number of peaks coming from neutron interactions visible in the background spectrum simulated for the shallow laboratory in depth of 50 m w.e. is higher. The count rates of identified peaks are listed in Table 1. Two peaks are occurring in both spectra, i.e., the ^7Li peak at the energy of 477.61 keV and the ^{208}Pb peak at the energy of 1380.89 keV. Expectedly, the intensity of peaks in the spectrum simulated for shallow laboratory is higher than in the spectrum simulated for 1000 m w.e. depth. Generally, the laboratory located in the depth of 1000 m w.e. is more suitable for low-background physics experiments. However, the shallow laboratory is still suitable for environmental radioactivity studies. The background of an HPGe detector with antic cosmic shielding (e.g. made of plastic scintillators) placed in a shallow laboratory can be decreased by 2 orders of magnitude in comparison with a standard surface laboratory [1]. It is expected that the muon induced background spectra simulated in 50 m w.e. laboratory could be decreased by a factor of 3 using the antic cosmic shielding as it is indicated in [1].

As copper peaks are prevailing in the 50 m w.e. background spectrum, the use of copper in the detector shielding for HPGe detectors located in shallow laboratories should be reconsidered. Copper due to interactions with neutrons forms a strong source of the background covering a wide part of the energy range of the HPGe detector. Reduction of copper thickness can decrease the background from this component as the background increases with the shield dimensions [24]. Ideally, copper should be replaced by other material or, at least, combined with neutron absorbing materials [35]. Copper is a significant contributor also to the background spectrum simulated in the deep underground laboratory therefore it is not recommended to use copper as shielding material from the point of view of the background induced by cosmic rays. On the other hand, from the point of view of radioactive contamination, the copper is still the best material [23].

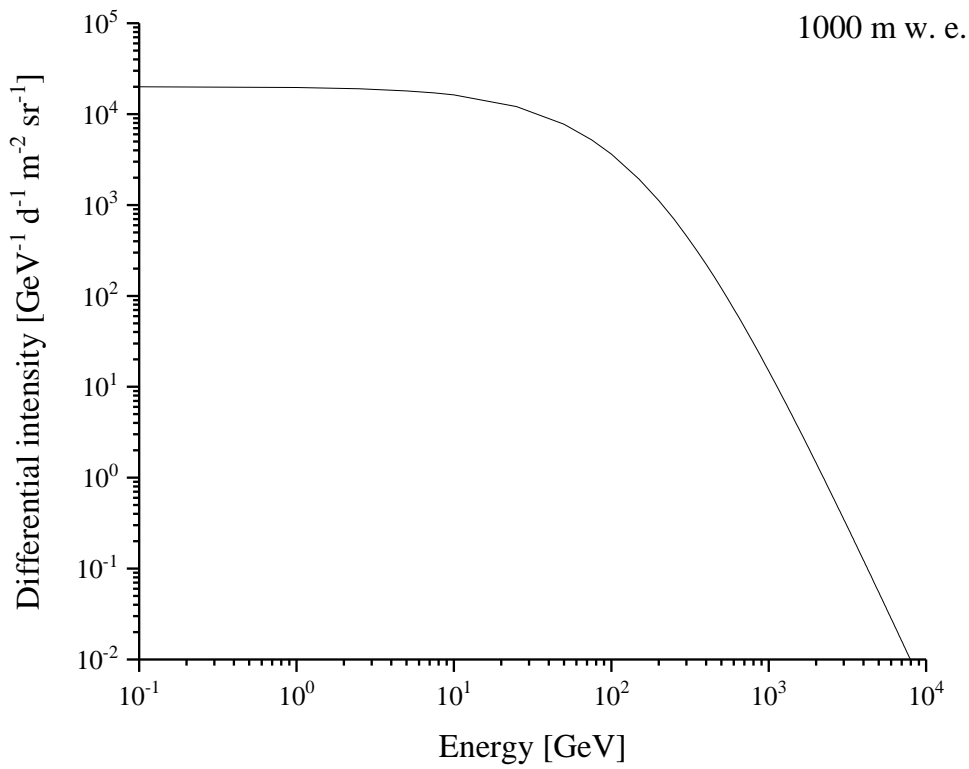
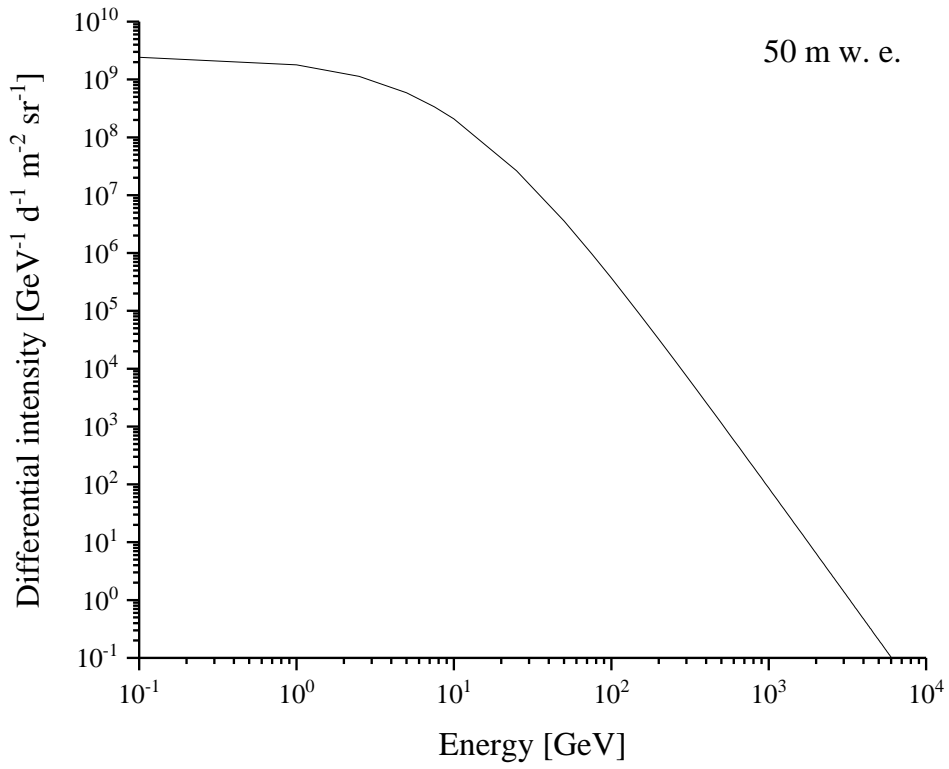


Fig. 3. Calculated muon vertical energy spectra in depths 50 m w.e. and 1000 m w.e.

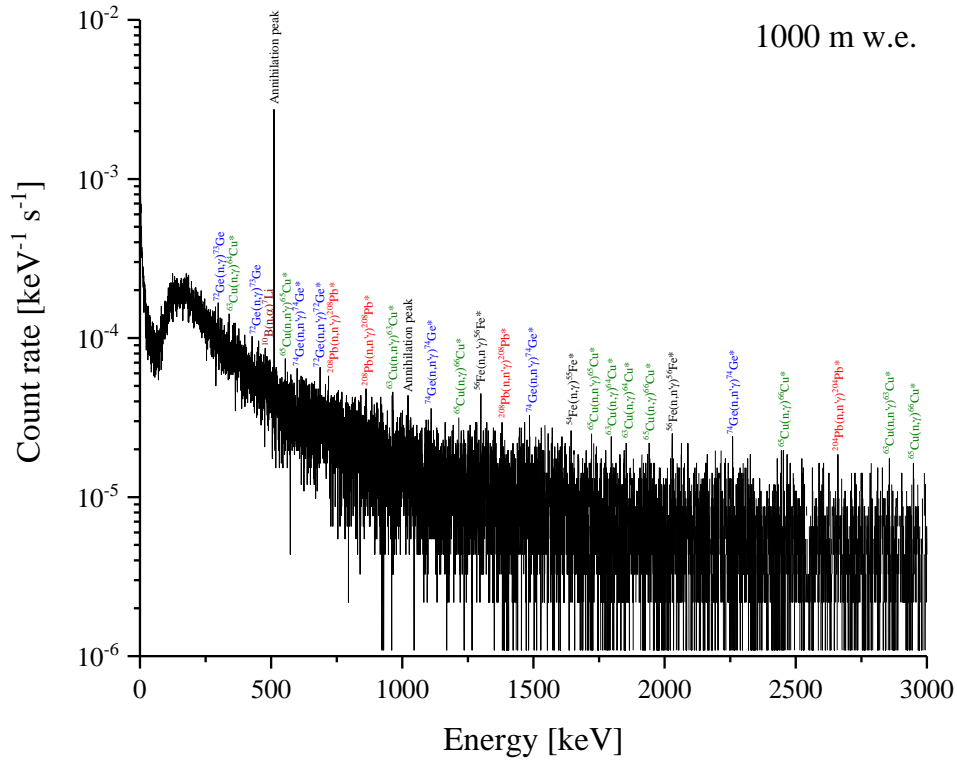
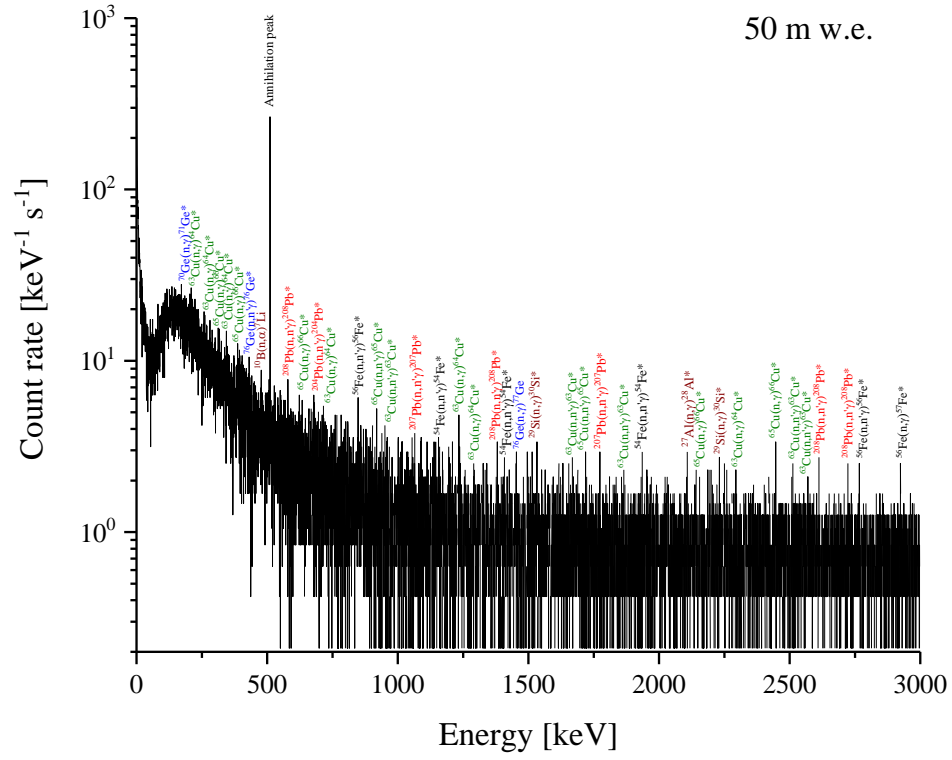


Fig. 4. Simulated HPGe detector background spectra for the energy range from 0-3 MeV in depths 50 m w.e. and 1000 m w.e.

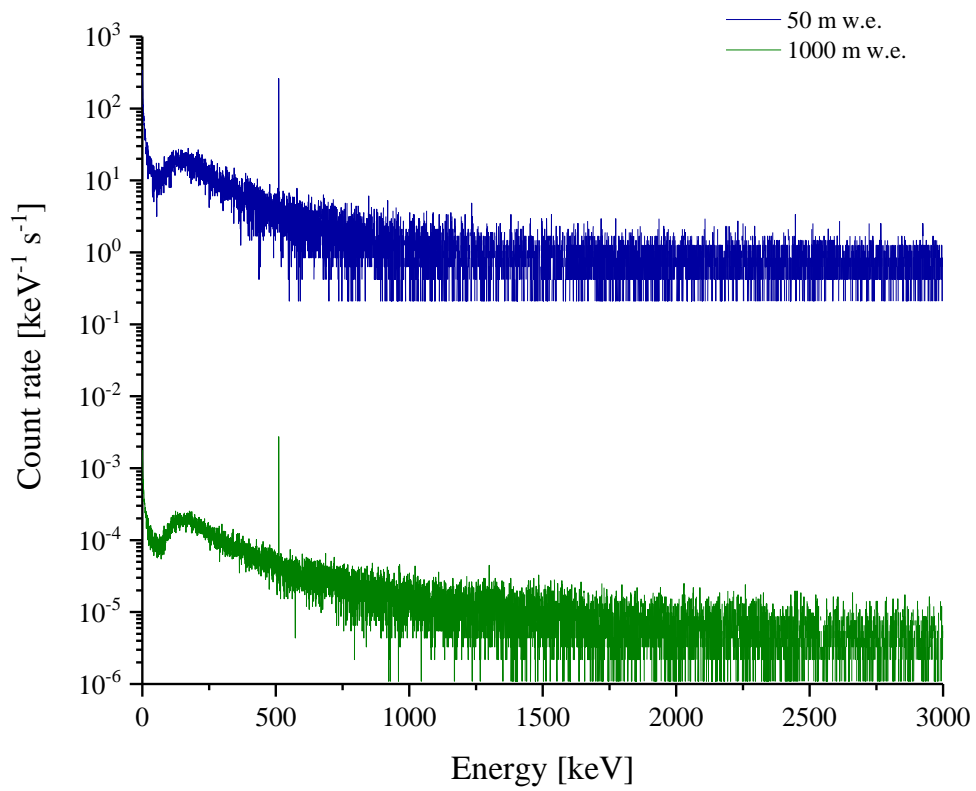


Fig. 5. Comparison of simulated HPGe detector background spectra for depths 50 m w.e. and 1000 m w.e.

Table 1

Calculated count rates in the simulated background γ -ray spectra.

50 m w.e.			1000 m w.e.		
Energy peaks [keV]	Nuclides and Reactions	Count rates [s ⁻¹]	Energy peaks [keV]	Nuclides and Reactions	Count rates $\times 10^{-5}$ [s ⁻¹]
10-3000	Continuum	8504 \pm 732	10-3000	Continuum	8498 \pm 684
174.96	⁷⁰ Ge(n, γ) ⁷¹ Ge*	11.8 \pm 3.0	297.30	⁷² Ge(n, γ) ⁷³ Ge	2.0 \pm 1.0
212.39	⁶³ Cu(n, γ) ⁶⁴ Cu*	7.5 \pm 1.8	343.94	⁶³ Cu(n, γ) ⁶⁴ Cu*	3.0 \pm 1.0
259.3	⁶³ Cu(n, γ) ⁶⁴ Cu*	5.8 \pm 1.7	430.30	⁷² Ge(n, γ) ⁷³ Ge	3.0 \pm 0.8
315.71	⁶⁵ Cu(n, γ) ⁶⁶ Cu*	5.7 \pm 1.4	477.61	¹⁰ B (n, α) ⁷ Li	1.0 \pm 0.4
343.94	⁶³ Cu(n, γ) ⁶⁴ Cu*	7.1 \pm 1.1	511.0	Annihilation	99.3 \pm 2.1
385.78	⁶⁵ Cu(n, γ) ⁶⁶ Cu*	3.1 \pm 1.2	550.0	⁶⁵ Cu(n, n' γ) ⁶⁵ Cu*	1.4 \pm 0.4
431.0	⁷⁶ Ge(n, n' γ) ⁷⁶ Ge*	3.3 \pm 1.0	595.85	⁷⁴ Ge(n, n' γ) ⁷⁴ Ge*	1.6 \pm 0.3
477.61	¹⁰ B (n, α) ⁷ Li	3.2 \pm 1.0	691.43	⁷² Ge(n, n' γ) ⁷² Ge*	4.6 \pm 1.0
511	Annihilation	96.7 \pm 2.8	722.25	²⁰⁸ Pb(n, n' γ) ²⁰⁸ Pb*	2.0 \pm 0.6
583.19	²⁰⁸ Pb(n, n' γ) ²⁰⁸ Pb*	2.0 \pm 0.9	860.56	²⁰⁸ Pb(n, n' γ) ²⁰⁸ Pb*	1.7 \pm 0.4
622.69	⁶⁵ Cu(n, γ) ⁶⁶ Cu*	1.7 \pm 0.5	962.06	⁶³ Cu(n, n' γ) ⁶³ Cu*	2.8 \pm 0.6
683.50	²⁰⁴ Pb(n, n' γ) ²⁰⁴ Pb*	2.4 \pm 0.6	1022	Annihilation	1.7 \pm 0.4
711.94	⁶³ Cu(n, γ) ⁶⁴ Cu*	2.0 \pm 0.5	1105.56	⁷⁴ Ge(n, n' γ) ⁷⁴ Ge*	1.7 \pm 0.4
846.76	⁵⁶ Fe(n, n' γ) ⁵⁶ Fe*	1.9 \pm 0.6	1212.52	⁶⁵ Cu(n, γ) ⁶⁶ Cu*	2.0 \pm 0.4
924.50	⁶⁵ Cu(n, n' γ) ⁶⁵ Cu*	1.7 \pm 0.6	1303.40	⁵⁶ Fe(n, n' γ) ⁵⁶ Fe*	1.3 \pm 0.3
955.0	⁶³ Cu(n, n' γ) ⁶³ Cu*	2.2 \pm 0.5	1380.89	²⁰⁸ Pb(n, n' γ) ²⁰⁸ Pb*	1.2 \pm 0.3
1063.66	²⁰⁷ Pb(n, n' γ) ²⁰⁷ Pb*	2.3 \pm 0.5	1489.35	⁷⁴ Ge(n, n' γ) ⁷⁴ Ge*	1.4 \pm 0.3
1153.10	⁵⁴ Fe(n, n' γ) ⁵⁴ Fe*	2.0 \pm 0.5	1640.40	⁵⁴ Fe(n, γ) ⁵⁵ Fe*	1.5 \pm 0.3
1232.13	⁶³ Cu(n, γ) ⁶⁴ Cu*	2.2 \pm 0.4	1724.92	⁶⁵ Cu(n, n' γ) ⁶⁵ Cu*	1.8 \pm 0.3
1293.92	⁶³ Cu(n, γ) ⁶⁴ Cu*	1.7 \pm 0.4	1799.48	⁶³ Cu(n, γ) ⁶⁴ Cu*	1.4 \pm 0.3
1380.89	²⁰⁸ Pb(n, n' γ) ²⁰⁸ Pb*	1.9 \pm 0.5	1852.40	⁶³ Cu(n, γ) ⁶⁴ Cu*	0.5 \pm 0.3
1408.10	⁵⁴ Fe(n, n' γ) ⁵⁴ Fe*	1.9 \pm 0.5	1944.97	⁶⁵ Cu(n, γ) ⁶⁶ Cu*	1.3 \pm 0.3
1457.84	⁷⁶ Ge(n, γ) ⁷⁷ Ge	1.4 \pm 0.4	2034.79	⁵⁶ Fe(n, n' γ) ⁵⁶ Fe*	1.6 \pm 0.3
1534.12	²⁹ Si(n, γ) ³⁰ Si*	1.5 \pm 0.5	2260.0	⁷⁴ Ge(n, n' γ) ⁷⁴ Ge*	0.3 \pm 0.2
1668.90	⁶³ Cu(n, n' γ) ⁶³ Cu*	1.0 \pm 0.4	2448.70	⁶⁵ Cu(n, γ) ⁶⁶ Cu*	0.8 \pm 0.2
1724.92	⁶⁵ Cu(n, n' γ) ⁶⁵ Cu*	1.4 \pm 0.4	2457.66	⁶⁵ Cu(n, γ) ⁶⁶ Cu*	0.9 \pm 0.3
1770.23	²⁰⁷ Pb(n, n' γ) ²⁰⁷ Pb*	1.3 \pm 0.4	2666.20	²⁰⁴ Pb(n, n' γ) ²⁰⁴ Pb*	0.5 \pm 0.3
1861.30	⁶³ Cu(n, n' γ) ⁶³ Cu*	1.1 \pm 0.4	2857.60	⁶³ Cu(n, n' γ) ⁶³ Cu*	0.7 \pm 0.2
1936.50	⁵⁴ Fe(n, n' γ) ⁵⁴ Fe*	1.2 \pm 0.3	2952.64	⁶⁵ Cu(n, γ) ⁶⁶ Cu*	0.7 \pm 0.2
2108.24	²⁷ Al(n, γ) ²⁸ Al*	1.3 \pm 0.3			
2144.22	⁶⁵ Cu(n, γ) ⁶⁶ Cu*	1.0 \pm 0.4			
2235.23	²⁹ Si(n, γ) ³⁰ Si*	1.3 \pm 0.4			
2291.42	⁶³ Cu(n, γ) ⁶⁴ Cu*	1.2 \pm 0.3			
2448.70	⁶⁵ Cu(n, γ) ⁶⁶ Cu*	1.2 \pm 0.4			
2512.0	⁶³ Cu(n, n' γ) ⁶³ Cu*	1.4 \pm 0.4			
2562.0	⁶³ Cu(n, n' γ) ⁶³ Cu*	1.7 \pm 0.4			
2614.51	²⁰⁸ Pb(n, n' γ) ²⁰⁸ Pb*	1.1 \pm 0.4			
2720.57	²⁰⁸ Pb(n, n' γ) ²⁰⁸ Pb*	1.2 \pm 0.3			
2763.0	⁵⁶ Fe(n, n' γ) ⁵⁶ Fe*	1.4 \pm 0.4			
2922.50	⁵⁶ Fe(n, γ) ⁵⁷ Fe*	1.8 \pm 0.4			

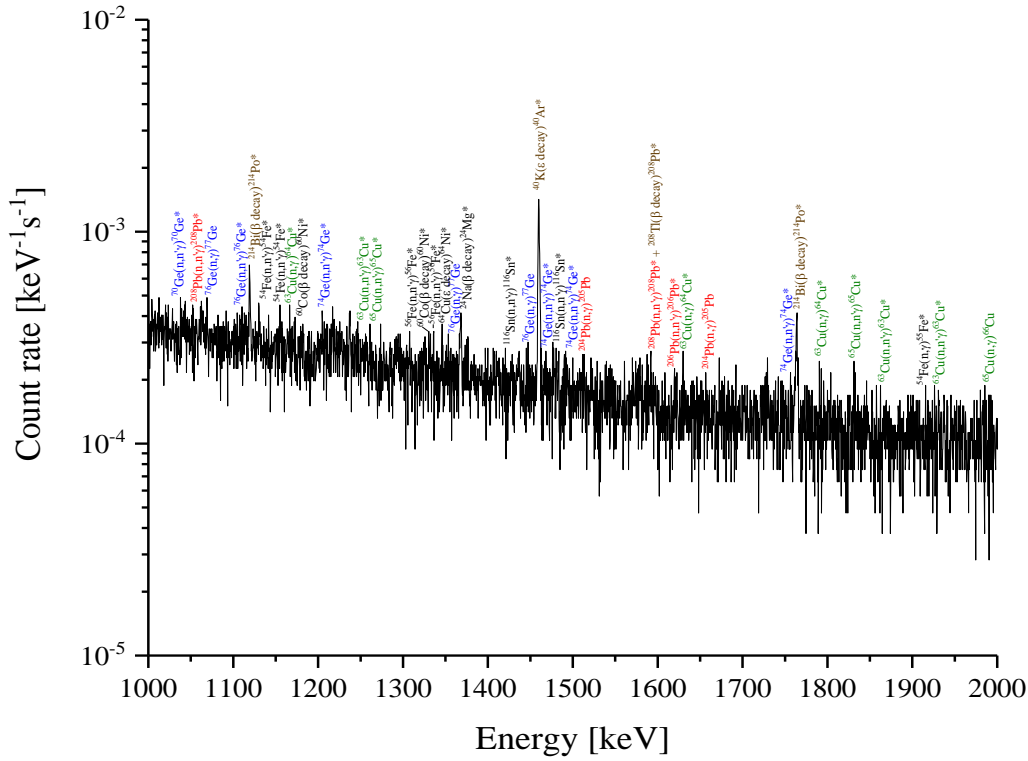


Fig. 7. Experimental HPGe detector background spectrum for energy range from 1-2 MeV.
(Ge peaks-blue, Cu peaks-green, Pb peaks-red, natural radionuclides-brown)

As information about radionuclide contamination of various parts of the setup was not available, no rigorous simulation of the background spectrum due to the contamination was possible. Moreover, a large part of the measured count rates except for ^{40}K may be caused by presence of radon (^{222}Rn) and thoron (^{220}Rn) in air which may diffuse inside the shield and decay close to the detector [24]. The activities of radon and thoron in the shield may vary with time if the laboratory does not have a ventilation system removing these inert gases and their progeny from the ambient air. Reliable quantification of radon and thoron concentrations inside the shield is difficult because of variable radon and thoron emanation and their diffusion to the shield cavity.

To estimate the contribution of radioactive contamination to the detector continuum, several simulations with ^{238}U , ^{232}Th , and ^{40}K in the setup materials, and ^{222}Rn in air inside the shield cavity were run. The resulting simulation spectra were normalized so that the simulated and the experimental count rates of the contamination peaks agreed while assuming that 35% of the ^{208}Tl peak at 2614.5 keV was induced by neutrons. It was found in the case of the surface laboratory that the simulated integral count rate of $0.033 \pm 0.006 \text{ s}^{-1}$ (50–2875 keV) due to radioactive contamination of the simulated spectrum made only 2.6% of the total experimental integral count rate of $1.26 \pm 0.07 \text{ s}^{-1}$. This number agrees well with the fraction of integral count rate of 2.4% obtained by subtracting the simulated spectrum from the experimental one. Indeed, continua observed in the experimental spectra of low-level HPGe spectrometers operating in surface or shallow laboratories are mostly induced by cosmic rays.

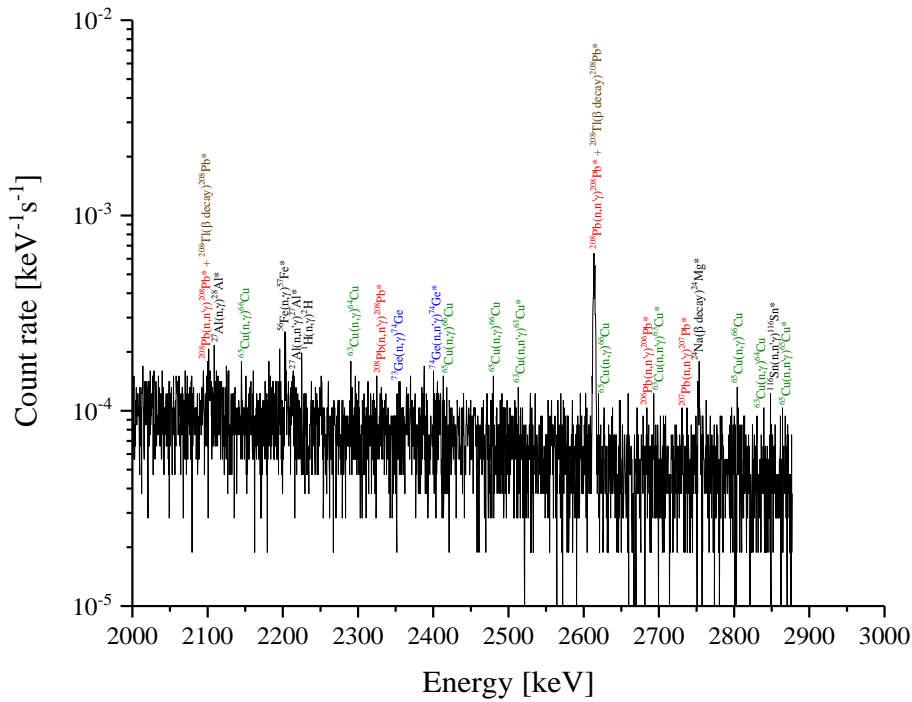


Fig. 8. Experimental HPGe detector background spectrum for energy range from 2-3 MeV.
(Ge peaks-blue, Cu peaks-green, Pb peaks-red, natural radionuclides-brown)

Natural radionuclides are present also in the background spectrum measured in underground laboratory in Modane with Obelix detector (Fig. 9.). Peaks caused by the natural radionuclides in the system were detected and traced to the primordial ^{40}K and a few members of the ^{238}U and ^{232}Th decay series (^{212}Bi , ^{214}Bi , ^{212}Pb , ^{214}Pb , ^{228}Ac , ^{208}Tl). They are present in the detector construction materials, the shield and its surroundings, especially in the walls. The list of radionuclides and their concentrations is given in Chapter 3.3 and [37]. The Monte Carlo simulation of the experimental background energy spectrum was conducted assuming these concentrations. It was found that the natural radionuclides in the detector parts and the laboratory walls form almost 94% of the continuum. Therefore, the major contributors to the Obelix detector background are the radionuclides present in the detector construction parts and laboratory walls. The most abundant are the daughter products of the ^{238}U , ^{232}Th decay series and ^{40}K as it is usually the case. It is impossible to remove the natural radioactivity in the laboratory walls consisting mainly of Fréjus rock present everywhere in LSM but effort should be made to optimize the detector shield. The concentration of radionuclides in the detector construction materials should be minimised by using even more radiopure materials. Significant reduction of long-lived radionuclides in these materials is a key issue. It is recommended to process the materials and assemble the detector parts in a place with a very low level of these radionuclides, as these radionuclides come to the detector parts from primary materials and the assembly rooms shall be very clean. Special attention should be paid to electronics, as the FET was one of the most radioactive parts. In underground laboratories is the reduction of γ -rays coming from decay of natural radionuclides one of key issues.

needed in this study. The detection limit $A^\#$ [Bq] according to the standard ISO 11929-3:2010 can be approximated by the following formula

$$A^\# = \frac{k^2 + 2k\sqrt{2B}}{\varepsilon Y t}$$

if the variance of the counting efficiency ε is negligible, which is usually the case when a radionuclide-specific standard is used for the efficiency calibration.

In this formula:

k = 1.645 for the confidence level of 0.95

Y = gamma-ray yield; in the case of ^{137}Cs , $Y = 0.851$

t = measuring time [s]

B = number of counts in the region of interest around the 662 keV peak of ^{137}Cs defined as

$$B = \sum_{i=1}^N n_i$$

where n_i is the number of counts in the channel i from the region of interest comprising N channels. The region of interest for calculating B typically includes $N = 2 + 4 \times \text{FWHM} + 2$ channels, where the FWHM is expressed in the number of channels. If the FWHM expressed in energy is 2.0 keV for 1.33 MeV of ^{60}Co , the FWHM expressed in energy for 0.662 MeV will be roughly 1.4 keV. The FWHM expressed in the number of channels is obtained by using the inverse energy calibration equation.

A typical measuring efficiency of 0.01 (1%) and a reasonable measuring time 7 days were assumed. Under these assumptions, the detection limits would be 7.3 mBq and 0.54 mBq in the 50 m w.e. and 1000 m w.e. laboratory, respectively. Increasing the laboratory depth from 50 m w.e. to 1000 m w.e. would result in a detection limit decrease by a factor of 13 at most. The presence of the background due to the material contamination will increase the detection limits and reduce the gain resulting from placing the laboratory to the depth of 1000 m w.e.

For illustration, count rates of peaks coming from natural radionuclides were listed in Table 2. Count rates for background spectrum of detector with relative efficiency of 100% located in depth of 1000 m w.e. were estimated based on information obtained during previous investigations, especially for the Obelix detector background. The same concentrations of radionuclides were assumed as in the Obelix detector and count rates were normalized to a 100% relative efficiency detector and to depth of 1000 m w.e. Integral count rates of individual continua formed by decay of natural radionuclides were calculated as well. The effect of natural radioactivity is negligible in background spectrum measured in surface laboratory as only 2.6% of continuum is formed by decay of natural radionuclides. However, in underground laboratories it gains significance. In deep underground laboratory in Modane it forms 94% of continuum and in planned Slovak laboratory in depth of 1000 m w.e. it is estimated to be 40%.

At this stage, only limited information on the planned underground laboratory was available, therefore it was not possible to provide more detailed design principles for the laboratory and shield design.

Table 2

Measured and estimated count rates of peaks coming from natural radionuclides.

Energy peaks [keV]	Natural Radionuclides and Reactions	Count rates [d ⁻¹]			
		HPGe detector in surface laboratory	Obelix in 4800 m w.e	100% HPGe detector in 50 m w.e (estimated) ×10 ⁵	100% HPGe detector in 1000 m w.e (estimated)
40-3000	Continuum formed by natural radionuclides	2850 ± 520	324 ± 17	1194 ± 92	5180 ± 410
72.81	X-rays of ²⁰⁸ Pb	9 ± 5	0.3 ± 0.1	3 ± 1	14 ± 4
74.97	X-rays of ²⁰⁸ Pb + X-rays of ²¹² Pb and ²¹⁴ Pb	23 ± 11	3.0 ± 0.6	9 ± 2	64 ± 8
84.21	X-rays of ²⁰⁸ Pb + γ-rays of ²²⁸ Th	-	2.8 ± 0.6	-	28 ± 4
238.63	²¹² Pb(β decay) ²¹² Bi*	-	1.6 ± 0.3	33 ± 6	55 ± 6
295.22	²¹⁴ Pb(β decay) ²¹⁴ Bi*	87 ± 17	-	14 ± 3	-
351.93	²¹⁴ Pb(β decay) ²¹⁴ Bi*	126 ± 16	0.6 ± 0.3	22 ± 6	11 ± 4
511.0	Annihilation	700 ± 40	2.5 ± 0.6	86 ± 9	90 ± 9
583.19	²⁰⁸ Pb(n, n'γ) ²⁰⁸ Pb* + ²⁰⁸ Tl(β decay) ²⁰⁸ Pb*	10 ± 7	0.3 ± 0.1	8 ± 2	9 ± 3
609.32	²¹⁴ Bi(β decay) ²¹⁴ Po*	180 ± 20	0.5 ± 0.2	16 ± 4	13 ± 4
911.40	²²⁸ Ac(β decay) ²²⁸ Th	-	0.8 ± 0.2	6 ± 2	13 ± 4
968.97	²²⁸ Ac(β decay) ²²⁸ Th	-	0.5 ± 0.1	-	7 ± 2
1120.29	²¹⁴ Bi(β decay) ²¹⁴ Po*	15 ± 6	0.3 ± 0.1	4 ± 1	43 ± 6
1460.80	⁴⁰ K(β decay) ⁴⁰ Ar*	99 ± 14	1.1 ± 0.3	11 ± 2	15 ± 4
1509.21	²¹⁴ Bi(β decay) ²¹⁴ Po*	-	0.2 ± 0.1	-	2 ± 1
1588.20	²²⁸ Ac(β decay) ²²⁸ Th	-	0.2 ± 0.1	-	2 ± 1
1677.10	²¹⁴ Bi(β decay) ²¹⁴ Po* + ²²⁸ Ac(β decay) ²²⁸ Th + ²¹² Bi(β decay) ²¹² Po*	-	0.3 ± 0.1	-	2 ± 1
1764.49	²¹⁴ Bi(β decay) ²¹⁴ Po*	22 ± 8	0.3 ± 0.1	3 ± 1	5 ± 1
2614.51	²⁰⁸ Pb(n, n'γ) ²⁰⁸ Pb* + ²⁰⁸ Tl(β decay) ²⁰⁸ Pb*	41 ± 12	0.3 ± 0.1	4 ± 1	9 ± 2

Conclusions

The main results obtained in this work may be summarised as follows:

- i. Within the study *Investigation of neutron interactions with Ge detectors*, investigations of interactions of neutrons (produced in the ^{241}Am -Be source) with Ge detector placed in low-level shielding were carried out experimentally and compared with Monte Carlo simulation using GEANT4 tool. Precise geometry of the setup was coded into the program, including individual material impurities. Reactions of elastic and inelastic scattering of fast neutrons were observed, as well as their capture by Ge and other nuclei present in the set up. Typical triangular shape -peaks of ^{70}Ge , ^{72}Ge , ^{73}Ge , ^{74}Ge and ^{76}Ge induced by inelastic scattering of neutrons were detected. A large number of other peaks induced by neutron interactions with all materials in the setup (including impurities) were observed. Gamma-lines resulting from neutron interactions with lead and copper parts of the setup (e.g. the peak at 2614.51 keV originating from the reaction of $^{208}\text{Pb}(n, n)^{208}\text{Pb}^*$), dominated in the spectra. The peak of ^{40}K (1466.11 keV) was detected only as an excited state resulting from neutron capture by ^{39}K . Impurities in materials are important targets for neutron interactions and their inclusion into simulation provide a better agreement with the experiment, also important for deep underground installations. Simulated background γ -spectra were in good agreement with the experimental ones, except for the lower-energy region below 250 keV.

This work provides a thorough analysis of peaks observed in γ -spectra measured by Ge spectrometers exposed to fast neutrons, and demonstrates GEANT4 as a useful tool for simulating neutron-induced background of Ge spectrometers.

- ii. The work *The neutron component of background of an HPGe detector operating in a surface laboratory* deals with experimental and theoretical (GEANT4) investigations of background induction mechanisms of a low-level 50% p-type HPGe gamma spectrometer placed in a descending-Z lead shield (Pb-Sn-Cu). The whole system is located on the surface, on the ground floor of a 3-storey building providing approximately 1 m of concrete bulk shielding. Particular attention is given to clarifying the role of secondary and tertiary cosmic-ray neutrons. A very good agreement, qualitative as well as quantitative, between the measured and simulated spectra was achieved, confirming that GEANT4 is a suitable detector simulation tool for this type of studies, even if very complex neutron interactions with matter are involved. Nevertheless, triangular peaks, which are characteristic of neutron interactions with Ge crystals, cannot be reproduced correctly at present. The shapes of these peaks reflect particularities of the detection mechanism such as the recoil dynamics and plasma effects in charge collection. The background continuum in an HPGe system of this class (low-level in a surface building with a moderate overhead shielding) is generated mostly by cosmic-ray muons and tertiary cosmic-ray neutrons. The latter are responsible for almost all γ -ray lines of cosmic-ray origin in the background spectrum. The main sources of neutron-induced γ -rays, except the Ge crystal, are lead, copper and tin present in the construction materials of the HPGe detector and in the shield. An extensive list of γ -lines potentially visible in a background spectrum was compiled and the main nuclear reactions generating them were identified. It was found, that the source of the well-known 2614.51 keV peak is not exclusively the β -decay of ^{208}Tl from the ^{232}Th decay series to an excited state of the stable daughter nuclide ^{208}Pb . The inelastic neutron scattering on ^{208}Pb nuclei abundantly present in the lead shield contributes by about 35% to this peak. Below about 500 keV, the shape of the background continuum predominantly generated by cosmic rays (mainly by muons and neutrons) in our case depends considerably on the thickness of the overhead concrete bulk shielding associated with the building in which the system is located. Generally, there has been reasonable agreement between the measured and simulated background γ -ray spectra. The integral counting rates in the energy range from 50 keV to 2875 keV were $1.26 \pm 0.07 \text{ s}^{-1}$ in the measured spectrum and $1.25 \pm 0.13 \text{ s}^{-1}$ in the simulated one, indicating a good agreement with the experiment.

Peaks caused by radioactive contamination of the system were detected and traced to the primordial ^{40}K and a few members of the ^{238}U and ^{232}Th decay series (^{214}Bi , ^{214}Pb , ^{208}Tl). Yet, in the case of the present system, the lack of knowledge about the contamination of the construction materials and interference of Radon and Thoron entering the shield cavity did not allow us to investigate this background source theoretically. To estimate the contribution of radioactive contamination to the detector continuum, a number of simulations with ^{238}U , ^{232}Th , and ^{40}K in the setup materials, and ^{222}Rn in air inside the shield cavity were run. It was found that only about 2.6% of the continuum is formed by decay of natural radionuclides.

Although Pb and Cu are very popular materials for construction of low-level HPGe detector systems thanks to their costs and achievable purity, they are not the ideal choice as far as the neutron background is concerned. Interaction cross-sections are large and too many γ -rays are produced in nuclear reactions of various types. Tin should be also avoided as a construction material.

- iii. The study *The effect of neutrons on the background of HPGe detectors operating deep underground* deals with investigation of a background spectrum of a 160% relative efficiency HPGe detector located in the deep underground laboratory (LSM) in Modane (4800 m w.e.). Special attention was paid to the neutron induced background and to the contribution of the radionuclides in the detector parts to the measured background. The experimental spectrum was reproduced by a GEANT4 simulation with a good agreement. Separate simulations of spectra induced by cosmic-ray muons and neutron were carried out, too. It was found that the contribution of muon events to the experimental spectrum is much less than 1%, and it was confirmed that the muon induced spectra are about three orders of magnitude lower than the experimental ones.

The contribution of radionuclides to the background measured underground is dominating. Almost 94% of the continuum of the experimental spectrum is formed by radiation coming from members of the ^{238}U , ^{232}Th decay series and ^{40}K . Hence, even more radiopure materials should be used to decrease the detector background significantly.

The detector background induced by neutrons coming mainly from (α , n) reactions and fission reactions due to Uranium and Thorium present in the Fréjus rock and in the wall concrete in LSM was investigated by Monte Carlo simulations. The total neutron invoked energy spectrum as well as individual contributions from thermal and fast neutrons were simulated. The comparison of integral count rates of the experimental spectrum and the simulated total neutron invoked energy spectrum showed that only about 6% of the measured background continuum is formed by interactions of neutrons. Fast neutrons contribute to the total spectrum induced by neutrons more than thermal neutrons, specifically about 65% of the total spectrum was induced by them. Furthermore, they contribute mainly to the lower continuum up to 250 keV, which is the region of interest for potential low mass WIMPs occurrence. Such events resulting from neutron interactions can imitate the searched signals. This gives this background source more importance. In addition, neutron interactions with the detector materials, especially with lead, copper and germanium, induce unwanted γ -rays contributing to the background spectrum. Peaks resulting from ^{208}Tl decay are superimposed with ^{208}Pb peaks coming from the inelastic neutron scattering. Similarly, the ^{57}Fe γ -rays at the energy of 692.41 keV coming from the electron-capture decay of ^{57}Co are combined with γ -rays of ^{72}Ge originating in neutron interactions with the germanium crystal. Nevertheless, the contribution of neutron induced γ -rays to the total count rates of these peaks is only about 2%. Neutron capture, elastic and inelastic scattering were simulated separately as well. It was found that inelastic scattering is the major contributor to the spectrum induced by neutrons. The effect of neutrons on the background of the HPGe detector operating underground, such as the Obelix, is manifested mainly by their contribution to the continuum up to 1 MeV, especially in the lower part up to 500 keV. Simulations of neutron interactions in the lead shield showed, that particles generated in the shield contribute only about 1% to the total count rate of the resulting spectrum.

In general, we can conclude that the background continuum of the Obelix detector obtained underground is generated mostly by concentration of radionuclides and only a small part of it is formed by neutron interactions. Contribution of muons is minimal and thus, negligible.

Lead and copper are very common materials used in the construction of low-level HPGe spectrometers, mainly due to their relatively low cost and high achievable radiopurity; however, they are not the best choice for underground experiments where neutron induced backgrounds play an important role. Their neutron cross-sections are large and many γ -rays are generated in neutron capture and inelastic scattering, which affects the measured spectrum. The most efficient way of avoiding the creation of neutron induced γ -rays from lead and copper, is to replace them by other types of materials or at least combine them with effective neutron suppressing materials. Another way of neutron background suppression is the use of neutron absorbing layers covering the walls and floor of the detector room. Further study of this subject is necessary.

- iv. The work *Simulation of muon induced background in an underground laboratory in Slovakia* is focused on calculations of muon energy spectra and investigation of muon induced backgrounds in two proposed underground laboratories, one in a depth of 50 m w.e. and the second one in a depth of 1000 m w.e. GEANT4 toolkit was used for the Monte Carlo simulations of the HPGe detector background induced by muons. The simulated background spectra were analysed and evaluated. It was found that the spectrum simulated for the underground laboratory in the depth of 1000 m w.e. is about five orders of magnitude lower than the one simulated for the shallow laboratory (50 m w.e.). The interactions of neutrons with the detector and the shield are more frequent at the depth of 50 m w.e. than in the depth 1000 m w.e., as it was expected. The number of peaks coming from neutron interactions visible in the background spectrum simulated for the shallow laboratory at the depth of 50 m w.e. is higher. The count rates of identified peaks were calculated. Expectedly, the intensity of peaks in the spectrum simulated for shallow laboratory is higher than in the spectrum simulated for 1000 m w.e. depth. In the background spectrum simulated at the 50 m w.e. shallow laboratory, the copper peaks are prevailing. In the background spectrum simulated in the 1000 m w.e. deep laboratory, the germanium peaks are prevailing up to 1500 keV, and the copper peaks dominate above 1500 keV. It was confirmed that the laboratory located at the depth of 1000 m w.e. is more suitable for low-background physics experiments but the laboratory at the depth of 50 m w.e. would be still suitable for environmental studies. Copper is a significant contributor to the detector background induced by cosmic rays in underground laboratories therefore it is not recommended using it as shielding material. The selection of ultra-high purity materials for the experimental setup is a key issue for underground experiments. The effect of natural radioactivity in planned Slovak laboratory was estimated. The contribution of natural radionuclides to the total background continuum would be about 40% at the depth of 1000 m w.e. and 10% at 50 m w.e. using HPGe detector with relative efficiency of 100%. The detection limits for ^{137}Cs in a hypothetical sample was determined in both depths. It would be 7.3 mBq and 0.54 mBq in the 50 m w.e. and 1000 m w.e. laboratory, respectively. The detection limit would decrease by one order of magnitude at most if the laboratory would be built in the 1000 m w.e. depth compared to the depth of 50 m w.e. Due to the limited information about the planned underground laboratory and the used detector, it was not possible to provide more detailed design principles.

References

- [1] R. Breier, P. Povinec, Simulation of background characteristics of low-level gamma-ray spectrometers using Monte Carlo methods, *Appl. Radiat. Isot.* 68 (2010) 1231-1235.
- [2] R. Breier, M. Laubenstein, P.P. Povinec, Monte Carlo simulation of background characteristics of a Ge detector operating underground in the Gran Sasso National Laboratory, *Appl. Radiat. Isot.* 126 (2016) 188-190.
- [3] J. Ljungvall, J. Nyberg, A study of fast neutron interactions in high-purity germanium detectors, *Nucl. Instrum. Methods Phys. Res. A* 546 (2005) 553-573.
- [4] E. Gete, D. F. Measday, B. A. Moftah, M. A. Saliba, T. J. Stocki, Neutron-induced peaks in Ge detectors from evaporation neutrons, *Nucl. Instrum. Methods Phys. Res. A* 388 (1996) 212-219.
- [5] K. W. Jones and H. W. Kraner, Stopping of 1- to 1.8-keV ^{73}Ge Atoms in Germanium, *Physical Review C* 4 (1971) 125-129.
- [6] V. A. Kudryavtsev, L. Pandola and V. Tomasello, Neutron- and muon-induced background in underground physics experiments, *Europ. Phys. J. A* 36 (2008) 171-180.
- [7] M. Baginova, P. Vojtyla, P. P. Povinec, Investigation of neutron interactions with Ge detectors, *Nucl. Instrum. Methods Phys. Res. A* 897 (2018) 22-31.
- [8] N. Jovancevic, M. Krmar, D. Mrda, J. Slivka, I. Bikit, Neutron induced background gamma activity in low-level Ge-spectroscopy systems, *Nucl. Instrum. Methods Phys. Res. A* 612 (2010) 303–308.
- [9] J. H. Chao, Neutron-induced gamma-rays in germanium detectors, *Appl. Radiat. Isot.* 44 (1993) 605-611.
- [10] GEANT4 Collaboration, Introduction to Geant4, available at <http://geant.cern.ch/> (accessed on June 19th, 2019).
- [11] S. Agostinelli et al., Geant4 - a simulation toolkit, *Nucl. Instrum. Methods Phys. Res. A* 506 (2003) 250-303.
- [12] J. Allison et al., Geant4 developments and applications, *IEEE Trans. Nucl. Sci.* 53 (2006) 270-278.
- [13] J. Allison et al., Recent developments in Geant4, *Nucl. Instrum. Methods Phys. Res. A* 835 (2016) 186-225.
- [14] J. W. Marsh, D. J. Thomas, M. Burke, High resolution measurements of neutron energy spectra from Am-Be and Am-B neutron sources, *Nucl. Instrum. Methods Phys. Res. A* 366 (1995) 340-348.
- [15] L. A. Sonzogni, National Nuclear Data Center, Brookhaven National Laboratory, available at <https://www.nndc.bnl.gov/nudat2/> (accessed on October 3rd, 2019).
- [16] J. F. Ziegler, Terrestrial cosmic rays, *IBM J. Res. Dev.* 40 Issue 1 (1996) 19-39.
- [17] P. K. F. Greider, *Cosmic Rays at Earth, Researcher's Reference and Data Book Manual*, 1st ed., Elsevier, Amsterdam, 2001.
- [18] L. N. Bogdanova, M. G. Gavrillov, V. N. Kornoukhov, A. S. Starostin, Cosmic muon flux at shallow depth underground, *Phys. Atom. Nucl.* 69 (2006) 1328-1333.
- [19] G. Chardin and G. Gerbier, *Proceedings of the 4th Int. Workshop on Identification of Dark Matter*, World Scientific, Singapore, 2003.
- [20] H. M. Kluck, *Measurement of the Cosmic-Induced Neutron Yield at the Modane Underground Laboratory*, Springer, Berlin, 2015.
- [21] M. Aglietta et al., Muon “depth-intensity” relation measured by the LVD underground experiment and cosmic-ray muon spectrum at sea level, *Phys.Rev. D* 58 (1998) 092005.
- [22] D. Barker, W. Z. Wei, D. M. Mei, and C. Zhang, Ionization Efficiency Study for Low Energy Nuclear Recoils in Germanium, *Astropart. Phys.* 48 (2013) 8-15.

- [23] P. P. Povinec, M. Betti, A. J. T. Jull, New isotope technologies in environmental physics, *Acta Physica Slovaca* 58-1 (2008) 1–154.
- [24] P. Vojtyla, A computer simulation of the cosmic-muon background induction in a Ge γ -spectrometer using GEANT, *Nucl. Instrum. Methods Phys. Res. B* 100 (1995) 87-96.
- [25] P. Povinec, *Analysis of Environmental Radionuclides*, 1st ed., Elsevier, Oxford, 2007.
- [26] P. Vojtyla, Fast computer simulations of background of low-level Ge γ -spectrometers induced by $^{210}\text{Pb}/^{210}\text{Bi}$ in shielding lead, *Nucl. Instrum. Methods Phys. Res. B* 117 (1996) 189-198.
- [27] C. Berger et al., Experimental study of muon bundles observed in the Fréjus detector, *Phys. Rev. D* 40 (1989) 2163-2171.
- [28] B. Schmidt et al., Muon-induced background in the EDELWEISS dark matter search, *Astropart. Phys.* 44 (2013) 28-39.
- [29] V. B. Brudanin et al., The Low-Background HPGe Γ -Spectrometer OBELIX for the Investigation of the Double Beta Decay to Excited States, *J. Appl. Phys.* 9 (2017) 22-29.
- [30] D. Malczewski, J. Kisiel, J. Dorda, Gamma background measurements in the Laboratoire Souterrain de Modane, *J. Radioanal. Nucl. Chem.* (2012) 751–756
- [31] V. Chazal et al., Neutron background measurements in the underground laboratory of Modane, *Astropart. Phys.* 9 (1998) 163-172.
- [32] G. Chardin and G. Gerbier, *Proceedings of the 4th Int. Workshop on Identification of Dark Matter*, World Scientific, Singapore, 2003.
- [33] K. Eitel, Measurements of neutron fluxes in the LSM underground laboratory, *J. Phys. Conf. Ser.* 375 (2012) 012016.
- [34] S. Rozov et al., Monitoring of the thermal neutron flux in the LSM underground laboratory, *J. Phys. G: Nucl. Phys.* (2010) (Preprint arXiv:1001.4383)
- [35] M. Baginova, P. Vojtyla, P. P. Povinec, The neutron component of background of an HPGe detector operating in a surface laboratory, *Appl. Radiat. Isot.* 166 (2020) 109422.
- [36] R. Breier et al., Environmental radionuclides as contaminants of HPGe gamma-ray spectrometers: Monte Carlo simulations for Modane underground laboratory, *J. Env. Radioact.* 190-191 (2018) 134-140.
- [37] M. Baginova, P. Vojtyla, P. P. Povinec, The effect of neutrons on the background of HPGe detectors operating deep underground, *Astroparticle Physics* 143 (2022) 102756.
- [38] D.-M. Mei and A. Hime, Muon-Induced Background Study for Underground Laboratories, *Phys. Rev. D* 73 (2005) 053004.
- [39] S. Turkat et al., A new ultra low-level HPGe activity counting setup in the Felsenkeller shallow-underground laboratory, *Astroparticle Physics* 148 (2023) 102816.
- [40] L. Done and M-R. Ioan, Minimum Detectable Activity in gammaspectrometry and its use in low level activity measurements, *Appl. Radiat. Isot.* 114 (2016) 28–32.

Attachments

List of conferences

1. International Conference on Environmental Radioactivity ENVIRA2017 (28.5-2.6. 2017, Vilnius, Lithuania) – talk title: “Investigation of neutron-induced background in HPGe detectors – first phase”.
2. 50th Fermilab Symposium (6.-8.6. 2017, Batavia, USA) – poster title: “Investigation of neutron-induced background in HPGe detectors – first phase”.
3. The Occupational Health & Safety and Environmental Protection Seminar (23.11. 2017, CERN Geneva, Switzerland) – talk title: “Neutrons as environmental source of HPGe detectors background operating underground”
4. Doctoral Student Assembly (19.4. 2018, CERN Geneva, Switzerland) – poster title: “Background induced by neutron interactions”.
5. 18th Radiochemical Conference RadChem 2018 (12.-19.5. 2018, Marianske Lazne, Czech republic) – talk title: “Neutrons and gamma-rays as environmental sources of HPGe detectors background operating underground”.
6. Radiation Protection Conference 2019 (14. 2. 2019, CERN Geneva, Switzerland) – talk title: “Neutrons and gamma-rays as environmental sources of HPGe detectors background operating underground”.

List of publications

1. M. Baginova, P. Vojtyla, P.P. Povinec, Investigation of neutron interactions with Ge detectors, Nucl. Instrum. Methods Phys. Res. A, 897 (2018), pp. 22-31
Citations recorded by Scopus: 9 (1 in 2018, 2 in 2019, 2 in 2020, 2 in 2021, 1 in 2022, 1 in 2023)
2. M. Baginova, P. Vojtyla, P.P. Povinec, The neutron component of background of an HPGe detector operating in a surface laboratory, Appl. Radiat. Isot., 166 (2020), Article 109422
Citations recorded by Scopus: 4 (2 in 2021, 2 in 2022)
3. M. Baginova, P. Vojtyla, P.P. Povinec, The effect of neutrons on the background of HPGe detectors operating deep underground, Astroparticle Physics 143 (2022), Article 102756

Author's Publications

Investigation of neutron interactions with Ge detectors

Nuclear Inst. and Methods in Physics Research, A 897 (2018) 22–31



Contents lists available at ScienceDirect

Nuclear Inst. and Methods in Physics Research, A

journal homepage: www.elsevier.com/locate/nima



Investigation of neutron interactions with Ge detectors

Miloslava Baginova^{a,b,*}, Pavol Vojtyla^a, Pavel P. Povinec^b

^a CERN, Geneva 1211, Switzerland

^b Faculty of Mathematics, Physics and Informatics, Comenius University, Mlynská dolina F1, 842 48 Bratislava, Slovakia

ARTICLE INFO

Keywords:

Monte Carlo simulation
Detector background
GEANT4
Neutron interactions
High-purity Ge detectors

ABSTRACT

Interactions of neutrons with a high-purity germanium detector were studied experimentally and by simulations using the GEANT4 tool. Elastic and inelastic scattering of fast neutrons as well as neutron capture on Ge nuclei were observed. Peaks induced by inelastic scattering of neutrons on ^{70}Ge , ^{72}Ge , ^{73}Ge , ^{74}Ge and ^{76}Ge were well visible in the γ -ray spectra. In addition, peaks due to inelastic scattering of neutrons on copper and lead nuclei, including the well-known peak of ^{208}Pb at 2614.51 keV, were detected. The GEANT4 simulations showed that the simulated spectrum was in a good agreement with the experimental one. Differences between the simulated and the measured spectra were due to the high γ -ray intensity of the used neutron source, physics implemented in GEANT4 and contamination of the neutron source.

1. Introduction

Background of high-purity germanium (HPGe) detectors induced by neutrons is a poorly understood component in low-level γ -spectrometry systems. In surface laboratories with passive shielding, as well as in underground laboratories, neutrons can be produced by interactions of high energy cosmic rays and by natural radionuclides in spontaneous fission and in (α, n) reactions. Predicting all background components correctly is crucial for designing efficient shielding and applying appropriate event-rejection strategies.

The suppression and rejection of background is one of the key issues in experiments looking for rare nuclear events, such as neutrinoless $\beta\beta$ decay experiments, dark matter searches or experiments with low-energy neutrinos. Monte Carlo simulations of neutron background play a crucial role in evaluation of the total background and for the optimization of rejection strategies (e.g. [1,2]).

No study with a complex information about neutron background has been available till now, however, several studies were dealing with neutron interactions with germanium detectors. The knowledge of germanium peak shapes is important because they could cause systematic errors. Past measurements of neutron interactions with Ge detectors were carried out using ^{252}Cf neutron sources and environmental neutrons (e.g. [3,4]). A comparison of results showed that there is no substantial difference between Ge experimental peaks with a wide spectrum of neutron energies. The broader germanium peaks were observed for high energy neutrons [4].

The energy deposition process of the recoiling Ge nuclei has been studied, as well as elastic scattering of neutrons with Ge detectors [4,5]. Monte Carlo simulations of ^{252}Cf induced γ -ray spectra in Ge detectors were also carried out, and a good agreement of simulated spectra with experimental ones was found, especially for the region of elastic neutron scattering up to 50 keV. However, no detail analysis of experimental γ -ray spectra was carried out till now. As such investigations are crucial for determination of all Ge background components (especially in underground laboratories), we decided to carry out analysis of ^{241}Am -Be neutron induced γ -ray spectra both experimentally, as well as by Monte Carlo simulations.

2. Experimental setup

2.1. ^{241}Am -Be source

In order to investigate neutron-induced background, interactions of neutrons with a Ge detector were studied experimentally as the first step. Monte Carlo simulations using the GEANT4 simulation tool developed at CERN [6–9] were carried out as the next.

The ^{241}Am -Be source with a nominal activity of 370 MBq was used as a neutron source in the experiment. The source was produced in 2009 and its working life is 15 years. It contained compacted mixture of powders of ^{241}Am oxide and ^9Be . The neutron intensity in 2016 was about 23 000 neutrons s^{-1} . The standard neutron spectrum has the average and the maximal neutron energies of 4.2 and 11 MeV, respectively [10,11]. Neutrons are produced in $^9\text{Be}(\alpha, n)^{12}\text{C}$ reactions,

* Corresponding author at: CERN, Geneva 1211, Switzerland.
E-mail address: miloslava.baginova@cern.ch (M. Baginova).

<https://doi.org/10.1016/j.nima.2018.04.036>

Received 11 December 2017; Received in revised form 13 April 2018; Accepted 18 April 2018

Available online 25 April 2018

0168-9002/© 2018 Elsevier B.V. All rights reserved.

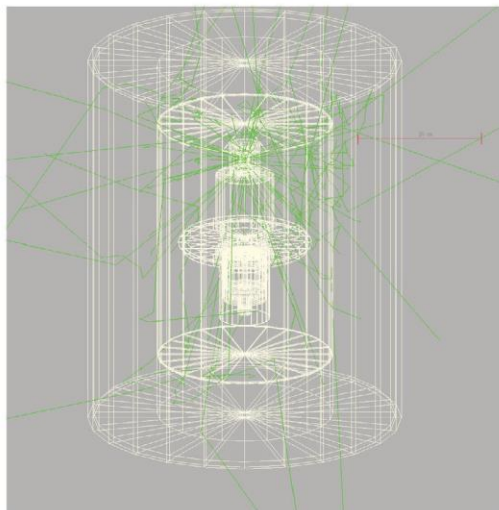


Fig. 1. Experimental setup with several simulated neutron and γ -ray interactions.

which are accompanied by emission of 4.44 MeV γ -rays from excited ^{12}C daughter nuclei. The shape of the neutron source is a cylinder with a diameter of 14 mm and a length of 12 mm. The active part was encapsulated in a case made of stainless steel and an aluminium shell.

2.2. Ge detector

The experimental setup consisted of an ^{241}Am -Be source placed coaxially 161.2 mm above a Canberra coaxial p-type Ge detector with a relative efficiency of 50%. The germanium crystal with a diameter of 66 mm and a height of 59 mm was enclosed in a thermoplastic foil and in an aluminium cryostat with a copper crystal holder. The cavity inside the crystal was 10 mm in diameter and 45 mm in height. The energy resolution of the detector was 2.07 keV for 1332.40 keV γ -rays of ^{60}Co . The energy calibration of the detector was done with ^{60}Co source. The detector efficiency calculation was done using LabSOCS software from Canberra. Two circular iron absorbers were placed above the detector to absorb abundant but low-energy γ -rays of ^{241}Am with the aim to reduce the dead time of the detector. A plastic beaker was used to place the source at a certain distance from the detector to further reduce the dead time and to minimize the energy summation effect. In this way, a dead time correction of only about 12.6% could be reached. The source-detector setup was placed in a shield consisting of 9.5 mm of carbon steel, 102 mm of lead, 1 mm of tin foil and 1.5 mm of copper cladding (from outside to inside). The outer shield dimensions were 508 mm in diameter and 635 mm in height. The γ -energy spectrum ranged from 10 to 3000 keV. Typical measuring time was 25 h. The background γ -spectrum (without ^{241}Am -Be source) was measured as well, and it was subtracted from measured neutron induced γ -spectra. A low nominal activity of the neutron source and short measuring time did not produce any neutron damage of the detector. The arrangement, as implemented in the GEANT4 simulation code is illustrated in Fig. 1.

2.3. Energy deposition mechanism

The principal energy deposition mechanisms of neutrons with energies up to 11 MeV in the Ge detector are elastic and inelastic scattering. The elastic scattering of neutrons gives the largest contribution to the interaction probability for Ge detector energy up to 50 keV [3]. The dominant process for slow and thermal neutrons is the neutron capture,

Table 1
Composition of natural germanium.

Isotopes	^{70}Ge	^{72}Ge	^{73}Ge	^{74}Ge	^{76}Ge
Abundance (%)	20.52	27.45	7.76	36.52	7.75
Number of neutrons	38	40	41	42	44

for fast neutrons the dominant processes are elastic and inelastic scattering, as indicated by cross sections of these reactions discussed below.

Natural germanium used in the detector is composed of 5 naturally occurring isotopes (Table 1). The purity of Ge crystals is usually at least 99.999%.

Cross sections for interactions of neutrons with germanium isotopes are shown in Fig. 2. They have common features, but different quantitative parameters as follows. For ^{70}Ge , the neutron capture dominates up to about 1.3 meV where elastic scattering gains significance until the resonance region extending from about 1 to 14 keV. In the resonance region, the cross sections fluctuate sharply within the same amplitude for both neutron capture and elastic scattering, however, the baseline for the elastic scattering may be several orders of magnitude higher. Beyond the resonance region, the elastic scattering takes over again. The inelastic scattering channel opens at about 1 MeV and drops sharply beyond about 10 MeV, the binding energy of a nucleon in a target nucleus. In the energy region of 1–10 MeV, elastic and inelastic scattering concur. However, around 3.5–4.5 MeV, the inelastic scattering is more probable.

For ^{72}Ge , elastic scattering starts to predominate at 0.3 meV. The resonance region extends from 2 keV to 11 keV. There are two strong resonances for the neutron capture below 2 keV. The inelastic scattering cross section predominates from 2.8 to 4.5 MeV.

For ^{73}Ge , the neutron capture predominates up to about 200 meV. The resonance region ranges from about 0.1 keV to 9 keV. The inelastic scattering channel opens at 13 keV but its cross-section becomes comparable to that of elastic scattering only at about 1.8 MeV. Nevertheless, from 2 to 4.5 MeV clearly predominates.

For ^{74}Ge , elastic scattering starts to predominate at about 0.13 meV. The resonance region is very narrow, 2.5–6 keV. Beyond the resonance region, the courses of cross-sections are very similar to those for ^{70}Ge and ^{72}Ge . The inelastic scattering is the most probable process from 2.4 to 4.5 MeV.

Finally, for ^{76}Ge , elastic scattering starts to dominate at 0.01 meV. Several isolated resonances are present in the region from 0.5 keV to 35 keV and the rest is similar to other stable Ge isotopes except for ^{73}Ge . The inelastic scattering channel opens at 0.6 MeV and becomes dominant for 2.5–4.5 MeV.

At neutron energies from 3.5 to 4.5 MeV, the inelastic scattering is the most probable interaction of neutrons with all naturally occurring germanium isotopes. This process is of interest for the background induction by fast neutrons as will be shown later. Let us recall that the elastic scattering of neutrons on Ge nuclei can contribute to the γ -spectrum only below 50 keV [3].

2.4. Monte Carlo simulation

GEANT4 developed at CERN for simulation of particle interactions with matter [6–9] was used for Monte Carlo simulations of interactions of neutrons with a Ge detector. It is based on C++ programming language with object-oriented programming features applicable for particle transport simulations in high as well as low-energy physics. It covers all relevant physical processes, including processes with γ -rays and neutrons. Cross sections for corresponding processes were taken from corresponding data files. For γ -ray interactions G4EMLOW 6.5 and for neutron interactions G4NDL 4.5 data files were used, respectively. The experimental neutron spectrum of the ^{241}Am -Be source was taken from [13]. The spectrum was digitized (Fig. 3) and used as the input source for GEANT4 simulations, together with γ -rays emitted by ^{241}Am and those generated in nuclear reactions inside the source.

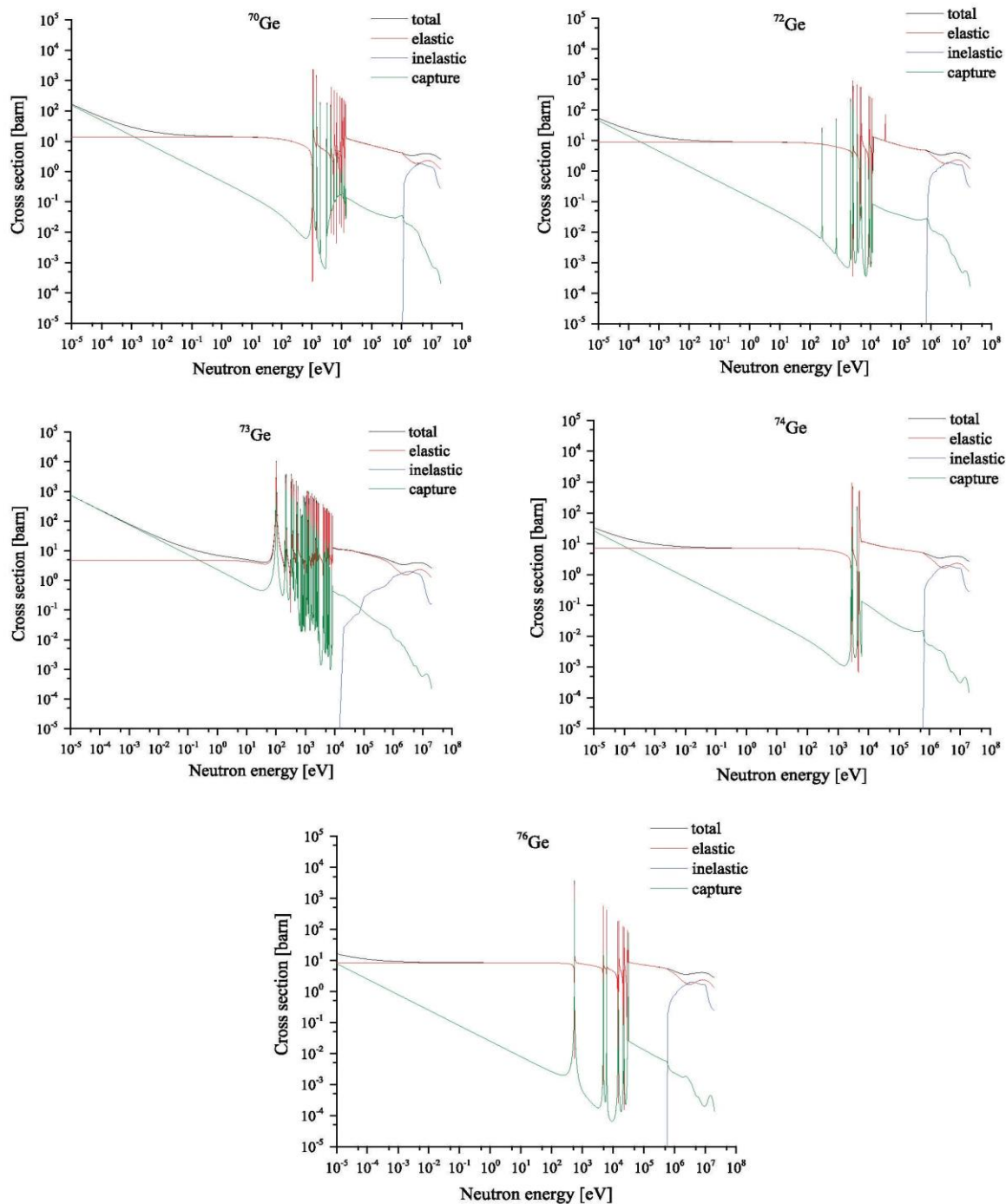


Fig. 2. Calculated cross sections for elastic and inelastic scattering and neutron capture in ^{70}Ge , ^{72}Ge , ^{73}Ge , ^{74}Ge , and ^{76}Ge . Source: Data taken from JENDL 4.0 database [12].

Gaussian energy distribution was used for γ -rays of ^{241}Am and γ -rays from $^9\text{Be}(\alpha, n)^{12}\text{C}$ reaction with mean energies of 59.54 keV and 4438.91 keV, with standard deviations of 0.24 keV and 1.55 keV, respectively. Values of mean energies were taken from NuDat 2.6 database [14], and values of standard deviations were taken from the

energy resolution of the Ge detector (Fig. 4), which was measured using radioactive standards and the resolution curve was calculated using the least square method. The resolution curve was then approximated up to 5 MeV. The aim was to simulate the instrumental spectrum of the detector used in the experiment.

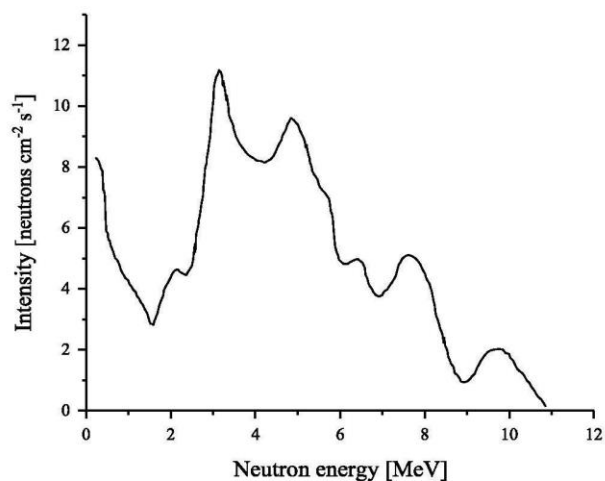


Fig. 3. Digitized neutron energy spectrum of the ^{241}Am -Be source measured in [13].

Real conditions were implemented into the Monte Carlo simulation. The simulated source matches the shape and dimensions of the real source and it emits particles isotropically.

The precise geometry setup was coded including individual material compositions. Special attention was paid to impurity in different materials. Investigation of impurities was carried out and every known material impurity was incorporated into simulation. The physics list SHIELDING, developed for neutron penetration studies and ion-ion collisions, was used in the simulations. It contains the best selection of electromagnetic and hadronic physical processes required to solve shielding problems including low background experiments. During simulation, every particle and process were tracked including particle's kinematics. The deposited energy was recorded each time a particle hit the detector.

3. Results and discussion

A detailed analysis of the experimental spectrum was carried out. To make the peaks more visible, the spectrum was split into three parts with energy ranges 0–1 MeV (Fig. 5), 1–2 MeV (Fig. 6) and 2–3 MeV (Fig. 7). Almost all peaks in the spectra were identified and explained. A typical feature of neutron interactions with a Ge detector are triangular γ -ray peaks. When a germanium detector is exposed to neutrons at energies of 1 MeV or more, triangular peaks may result from summation of the recoil energy of a Ge nucleus deposited within the detector itself and the energy of a photon emitted during de-excitation of the nucleus previously excited during inelastic scattering [4]. In the experiment, such peaks were observed at the energies of 68.80 keV, 562.93 keV, 595.84 keV, 689.60 keV, 834.01 keV, 1039.51 keV, 1108.41 keV, 1204.20 keV and 1463.75 keV.

The 68.80 keV peak corresponds to the reaction $^{73}\text{Ge}(n, n'\gamma)^{73}\text{Ge}^*$ (the symbol “*” indicates excited states for very short living radionuclides with half-lives less than 1 ms). The 562.93 keV and 1108.41 keV peaks originate from inelastic scattering of neutrons on ^{76}Ge while the 689.60 keV and 834.01 keV peaks are results of the reaction $^{72}\text{Ge}(n, n'\gamma)^{72}\text{Ge}^*$. The peaks at energies of 595.84 keV, 1204.20 keV and 1463.75 keV originate from inelastic scattering of neutrons on ^{74}Ge . And finally, the 1039.51 keV peak corresponds to the reaction $^{70}\text{Ge}(n, n'\gamma)^{70}\text{Ge}^*$.

In the case of the 691.43 keV peak (Fig. 5), the induction mechanism is slightly different. The excited nucleus of ^{72}Ge de-excites by an E0 transition, which is an internal conversion process for this nuclide: $^{72}\text{Ge}(n,$

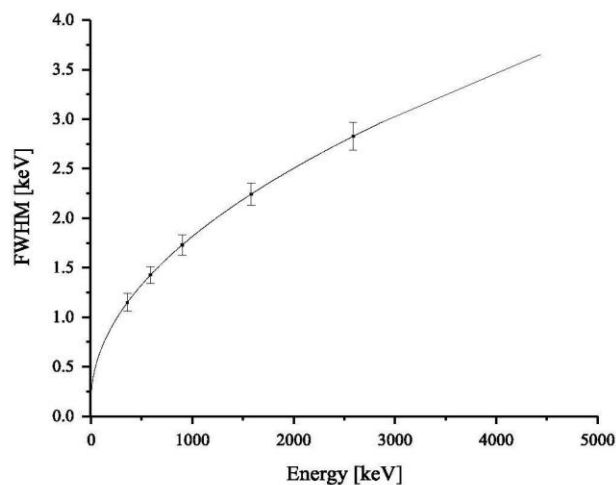


Fig. 4. Energy resolution of the Ge detector used in the experiment.

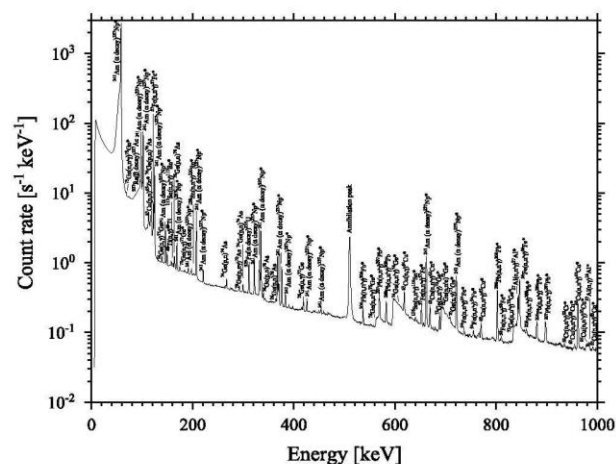


Fig. 5. Experimental γ -spectrum of neutron and γ -ray interactions with Ge detector for energy range of 0–1 MeV.

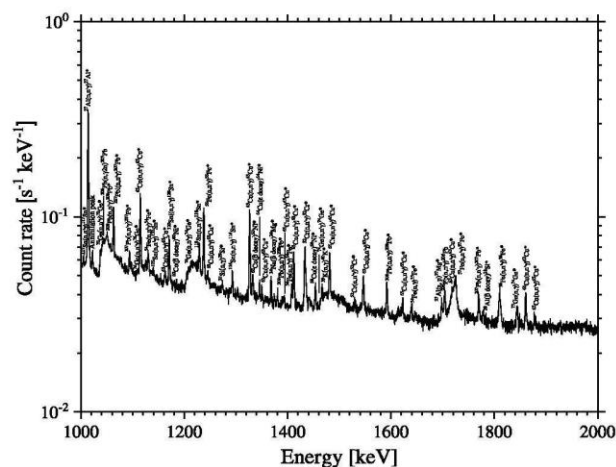


Fig. 6. Experimental γ -spectrum of neutron and γ -ray interactions with Ge detector for energy range of 1–2 MeV.

(abundance of 69.15%). ^{65}Zn (line 115.09 keV) was produced in (p, n) reaction on ^{65}Cu (abundance of 30.85%). ^{64}Ni (line 1345.84 keV) was produced in electron capture decay of ^{64}Cu .

^{74}As at energies of 267.43 keV and 299.97 keV, ^{76}As at energies of 139.68 keV, 165.05 keV, 339.33 keV and 363.91 keV were produced in (p, n) reactions on ^{74}Ge and ^{76}Ge nuclei. Peaks resulting from the neutron capture on Ge isotopes were detected, too. Namely, at 138.9 keV from $^{74}\text{Ge}(n, \gamma)^{75}\text{Ge}$, at 418.50 keV from $^{76}\text{Ge}(n, \gamma)^{77}\text{Ge}$, at 174.96 keV and 708.19 keV from $^{70}\text{Ge}(n, \gamma)^{71}\text{Ge}$, and at 1844.62 keV from $^{73}\text{Ge}(n, \gamma)^{74}\text{Ge}$. ^{70}As at energy of 293.66 keV originated from (p, $n\gamma$) reaction on ^{70}Ge . The well-known ^{60}Co peaks at 1173.23 keV and 1332.51 keV represents excited levels in stable ^{60}Ni (abundance of 26.223%) after inelastic scattering of neutrons. Another source could be the β -decay of ^{60}Co produced by activation of iron absorbers.

The peak with highest count rate in the spectrum at the energy of 58.54 keV is the γ -line of ^{237}Np that is a decay product of ^{241}Am . The other observed lines have energies of 98.97 keV, 102.98 keV, 125.3 keV, 146.55 keV, 169.56 keV, 191.96 keV, 208.10 keV, 221.80 keV, 322.52 keV, 332.35 keV, 335.37 keV, 368.62 keV, 370.94 keV, 376.65 keV, 383.81 keV, 426.47 keV, 454.66 keV, 662.40 keV and 722.01 keV.

The peak at the energy of 96.80 keV (^{227}Ac) is coming from β -decay of ^{227}Ra . The peak at the energy of 311.78 keV (^{235}U) originates from α -decay of ^{239}Pu . ^{227}Ra and ^{239}Pu are radioactive contaminants of the ^{241}Am -Be source. ^{227}Ra is produced by the source neutrons captured on ^{226}Ra that is present in the neutron source as an impurity.

The peaks at the energies of 511 keV and 1022 keV come from annihilation of electron-positron pairs generated by photon interactions with materials of the setup.

Presence of copper and lead influences the γ -spectrum strongly. Interactions of neutrons with these materials produce many γ -lines visible in the spectrum, which can hide or imitate searched signals. This is an unwanted effect, especially in experiments looking for rare nuclear processes. For example γ -rays resulting from neutron inelastic scattering or neutron capture reactions may imitate signatures of the neutrinoless $\beta\beta$ decay [18]. Possible replacement of copper and lead as shielding materials in underground experiments would require, however, further investigations.

Aluminium has only a few strong γ -lines in the spectrum, and it is certainly a significant background component. To avoid its contribution is, however, very difficult, because aluminium is the most commonly used material for cryostats and entrance windows. Nevertheless, the problem can be solved by elaboration of appropriate event-rejection strategy.

Similarly, γ -lines from tin parts of the setup are important potential sources of background. However, tin layers are usually not present in shields of Ge detectors located deeply underground. As it was shown previously, descending-Z shields consisting of lead, tin and copper are superior as far as the muon background is concerned [19]. Once it is suppressed, passively and/or actively, more materials remain for consideration.

To minimize the background induced by neutron interactions with impurities in the materials, it is necessary to use ultra-pure materials for experimental setups, and to know the identity and the amount of the residual elements.

In shallow as well as in deep underground laboratories fast neutrons are always present. They are produced by cosmic-ray interactions generating hadron showers as well as by capture of negative muons, predominantly on heavy nuclei like lead. Hence, inelastic scattering will always contribute to the background of Ge detectors in the energy region of interest manifesting itself by Ge peaks observed experimentally. If the spectrum statistics is sufficient to recognize such peaks, the contribution of neutrons to the total background can be unfolded. However, validated Monte Carlo simulations should be always carried out for estimation of the neutron background component.

4. Comparison of experimental and simulated γ -spectra

The experimental and simulated γ -spectra are shown in Fig. 8. The experimental spectrum was compared with the GEANT4 simulation of neutron and γ -ray interactions with the detector and the shield. The simulated spectrum reproduces the main features of the measured spectrum fairly well considering the complexity of the interactions. Integral count rates were compared for the experimental and the simulated spectra for the energy region from 250 keV to 2880 keV. This energy range was chosen due to a difference between experimental and simulated data for a lower continuum below 250 keV (explained below) and the end of the measured spectrum at 2880 keV. The integral count rate measured in the experiment ($210 \pm 2 \text{ s}^{-1}$) was in reasonable agreement with computed ($197 \pm 9 \text{ s}^{-1}$) result.

All peaks in the experimental γ -spectrum are clearly visible in the simulation, except peaks from the β decay of ^{227}Ra and α decay of ^{239}Pu resulting from contamination of the source, and γ -lines of ^{237}Np emitted after the α decay of ^{241}Am . The γ -emission of ^{241}Am is represented in the simulated spectrum only by the strongest γ -line at the energy of 59.54 keV and no other weaker γ -lines resulting from the ^{241}Am decay was generated in the simulation. The beginning of the simulated spectrum up to energy of 250 keV has a different shape than the beginning of the experimental spectrum, which may be due to a lower γ -ray intensity of the simulated ^{241}Am -Be source. The γ -ray intensity of neutron source is important information as well as intensity of neutrons. Intensity of γ -rays was calculated on the base of known neutron flux of ^{241}Am -Be source and γ -emission of ^{241}Am isotope, determined from the activity of the neutron source. The intensity of 4.44 MeV γ -rays was calculated as 75% of the neutron intensity [20]. Nevertheless, the real γ -ray intensity of the neutron source was evidently higher.

The triangular Ge peaks in the simulated γ -spectrum are lower and less sharp than in the measured spectrum, which is given by the physics implemented in GEANT4. The software is not yet capable to simulate appropriately Ge peaks at lower neutron energies, while for higher neutron energies, above 10 MeV, it simulates well. The average neutron energy in the simulation was 4.2 MeV.

^{27}Al peak (2982.0 keV) resulting from inelastic scattering of neutrons on aluminium nuclei is visible in the simulated spectra. This peak is not present in the experimental spectrum that extends only till 2880 keV. Also, a peak at the energy of 477.61 keV coming from $^{10}\text{B}(n, \alpha)^7\text{Li}$ reaction is not visible in the measured spectrum. This peak is hidden in the continuum of photons generated during the experiment, but not simulated. The ^{241}Am -Be source emits much more γ -rays than neutrons (5800:1 for 370 MBq source) and the region till 500 keV is significantly affected by γ -rays from ^{241}Am . Also, the amount of boron in the setup is too small, so the thermal neutron capture by boron and subsequent emission of α -particle and 477.61 keV γ -ray is not visible in the experimental spectrum.

New simulation was carried out with the aim to achieve better agreement between the experiment and the simulation, and to assess the impact of further γ -rays of ^{241}Am on the shape of simulated spectrum. Instead of Gaussian energy distribution of ^{241}Am γ -rays, ^{241}Am ion was coded as input parameter for particle gun including complete decay process. Both spectra are visible separately in Fig. 9. The comparison of the experiment with the simulation shows that inclusion of ^{241}Am ion into simulation increased the γ -ray intensity of the simulated ^{241}Am -Be source, and additional ^{237}Np peaks from ^{241}Am decay are visible in the simulated spectrum. Therefore the shape of the beginning of the simulated spectrum was lifted up. However, there is still a little difference in the region till 115 keV, especially between the measured and simulated photopeak of ^{241}Am . The measured photopeak is about one order of magnitude higher than the simulated one. This can be probably explained by non-exact inputs for the ^{241}Am source implemented in GEANT4. The integral count rate measured in the energy region from 115 keV to 2880 keV ($378 \pm 3 \text{ s}^{-1}$) was in reasonable agreement with

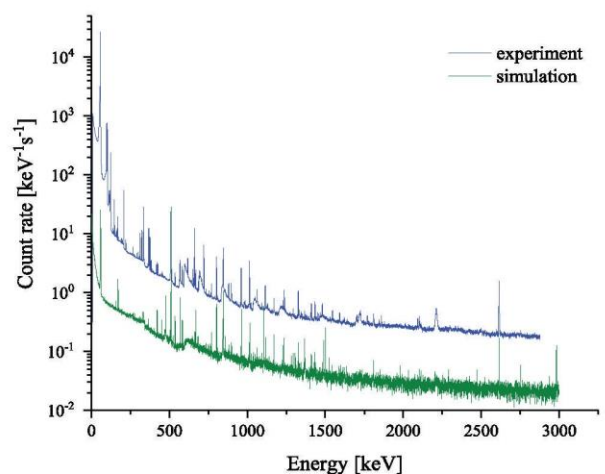
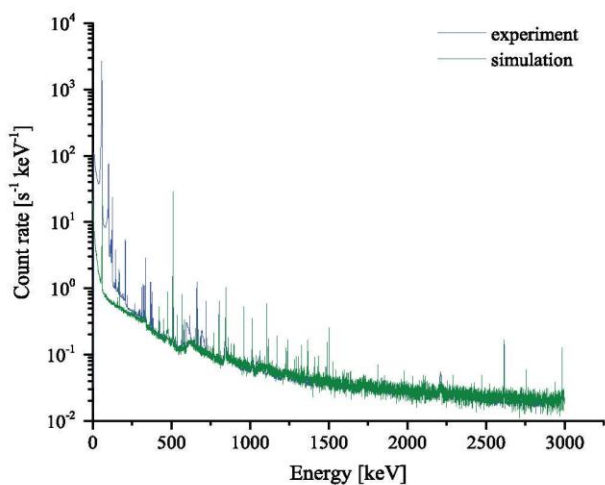


Fig. 8. Comparison of experimental and simulated γ -spectra (the experimental spectrum shown in the bottom figure has been multiplied by 10 for better visibility). The simulation was carried out with Gaussian energy distribution of ^{241}Am γ -rays coded in GEANT4.

calculated ($369 \pm 11 \text{ s}^{-1}$) one. All measured and calculated results are listed in the accompanying Table 2 to this paper.

5. Conclusions

Investigations of interactions of neutrons (produced in the ^{241}Am -Be source) with Ge detector placed in low-level shielding were carried out experimentally and compared with Monte Carlo simulation using GEANT4 tool. Precise geometry of the setup was coded including individual material impurities. Reactions of elastic and inelastic scattering of fast neutrons were observed, as well as their capture by Ge and other nuclei present in the set up. Typical triangular shape γ -peaks of ^{70}Ge , ^{72}Ge , ^{73}Ge , ^{74}Ge and ^{76}Ge induced by inelastic scattering of neutrons were detected. A large number of other peaks induced by neutron interactions with all materials in the setup (including impurities) were observed. Gamma-lines resulting from neutron interactions with lead and copper parts of the setup (e.g. the peak at 2614.51 keV originating from the reaction of $^{208}\text{Pb}(n, n'\gamma)^{208}\text{Pb}^*$), dominated in the spectra. The peak of ^{40}K (1466.11 keV) was detected only as an excited state resulting

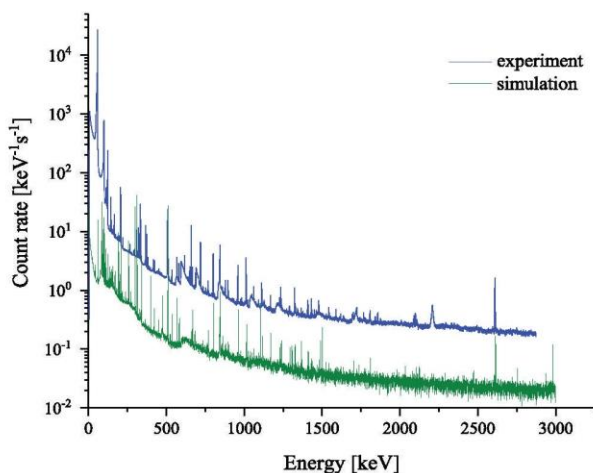
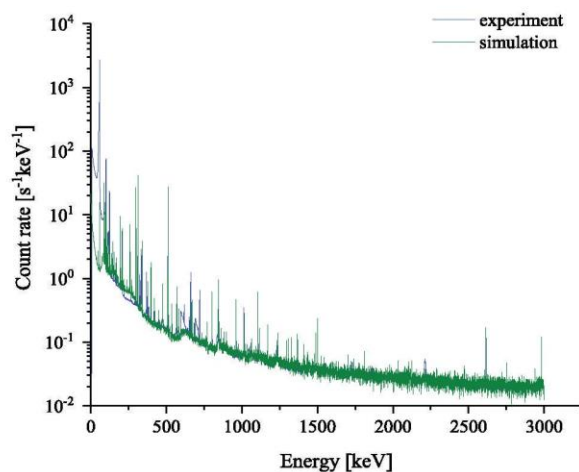


Fig. 9. Comparison of experimental and simulated γ -spectra (the experimental spectrum shown in the bottom figure has been multiplied by 10 for better visibility). The simulation was carried out using ^{241}Am ion in GEANT4 instead of Gaussian energy distribution as a source of ^{241}Am γ -rays.

from neutron capture by ^{39}K . Impurities in materials are important targets for neutron interactions and their inclusion into simulation provide a better agreement with the experiment, also important for deep underground installations. Simulated background γ -spectra were in good agreement with the experimental ones, except for a lower-energy range below 250 keV.

This work provides a thorough analysis of peaks observed in γ -spectra measured by Ge spectrometers exposed to fast neutrons, and demonstrates GEANT4 as a useful tool for simulating neutron-induced background of Ge spectrometers.

Acknowledgements

The authors are thankful to CERN for providing Ph.D. fellowship to Miloslava Baginova. Special thanks to Fabrice Malacrida for his help with the neutron source and the experiment. Support provided by the Slovak Research and Development Agency (project no. 15-0576) is highly acknowledged.

Table 2
Table of measured and simulated count rates.

Energy peaks [keV]	Nuclides and Reactions	Count rates [s^{-1}]	
		Experiment	Simulation (^{241}Am ion in GEANT4)
115–2880	Continuum	378 ± 3	369 ± 11
59.54	^{241}Am (α decay) $^{237}\text{Np}^*$	2450 ± 30	5.42 ± 0.21
68.80	$^{73}\text{Ge}(\text{n}, \text{n}'\gamma)^{73}\text{Ge}^*$	0.82 ± 0.06	0.06 ± 0.06
96.80	$^{227}\text{Ra}(\beta$ decay) ^{227}Ac	1.66 ± 0.05	–
98.97	^{241}Am (α decay) $^{237}\text{Np}^*$	66.55 ± 0.80	7.32 ± 0.31
102.98	^{241}Am (α decay) $^{237}\text{Np}^*$	73.1 ± 0.8	1.67 ± 0.17
115.09	$^{65}\text{Cu}(\text{p}, \text{n})^{65}\text{Zn}^*$	3.11 ± 0.05	2.39 ± 0.14
118.68	$^{76}\text{Ge}(\text{p}, \text{n})^{76}\text{As}$	2.33 ± 0.04	0.12 ± 0.08
122.06	$^{57}\text{Fe}(\text{n}, \text{n}'\gamma)^{57}\text{Fe}^*$	4.82 ± 0.03	0.13 ± 0.08
125.30	^{241}Am (α decay) $^{237}\text{Np}^*$	23.9 ± 0.1	1.11 ± 0.06
139.68	$^{74}\text{Ge}(\text{n}, \gamma)^{75}\text{Ge}$	0.29 ± 0.03	0.69 ± 0.18
146.55	^{241}Am (α decay) $^{237}\text{Np}^*$	3.28 ± 0.03	0.54 ± 0.12
149.56	$^{48}\text{Ti}(\text{n}, \gamma)^{49}\text{Ti}$	0.54 ± 0.03	0.10 ± 0.07
158.56	$^{117}\text{Sn}(\text{n}, \text{n}'\gamma)^{117}\text{Sn}^*$	0.19 ± 0.02	0.11 ± 0.08
165.05	$^{76}\text{Ge}(\text{p}, \text{n})^{76}\text{As}$	0.48 ± 0.03	0.17 ± 0.08
169.56	^{241}Am (α decay) $^{237}\text{Np}^*$	1.37 ± 0.03	1.31 ± 0.11
174.96	$^{70}\text{Ge}(\text{n}, \gamma)^{71}\text{Ge}^*$	0.15 ± 0.02	0.05 ± 0.06
191.96	^{241}Am (α decay) $^{237}\text{Np}^*$	0.19 ± 0.03	3.28 ± 0.16
197.37	$^{120}\text{Sn}(\text{n}, \text{n}'\gamma)^{120}\text{Sn}^*$	0.72 ± 0.02	0.30 ± 0.05
208.01	^{241}Am (α decay) $^{237}\text{Np}^*$	6.22 ± 0.08	2.10 ± 0.11
221.80	^{241}Am (α decay) $^{237}\text{Np}^*$	0.34 ± 0.02	0.08 ± 0.08
267.43	$^{74}\text{Ge}(\text{p}, \text{n})^{74}\text{As}$	0.20 ± 0.02	0.03 ± 0.05
293.66	$^{70}\text{Ge}(\text{p}, \text{n})^{70}\text{As}$	0.10 ± 0.02	0.03 ± 0.05
299.97	$^{74}\text{Ge}(\text{p}, \text{n})^{74}\text{As}$	0.17 ± 0.02	2.10 ± 0.10
311.78	$^{239}\text{Pu}(\alpha$ decay) ^{235}U	0.92 ± 0.02	–
322.52	^{241}Am (α decay) $^{237}\text{Np}^*$	1.06 ± 0.02	0.04 ± 0.04
332.35	^{241}Am (α decay) $^{237}\text{Np}^*$	0.94 ± 0.02	0.03 ± 0.03
335.37	^{241}Am (α decay) $^{237}\text{Np}^*$	3.26 ± 0.02	0.12 ± 0.05
339.33	$^{76}\text{Ge}(\text{p}, \text{n})^{76}\text{As}$	0.10 ± 0.01	1.30 ± 0.05
363.91	$^{76}\text{Ge}(\text{p}, \text{n})^{76}\text{As}$	0.04 ± 0.02	0.02 ± 0.02
368.62	^{241}Am (α decay) $^{237}\text{Np}^*$	1.21 ± 0.02	0.01 ± 0.02
370.94	^{241}Am (α decay) $^{237}\text{Np}^*$	0.17 ± 0.02	0.04 ± 0.04
376.65	^{241}Am (α decay) $^{237}\text{Np}^*$	0.93 ± 0.02	0.05 ± 0.03
383.81	^{241}Am (α decay) $^{237}\text{Np}^*$	0.19 ± 0.02	0.05 ± 0.04
418.50	$^{76}\text{Ge}(\text{n}, \gamma)^{77}\text{Ge}$	0.16 ± 0.01	0.73 ± 0.07
426.47	^{241}Am (α decay) $^{237}\text{Np}^*$	0.15 ± 0.01	0.02 ± 0.03
454.66	^{241}Am (α decay) $^{237}\text{Np}^*$	0.07 ± 0.02	0.02 ± 0.01
511	Annihilation	6.11 ± 0.08	9.99 ± 0.50
537.47	$^{206}\text{Pb}(\text{n}, \text{n}'\gamma)^{206}\text{Pb}^*$	0.13 ± 0.02	0.11 ± 0.03
562.93	$^{76}\text{Ge}(\text{n}, \text{n}'\gamma)^{76}\text{Ge}^*$	0.07 ± 0.02	0.02 ± 0.03
569.70	$^{207}\text{Pb}(\text{n}, \text{n}'\gamma)^{207}\text{Pb}^*$	0.31 ± 0.02	0.29 ± 0.03
583.18	$^{208}\text{Pb}(\text{n}, \text{n}'\gamma)^{208}\text{Pb}^*$	0.22 ± 0.02	0.18 ± 0.03
595.84	$^{74}\text{Ge}(\text{n}, \text{n}'\gamma)^{74}\text{Ge}^*$	0.20 ± 0.02	0.02 ± 0.03
608.35	$^{74}\text{Ge}(\text{n}, \text{n}'\gamma)^{74}\text{Ge}^*$	0.02 ± 0.02	0.03 ± 0.03
617.43	$^{63}\text{Cu}(\text{n}, \gamma)^{64}\text{Cu}^*$	0.31 ± 0.02	0.04 ± 0.03
641.10	$^{116}\text{Sn}(\text{n}, \text{n}'\gamma)^{116}\text{Sn}^*$	0.04 ± 0.02	0.02 ± 0.01
650.40	$^{57}\text{Fe}(\text{n}, \text{n}'\gamma)^{57}\text{Fe}^*$	0.18 ± 0.01	0.01 ± 0.02
662.40	^{241}Am (α decay) $^{237}\text{Np}^*$	1.89 ± 0.02	0.10 ± 0.04
669.62	$^{63}\text{Cu}(\text{n}, \text{n}'\gamma)^{63}\text{Cu}^*$	0.23 ± 0.02	0.18 ± 0.04
689.60	$^{72}\text{Ge}(\text{n}, \text{n}'\gamma)^{72}\text{Ge}^*$	0.10 ± 0.01	0.01 ± 0.02
691.43	$^{72}\text{Ge}(\text{n}, \text{n}'\gamma)^{72}\text{Ge}^*$	0.34 ± 0.02	0.04 ± 0.03
708.19	$^{70}\text{Ge}(\text{n}, \gamma)^{71}\text{Ge}^*$	0.04 ± 0.01	0.02 ± 0.03
722.01	^{241}Am (α decay) $^{237}\text{Np}^*$	0.91 ± 0.02	0.06 ± 0.05
736.40	$^{54}\text{Fe}(\text{n}, \text{n}'\gamma)^{54}\text{Fe}^*$	0.05 ± 0.01	0.04 ± 0.03
756.60	$^{54}\text{Fe}(\text{n}, \text{n}'\gamma)^{54}\text{Fe}^*$	0.03 ± 0.01	0.02 ± 0.02
770.60	$^{65}\text{Cu}(\text{n}, \text{n}'\gamma)^{65}\text{Cu}^*$	0.10 ± 0.01	0.10 ± 0.03
803.06	$^{206}\text{Pb}(\text{n}, \text{n}'\gamma)^{206}\text{Pb}^*$	0.58 ± 0.02	0.30 ± 0.03
810.76	$^{58}\text{Fe}(\text{n}, \text{n}'\gamma)^{58}\text{Fe}^*$	0.02 ± 0.01	0.01 ± 0.01
834.01	$^{72}\text{Ge}(\text{n}, \text{n}'\gamma)^{72}\text{Ge}^*$	0.15 ± 0.02	0.03 ± 0.03
843.76	$^{27}\text{Al}(\text{n}, \text{n}'\gamma)^{27}\text{Al}^*$	0.23 ± 0.01	0.57 ± 0.04
846.76	$^{56}\text{Fe}(\text{n}, \text{n}'\gamma)^{56}\text{Fe}^*$	0.66 ± 0.01	0.78 ± 0.04
860.56	$^{208}\text{Pb}(\text{n}, \text{n}'\gamma)^{208}\text{Pb}^*$	0.03 ± 0.02	0.61 ± 0.04
880.98	$^{206}\text{Pb}(\text{n}, \text{n}'\gamma)^{206}\text{Pb}^*$	0.14 ± 0.01	0.50 ± 0.03
897.77	$^{207}\text{Pb}(\text{n}, \text{n}'\gamma)^{207}\text{Pb}^*$	0.18 ± 0.01	0.08 ± 0.03
935.54	$^{52}\text{Cr}(\text{n}, \text{n}'\gamma)^{52}\text{Cr}^*$	0.01 ± 0.01	0.02 ± 0.02
955.0	$^{63}\text{Cu}(\text{n}, \text{n}'\gamma)^{63}\text{Cu}^*$	0.03 ± 0.01	0.04 ± 0.03
962.06	$^{63}\text{Cu}(\text{n}, \text{n}'\gamma)^{63}\text{Cu}^*$	0.40 ± 0.01	0.21 ± 0.03
978.80	$^{65}\text{Cu}(\text{n}, \text{n}'\gamma)^{65}\text{Cu}^*$	0.02 ± 0.01	0.01 ± 0.01
983.02	$^{27}\text{Al}(\text{n}, \gamma)^{28}\text{Al}^*$	0.03 ± 0.01	0.02 ± 0.02
990.0	$^{63}\text{Cu}(\text{n}, \text{n}'\gamma)^{63}\text{Cu}^*$	0.02 ± 0.01	0.02 ± 0.01
1004.51	$^{117}\text{Sn}(\text{n}, \text{n}'\gamma)^{117}\text{Sn}^*$	0.01 ± 0.01	0.03 ± 0.03

(continued on next page)

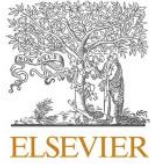
Table 2 (continued)

Energy peaks [keV]	Nuclides and Reactions	Count rates [s ⁻¹]	
		Experiment	Simulation (²⁴¹ Am ion in GEANT4)
1014.52	²⁷ Al(n, n'γ) ²⁷ Al*	0.59 ± 0.01	0.08 ± 0.02
1022	Annihilation	0.02 ± 0.01	0.02 ± 0.01
1039.51	⁷⁰ Ge(n, n'γ) ⁷⁰ Ge*	0.03 ± 0.02	0.03 ± 0.02
1043.75	²⁰⁶ Pb(n, γ2n) ²⁰⁵ Pb*	0.01 ± 0.01	0.01 ± 0.02
1050.90	²⁰⁸ Pb(n, n'γ) ²⁰⁸ Pb*	0.02 ± 0.01	0.02 ± 0.02
1063.66	²⁰⁷ Pb(n, n'γ) ²⁰⁷ Pb*	0.09 ± 0.01	0.04 ± 0.03
1094.70	²⁰⁷ Pb(n, n'γ) ²⁰⁷ Pb*	0.02 ± 0.01	0.02 ± 0.01
1108.41	⁷⁶ Ge(n, n'γ) ⁷⁶ Ge*	0.01 ± 0.01	0.27 ± 0.02
1115.55	⁶⁵ Cu(n, n'γ) ⁶⁵ Cu*	0.16 ± 0.01	0.10 ± 0.01
1129.90	⁵⁴ Fe(n, n'γ) ⁵⁴ Fe*	0.03 ± 0.01	0.01 ± 0.01
1140.52	¹²² Sn(n, n'γ) ¹²² Sn*	0.01 ± 0.01	0.01 ± 0.01
1162.60	⁶⁵ Cu(n, n'γ) ⁶⁵ Cu*	0.02 ± 0.01	0.01 ± 0.02
1171.25	¹²⁰ Sn(n, n'γ) ¹²⁰ Sn*	0.07 ± 0.01	0.06 ± 0.01
1173.23	⁶⁰ Co(β decay) ⁶⁰ Ni*	0.01 ± 0.01	0.01 ± 0.02
1204.20	⁷⁴ Ge(n, n'γ) ⁷⁴ Ge*	0.01 ± 0.01	0.01 ± 0.01
1229.68	¹¹⁸ Sn(n, n'γ) ¹¹⁸ Sn*	0.05 ± 0.01	0.03 ± 0.02
1238.27	⁵⁶ Fe(n, n'γ) ⁵⁶ Fe*	0.12 ± 0.01	0.04 ± 0.01
1245.20	⁶³ Cu(n, n'γ) ⁶³ Cu*	0.01 ± 0.01	0.02 ± 0.02
1273.36	²⁸ Si(n, γ) ²⁹ Si*	0.02 ± 0.01	0.01 ± 0.01
1293.56	¹¹⁶ Sn(n, n'γ) ¹¹⁶ Sn*	0.03 ± 0.01	0.04 ± 0.02
1327.03	⁶³ Cu(n, n'γ) ⁶³ Cu*	0.14 ± 0.01	0.07 ± 0.03
1332.51	⁶⁰ Co(β decay) ⁶⁰ Ni*	0.02 ± 0.01	0.01 ± 0.01
1345.84	⁶⁴ Cu(ε decay) ⁶⁴ Ni*	0.01 ± 0.01	0.01 ± 0.01
1350.10	⁶³ Cu(n, n'γ) ⁶³ Cu*	0.01 ± 0.01	0.01 ± 0.01
1368.63	²⁴ Na(β decay) ²⁴ Mg*	0.03 ± 0.01	0.04 ± 0.02
1380.89	²⁰⁸ Pb(n, n'γ) ²⁰⁸ Pb*	0.01 ± 0.01	0.01 ± 0.01
1392.55	⁶³ Cu(n, n'γ) ⁶³ Cu*	0.01 ± 0.01	0.03 ± 0.02
1408.10	⁵⁴ Fe(n, n'γ) ⁵⁴ Fe*	0.02 ± 0.01	0.02 ± 0.01
1412.08	⁶³ Cu(n, n'γ) ⁶³ Cu*	0.07 ± 0.01	0.03 ± 0.01
1434.07	⁵² Cr(n, n'γ) ⁵² Cr*	0.10 ± 0.01	0.02 ± 0.01
1454.28	⁵⁸ Cu(ε decay) ⁵⁸ Ni*	0.03 ± 0.01	0.01 ± 0.01
1463.75	⁷⁴ Ge(n, n'γ) ⁷⁴ Ge*	0.02 ± 0.02	0.02 ± 0.01
1466.11	³⁹ K(n, γ) ⁴⁰ K*	0.01 ± 0.01	0.02 ± 0.01
1481.84	⁶⁵ Cu(n, n'γ) ⁶⁵ Cu*	0.06 ± 0.01	0.02 ± 0.01
1530.67	⁵² Cr(n, n'γ) ⁵² Cr*	0.01 ± 0.01	0.01 ± 0.01
1547.04	⁶³ Cu(n, n'γ) ⁶³ Cu*	0.03 ± 0.01	0.02 ± 0.01
1592.51	Single escape peak of 2614.51 keV	0.03 ± 0.01	0.02 ± 0.01
1623.42	⁶⁵ Cu(n, n'γ) ⁶⁵ Cu*	0.01 ± 0.01	0.01 ± 0.01
1640.40	⁵⁴ Fe(n, γ) ⁵⁵ Fe*	0.01 ± 0.01	0.02 ± 0.01
1698.46	²⁷ Al(β decay) ²⁷ Mg*	0.01 ± 0.01	0.01 ± 0.01
1704.45	²⁰⁶ Pb(n, n'γ) ²⁰⁶ Pb*	0.03 ± 0.01	0.03 ± 0.01
1716.80	⁶³ Cu(n, n'γ) ⁶³ Cu*	0.01 ± 0.01	0.02 ± 0.02
1725.09	⁵⁷ Fe(n, n'γ) ⁵⁷ Fe*	0.02 ± 0.01	0.01 ± 0.01
1770.23	²⁰⁷ Pb(n, n'γ) ²⁰⁷ Pb*	0.03 ± 0.01	0.02 ± 0.01
1778.97	²⁸ Al(β decay) ²⁸ Si*	0.01 ± 0.01	0.02 ± 0.01
1810.76	⁵⁶ Fe(n, n'γ) ⁵⁶ Fe*	0.04 ± 0.01	0.03 ± 0.02
1844.62	⁷³ Ge(n, γ) ⁷⁴ Ge*	0.03 ± 0.01	0.03 ± 0.02
1861.30	⁶³ Cu(n, n'γ) ⁶³ Cu*	0.03 ± 0.01	0.01 ± 0.01
1879.0	⁶⁵ Cu(n, n'γ) ⁶⁵ Cu*	0.01 ± 0.01	0.02 ± 0.02
2092.78	²⁰⁷ Pb(n, n'γ) ²⁰⁷ Pb*	0.04 ± 0.01	0.02 ± 0.01
2103.51	Double escape peak of 2614.51 keV	0.05 ± 0.01	0.02 ± 0.01
2113.14	⁵⁶ Fe(n, n'γ) ⁵⁶ Fe*	0.01 ± 0.01	0.01 ± 0.01
2212.01	²⁷ Al(n, n'γ) ²⁷ Al*	0.07 ± 0.02	0.03 ± 0.01
2224.56	¹ H(n, γ) ² H	0.01 ± 0.01	0.01 ± 0.01
2614.51	²⁰⁸ Pb(n, n'γ) ²⁰⁸ Pb*	0.44 ± 0.01	0.19 ± 0.02
2754.01	²⁴ Na(β decay) ²⁴ Mg*	0.01 ± 0.01	0.01 ± 0.01

References

- [1] R. Breier, P. Povinec, Simulation of background of low-level gamma-ray spectrometers using Monte Carlo methods, *Appl. Radiat. Isot.* 68 (2010) 1231–1235.
- [2] R. Breier, M. Laubenstein, P.P. Povinec, Monte Carlo simulation of background characteristics of a Ge detector operating underground in the Gran Sasso National Laboratory, *Appl. Radiat. Isot.* 126 (2016) 188–190.
- [3] J. Ljungvall, J. Nyberg, A study of fast neutron interactions in high-purity germanium detectors, *Nucl. Instrum. Methods Phys. Res. A* 546 (2005) 553–573.
- [4] E. Gete, D.F. Measday, B.A. Mofteh, M.A. Saliba, T.J. Stocki, Neutron-induced peaks in ge detectors from evaporation neutrons, *Nucl. Instrum. Methods Phys. Res. A* 388 (1996) 212–219.
- [5] K.W. Jones, H.W. Kraner, Stopping of 1- to 1.8-keV⁷³Ge atoms in germanium, *Phys. Rev. C* 4 (1971) 125–129.
- [6] GEANT4 Collaboration, Introduction to Geant4, available at <http://geant.cern.ch/>. (Accessed 3 October 2017).
- [7] S. Agostinelli, et al., Geant4 - a simulation toolkit, *Nucl. Instrum. Methods Phys. Res. A* 506 (2003) 250–303.
- [8] J. Allison, et al., Geant4 developments and applications, *IEEE Trans. Nucl. Sci.* 53 (2006) 270–278.
- [9] J. Allison, et al., Recent developments in geant4, *Nucl. Instrum. Methods Phys. Res. A* 835 (2016) 186–225.
- [10] J. Scherzinger, R. Al Jebali, J.R.M. Annand, K.G. Fissum, R. Hall-Wilton, S. Koufigar, N. Mauritzson, F. Messi, H. Perrey, E. Rofors, A comparison of untagged gamma-ray and tagged-neutron yields from ²⁴¹AmBe and ²³⁸PuBe sources, *Appl. Radiat. Isot.* 127 (2017) 98–102.
- [11] D.V. Ellis, J.M. Singer, *Well Logging for Earth Scientists*, Springer, New York, 2007, pp. 325–382.

- [12] Nuclear Data Center, Japan Atomic Energy Agency (JAEA), available at <http://www.ndc.jaea.go.jp/jendl/j40/j40.html>. (Accessed 3 October 2017).
- [13] J.W. Marsh, D.J. Thomas, M. Burke, High resolution measurements of neutron energy spectra from Am-Be and Am-B neutron sources, *Nucl. Instrum. Methods Phys. Res. A* 366 (1995) 340–348.
- [14] L.A. Sonzogni, National Nuclear Data Center, Brookhaven National Laboratory, available at <https://www.nndc.bnl.gov/nudat2/><https://www.nndc.bnl.gov/nudat2/>. (Accessed 3 October 2017).
- [15] D. Barker, W.Z. Wei, D.M. Mei, C. Zhang, Ionization efficiency study for low energy nuclear recoils in Germanium, *Astropart. Phys.* 48 (2013) 8–15.
- [16] L.G. Evans, P.N. Peplowski, E.A. Rhodes, D.J. Lawrence, T.J. McCoy, L.R. Nittler, S.C. Solomon, A.L. Sprague, K.R. Stockstill-Cahill, R.D. Starr, S.Z. Weider, W.V. Boynton, D.K. Hamara, J.O. Goldsten, Major-element abundances on the surface of Mercury: Results from the MESSENGER Gamma-Ray Spectrometer, *J. Geophys. Res.* 117 (2012) 1–14.
- [17] M.M. Sternfelsa, F.A. Lowenheim, Tin plating from the potassium stannate bath, *J. Electrochem. Soc.* 82 (1942) 77–100.
- [18] V.A. Kudryavtsev, L. Pandola, V. Tomasello, Neutron- and muon-induced background in underground physics experiments, *Eur. Phys. J. A* 36 (2008) 171–180.
- [19] P.P. Povinec, M. Betti, A.J.T. Jull, New isotope technologies in environmental physics, *Acta Phys. Slovaca* 58 (1) (2008) 1–154.
- [20] I. Murata, I. Tsuda, R. Nakamura, S. Nakayama, M. Matsumoto, H. Miyamar, Neutron and gamma-ray source-term characterization of AmBe sources in Osaka University, *Progress Nucl. Sci. Tech.* 4 (2014) 345–348.



Contents lists available at ScienceDirect

Applied Radiation and Isotopes

journal homepage: <http://www.elsevier.com/locate/apradiso>



The neutron component of background of an HPGe detector operating in a surface laboratory

M. Baginova^{a,b,*}, P. Vojtyla^a, P.P. Povinec^b

^a CERN, Geneva, 1211, Switzerland

^b Faculty of Mathematics, Physics and Informatics, Comenius University, 842 48, Bratislava, Slovakia

ARTICLE INFO

Keywords:

Monte Carlo simulation
Neutron induced background
GEANT4
High-purity Ge detector

ABSTRACT

Investigation of neutron-induced background was carried out by studying interactions of cosmic-ray neutrons with an HPGe detector inside its shield placed on a ground floor of a 3-storey building. The study was conducted experimentally and by Monte Carlo simulations using GEANT4 simulation tool. Detailed analysis of measured background γ -ray spectra showed that many γ -lines visible in the spectra were induced by neutrons. The majority of detected γ -rays originated in germanium, copper, lead and tin. Iron and aluminium components were less important background sources. Inelastic scattering and neutron capture were the most often occurring processes of neutron interactions with the detector and its shielding. The contamination by natural radionuclides, specifically of ^{40}K , ^{214}Pb , ^{214}Bi and ^{208}Tl , was also present in the background spectra. Nevertheless, approximately 35% of ^{208}Tl peak at the energy of 2614.51 keV was produced by inelastic scattering of neutrons on ^{208}Pb nuclei. The experimental background was compared with GEANT4 simulations, which were carried out without and with the shielding layer of the building. The final integral counting rates for measured spectrum in the energy range from 50 keV to 2875 keV was $1.26 \pm 0.07 \text{ s}^{-1}$ and for simulated one $1.25 \pm 0.13 \text{ s}^{-1}$, indicating a good agreement with the experiment.

1. Introduction

High-purity germanium (HPGe) detectors have been very often used for analysis of radionuclides at very low levels, as well as in experiments looking for rare events, especially those operating in deep underground laboratories. Success of such experiments depends mainly on the detector background that can overlap the useful signal coming from the detector. For this reason, it is very important to know all sources of background of HPGe detectors and minimize or eliminate their influence on the searched signals. A significant source of the Ge detector background has been due to neutrons. Neutrons interacting with the HPGe detector materials and the shield produces many γ -rays that can hide or imitate the searched signal (Kudryavtsev et al., 2008). Neutrons are present not only in surface laboratories but also in deep underground laboratories, either as a result of spontaneous fission of natural long-lived radionuclides, (α, n) reactions, or muon interactions with surrounding rocks and detector materials (Baginova et al., 2018).

Reliable identification and investigation of neutron-induced background is a challenge due to diversity of neutron interactions with detectors and shielding materials. There are several studies dealing with

neutron induced background of Ge detectors focusing mainly on neutron interactions with Ge nuclei (e.g. Jovancevic et al., 2010; Chao, 1993). Neutrons interacting with Ge crystals produce several γ -lines resulting from capture of thermal neutrons and inelastic scattering of fast neutrons on individual Ge nuclei. These γ -lines can be used for estimation of the flux of thermal and fast neutrons around a detector. Different types of Ge detectors and various shielding materials were used for background measurements. It has been found out that the production of neutrons induced by cosmic muons significantly depends on the atomic number Z of the shielding material, as it increases with rising Z . Therefore, a shield with high Z , which is commonly used for reduction of γ -rays coming from natural radionuclides and from interactions of cosmic rays is a source of neutrons, too (Jovancevic et al., 2010). This has to be taken into account especially when building large shields for surface laboratories, compromising the composition and thickness of the shield (Povinec et al., 2008).

Germanium γ -ray peaks were used for identification of neutron sources in the Ge detector environments, as well as for calculation of their contribution to detector background. It was found that the germanium crystal itself is one of the most intensive sources of neutron-

* Corresponding author. CERN, Geneva, 1211, Switzerland.
E-mail address: miloslava.baginova@cern.ch (M. Baginova).

induced γ -rays in an HPGe detector (Chao, 1993).

However, a study providing complex information on the neutron induced background in Ge spectrometers is still missing. In order to bring additional information about the neutron-induced background and to contribute to better understanding of low-background detector systems, γ -ray background of an HPGe detector operating in a surface laboratory was measured and compared with Monte Carlo simulations in the present study. The knowledge obtained in (Baginova et al., 2018) provided useful hints for this work.

2. Cosmic rays at the sea level

Background of low-level Ge detectors operating in surface laboratories is mainly caused by secondary cosmic rays, radioactive contamination of materials used for construction of detectors and their shields, and by decay products of radon. Interactions of primary high-energy cosmic ray particles with atmospheric nuclei produce secondary particles, which interact further in the atmosphere producing next generations of particle cascades. The ability of a particle to reach sea level depends on the particle type, energy, zenith angle of propagation and mean lifetime at rest. Cosmic rays at sea level consist of hadrons, electrons, γ -rays, muons, nuclei and antinucleons with energy up to a few TeV. These particles form at sea level soft, nucleonic and hard components of cosmic rays. Electrons, positrons and γ -rays belong to the soft component. The nucleonic component consists mainly of protons and neutrons, and the hard component contains mostly muons. The hard component is dominant at the sea level, as the most numerous particles at the sea level are muons with abundance of about 63%. The second most abundant particles are neutrons with occurrence of about 21% and the third numerous particles are electrons, positrons and γ -rays with abundance of about 15%. The rest, about 1% of cosmic rays at the sea level is formed by protons, pions and nuclei (Greider, 2001; Bogdanova et al., 2006).

Although muons are the dominant particle type at the sea level, we can reduce their effect by operating detectors deep underground where muon fluxes are lower by several orders of magnitude. In surface laboratories we may apply anti-cosmic (anti-coincidence) pulse-rejection techniques. Therefore, the most difficult cosmic-ray component to deal with are neutrons, as the fluxes of protons, the second part of the nucleonic component, are very small.

3. Neutron cross sections

Neutrons interact with matter by different processes depending on their energy and material cross sections. Slow and thermal neutrons interact by neutron capture, while fast neutrons interact by elastic and inelastic scattering. Neutron cross sections for individual isotopes forming the materials of Ge detector and the shield are very important for investigation of neutron induced background. Isotopes with large cross sections, such as isotopes of lead and copper, interact with neutrons easily so that they can significantly contribute to the neutron background. Lead and copper are materials frequently used in certain parts of HPGe detectors. The crystal holder is usually made of copper, as well as the internal part of the shield is covered with a copper layer. Lead is almost always the largest part of the detector shield. Usually, lead is one of the most frequently used material for construction of massive shields for HPGe detectors operating deep underground. The amount of lead in a shield of an HPGe detector commonly used in a surface laboratory is around 1 ton. Therefore, due to its high cross sections and mass, the shield is a significant contributor to the neutron background.

Lead as an element consists of four naturally occurring isotopes: ^{204}Pb (1.4%), ^{206}Pb (24.1%), ^{207}Pb (22.1%), and ^{208}Pb (52.4%). Copper has two naturally occurring isotopes, ^{63}Cu and ^{65}Cu , with abundances of 69.15% and 30.85%, respectively. The cross sections for individual lead and copper isotopes for interactions with neutrons are shown in Fig. 1.

Quantitative parameters of cross sections of individual isotopes were

compared and following was found. For all four lead isotopes the elastic scattering significantly dominates until the resonance region, which can be split into two parts. The first part is characterized by sharp fluctuations of cross sections for both, neutron capture and elastic scattering. In the second part, the elastic scattering dominates, and the cross sections fluctuate with decreasing amplitude.

For ^{204}Pb , the resonance region opens at 3.7 keV and ranges up to 1.8 MeV. Within the first part of the region up to about 75 keV, the neutron capture and elastic scattering are equally probable. Beyond the resonance region, the elastic scattering gains significance again. The channel of inelastic scattering opens at about 200 keV and drops sharply beyond 10 MeV. In the energy region of 1.8–10 MeV, elastic and inelastic scattering occur. Nevertheless, around 8–9 MeV, the inelastic scattering is more probable.

For ^{206}Pb , the resonance region extends from about 3 keV to 2.5 MeV. In the first part of the region up to about 320 keV, the elastic scattering gradually takes over. In the energy region of 8–9 MeV, elastic and inelastic scattering are equally probable.

For ^{207}Pb , the resonance region is wider and ranges from about 3 keV to 4.5 MeV. In the first part of the region, up to about 680 keV, the elastic scattering clearly outweighs. In the second part of the resonance region, the inelastic scattering cross section increases quickly. The elastic and inelastic scattering are equally probable processes from 6.5 to 8.0 MeV.

For ^{208}Pb , the resonance region ranges from about 43 keV to 5.5 MeV, where the elastic scattering highly predominates. The channel of inelastic scattering opens at 900 keV and, from 7.5 to 8.5 MeV, the elastic and inelastic scattering are equally probable.

The inelastic scattering is a significant process for all lead isotopes around the energy of 8 MeV, the binding energy per nucleon in a lead nucleus.

The behaviour of cross sections for both copper isotopes is very similar to lead isotopes.

For ^{63}Cu , the neutron capture predominates up to 19 meV. Above this energy the elastic scattering gains significance until the resonance region, which extends from about 400 eV up to 1.1 MeV. Inside the region, the neutron capture is the most probable reaction up to 1 keV. From 50 keV the elastic scattering dominates. The inelastic channel opens at 680 keV and it is equally probable as elastic scattering in the energy range of 2.5–6 MeV.

Finally, for ^{65}Cu , the elastic scattering dominates up to 230 eV, where the resonance region starts. The region ranges up to 1.1 MeV. In the region up to 50 keV, cross sections of the elastic scattering and neutron capture are comparable. Above this energy, the elastic scattering takes over. The inelastic channel opens at 780 keV and in the energy range of 3.5–5 MeV, both, the elastic and inelastic scattering are equally probable.

In the energy range of 3.5–5 MeV, neutrons interact easily by inelastic scattering with both copper isotopes. The neutron capture is the preferred process for thermal neutrons and a very probable process for slow neutrons from 400 eV to 50 keV.

4. Detector background

4.1. Experimental setup

Investigation of neutron induced-background was carried out by a study of cosmic ray interactions with an HPGe detector inside a shield. The study was conducted experimentally and by Monte Carlo simulations using the GEANT4 simulation tool developed at CERN (<http://geant.cern.ch/>; Agostinelli et al., 2003; Allison et al., 2006, 2016).

A Mirion Technologies (Canberra) coaxial low-level p-type HPGe detector GC-5019 with a relative efficiency of 50% was used for background measurement. The germanium crystal was a cylinder with a cavity inside the crystal. The dimensions of the crystal were 66 mm in diameter and 59 mm in height. The cavity was 10 mm in diameter and

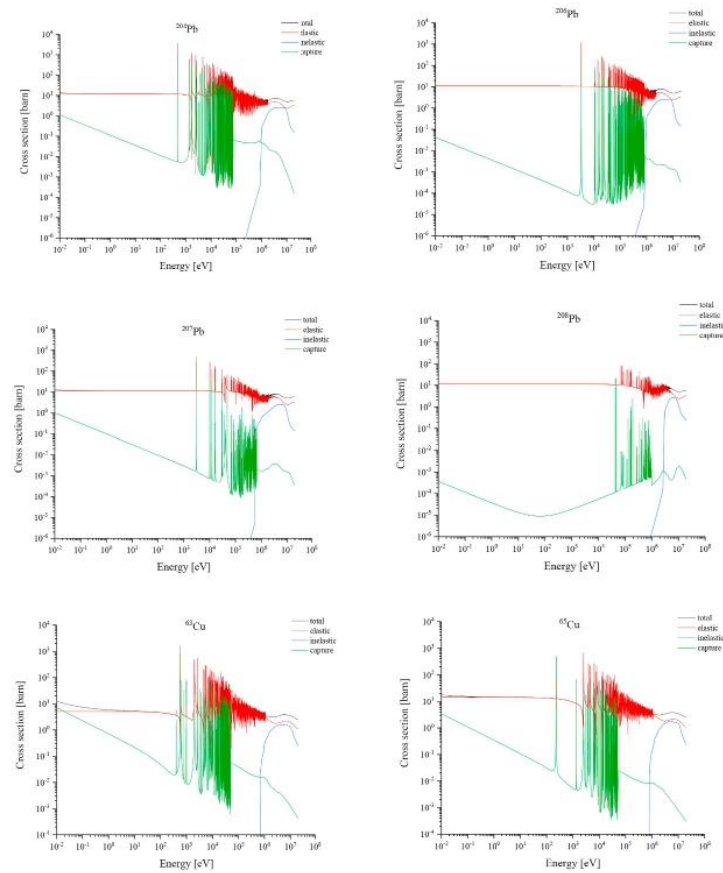


Fig. 1. Calculated cross sections for elastic and inelastic scattering and neutron capture in lead and copper isotopes. Data taken from JENDL 4.0 database (<http://www.ndc.jaea.go.jp/jendl/j40/j40.html>).

45 mm in height. The crystal was placed in a thermoplastic foil and in a copper crystal holder, which was enclosed in an aluminium “swan-neck” cryostat. The detector was placed in a low-level shield consisting of (from outside to inside) 9.5 mm of carbon steel, 92 mm of common lead, 10 mm of old low-activity lead, 1 mm of tin foil, and 1.5 mm of copper cladding. The outer dimensions of the shield were 508 mm in diameter and 635 mm in height. The preamplifier was placed outside the shield. The “swan-neck” prevented a direct sight of the crystal on a Dewar vessel and the floor below. The energy resolution of the detector was 2.07 keV for 1332.40 keV γ -rays of ^{60}Co . The Canberra GENIE 2000 software was used for γ -ray spectrum analysis. The spectrum was acquired in the energy range from 10 to 3000 keV during 84 h of live time. The measurement was carried out after an experiment with an Am-Be neutron source (Baginova et al., 2018), in which two circular iron absorbers and one plastic beaker were placed above the detector with the aim of reducing the dead time by increasing the source-detector distance and absorbing the ^{241}Am gamma rays. As the same background spectrum was used in this work, the iron absorbers and the plastic beaker were left inside the shield. The setup, as it was implemented in the GEANT4 simulation code, is shown in Fig. 2a, Fig. 2b.

4.2. Monte Carlo simulations

The GEANT4 simulation code was used for Monte Carlo simulations of Ge detector background. GEANT4 is an object-oriented simulation toolkit, which provides an extensive set of software components for simulation of particle interactions with matter in a wide energy range. The code includes all aspects of the simulation process, such as the

geometry, materials, particles, the tracking, physics processes and the detector response. The software is capable to generate and store events and tracks, to visualize the detector and particle trajectories, and to record the simulation data, energy deposition included. GEANT4 disposes with extensive databases of cross sections, which are stored in individual data files for specific processes (<http://geant.cern.ch/>; Agostinelli et al., 2003; Allison et al., 2006, 2016). The GEANT4 simulation code is equally suitable for simulations in High Energy Physics as in Low Energy Physics. The code was already validated for low background experiments, such as dark matter or neutrinoless $\beta\beta$ decay searches, where the precision of simulations is very important. For example, the detector geometry and its surrounding, the source particles and the background spectra were simulated by GEANT4 in underground experiments such as CRESST, COSINE, EDELWEISS or SuperNEMO (e.g. Abdelhameed et al., 2019; Adhikari et al., 2018; Armengaud et al., 2017; M. Kauer and the SuperNEMO Collaboration 2009, 2008). Nevertheless, GEANT4 is commonly used also for cosmic-ray background simulations, (e.g. Shun-Li et al., 2015; Medhat and Wang, 2014; Hung et al., 2017). In all these studies, simulations well agreed with experimentally measured spectra.

The detector and shield geometry were coded in GEANT4, including composition of shielding materials and impurities. Detailed drawings of the detector setup were provided by Mirion Technologies/Canberra for the study.

The setup was placed into a box with dimensions of $7 \times 4 \times 3 \text{ m}^3$ representing the laboratory with concrete walls of 32 cm thickness. The laboratory with the HPGe detector is located in a basement of a building and the cosmic rays from an open area pass through masonry structures

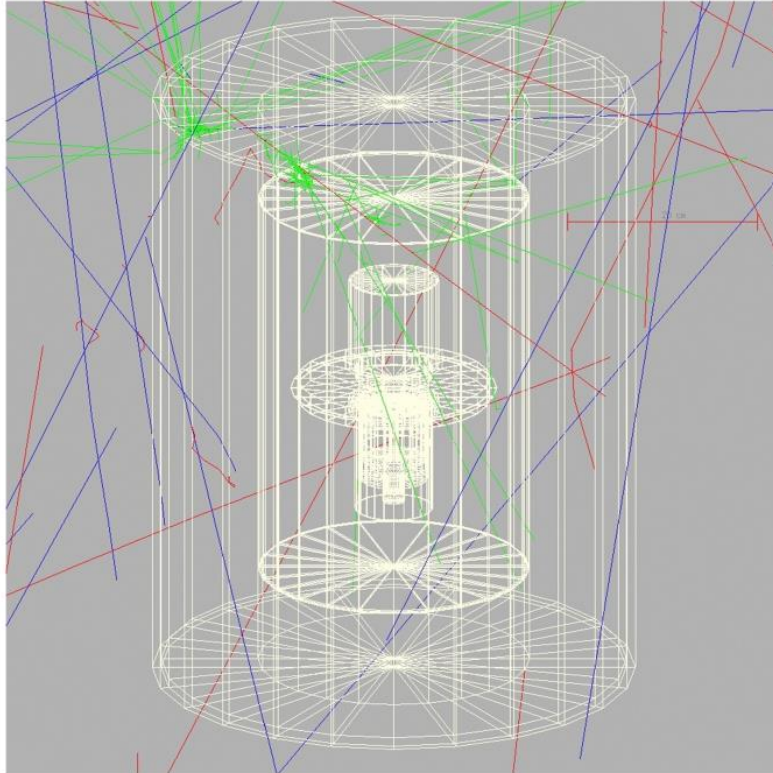


Fig. 2a. GEANT 4 simulation of the experimental setup with several simulated cosmic ray interactions (trajectories of positive particles are blue, of negative particles are red and of neutral particles are green). (For interpretation of the references to colour in this figure legend, the reader is referred to the web version of this article.)

of the building. The detailed structure of the overhead material layers was not known but its concrete equivalent was estimated to be 1 m, arranged as a ceiling equivalent to a roof and two floors. We expect that the nucleonic and soft components of cosmic rays were reduced approximately by a factor of 4 (Ziegler, 1996).

The cosmic rays at sea level were used as source of particles impinging on the setup, without and with the concrete overhead shielding. The source consisted of muons, neutrons, electrons, positrons, γ -rays, protons and pions. The measured energy spectra of individual cosmic ray particles taken from (Greider, 2001) were implemented into GEANT4 simulation. The intensity of particles was coded based on their abundances in cosmic rays at sea level as indicated in (Bogdanova et al., 2006). The assumed relative abundances of different particle types were: muons (63%), neutrons (21%), electrons and positrons (7.5%), γ -rays (7.5%), and protons and pions (1%). The fluxes of positive and negative muons, positive and negative pions, as well as electrons and positrons were calculated from charge ratios reported in (Greider, 2001). The cosmic-ray particle source was modelled as a plane ($10 \times 10 \text{ m}^2$) placed above the laboratory. See (Greider, 2001) for detailed information on spectral fluxes of the different cosmic-ray particle types.

SHIELDING 2.1 was selected as the most suitable GEANT physics list. It is an ideal choice to study neutron interactions in underground or low background experiments thanks to an appropriate composition of electromagnetic and hadronic physics processes.

The G4NDL 4.5 and G4NEUTRONXS 1.4 data files were used for neutron processes and G4EMLOW 6.5 data file for γ -ray interactions. G4NEUTRONXS 1.4 is suitable for elements with natural composition, and G4NDL 4.5 is used especially for thermal neutron cross sections.

The correct coding of the given detector and shield to GEANT4 and the software setup with the selection of the physics data files were validated in a previous work (Baginova et al., 2018). Interactions of

neutrons from a ^{241}Am -Be neutron source with an HPGe detector was investigated experimentally and by Monte Carlo simulations. The integral count rates of the two spectra were compared and a good agreement was found (experiment $378 \pm 3 \text{ s}^{-1}$, simulation $369 \pm 11 \text{ s}^{-1}$). Count rates of many neutron induced peaks were compared, too. For example, the measured ^{65}Cu peak at the energy of 770.60 keV resulting from inelastic scattering of neutrons on Cu nuclei had a count rate of $0.1 \pm 0.01 \text{ s}^{-1}$ to be compared with the simulated one of $0.1 \pm 0.03 \text{ s}^{-1}$. Similarly, the measured count rate of $0.31 \pm 0.02 \text{ s}^{-1}$ of the ^{207}Pb peak at the energy of 569.70 keV matched the count rate of the simulated peak $0.29 \pm 0.03 \text{ s}^{-1}$.

5. Results and discussion

5.1. Evaluation of the experimental background γ -ray spectrum

The measured background γ -ray spectrum was analysed and evaluated in detail. To make the peaks and reaction formulas more visible, the γ -ray spectra are shown in three energy regions: 0–1 MeV (Fig. 3.), 1–2 MeV (Fig. 4.) and 2–3 MeV (Fig. 5.). Many peaks were identified and explained also using information from the previous experiment with Am-Be neutron source (Baginova et al., 2018). Different colours are used to mark peaks from different contributors. Very short-lived radionuclides (excited states with half-lives $< 1 \text{ ms}$) are marked with the asterisk.

The observed count rates depend on the particle spectral fluxes, isotope-specific nuclear-reaction cross-sections, isotope abundances, γ -ray emission probabilities and detection efficiencies. Apparently, these are complex processes to combine and could be analysed on demand by using the information provided by GEANT4 code, for example.

Triangular γ -ray peaks, which are typical for interactions of fast

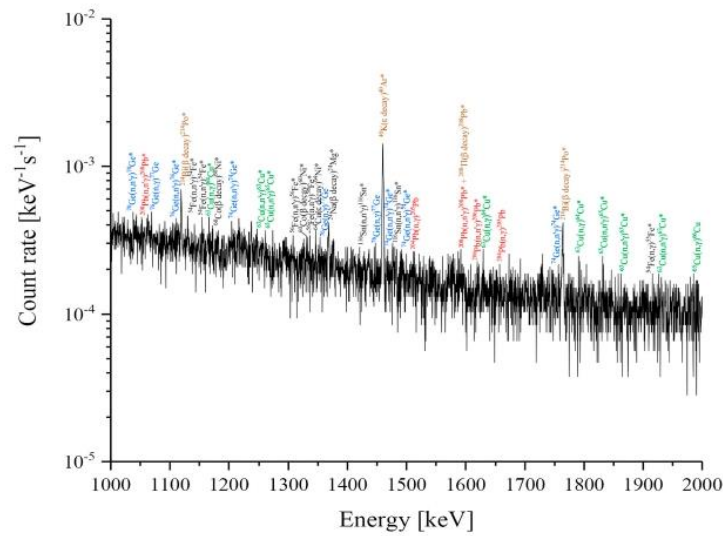


Fig. 4. Experimental HPGe detector background spectrum for energy range from 1 to 2 MeV. (Ge peaks-blue, Cu peaks-green, Pb peaks-red, contamination-brown)

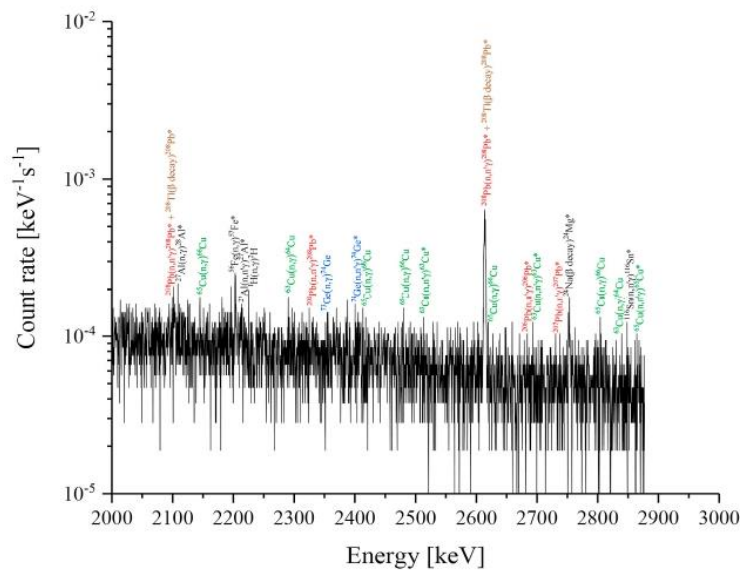


Fig. 5. Experimental HPGe detector background spectrum for energy range from 2 to 3 MeV. (Ge peaks-blue, Cu peaks-green, Pb peaks-red, contamination-brown)

neutrons with individual Ge nuclei, are present in the spectra. Their origin and occurrence have been fully explained in our previous paper (Baginova et al., 2018). The triangular shape of the Ge peaks is well visible only in the energy range from 0 to 1 MeV, but not at higher energies due to poor statistics. Whereas, neutrons interact with all Ge isotopes (^{70}Ge - 20.52%, ^{72}Ge - 27.45%, ^{73}Ge - 7.76%, ^{74}Ge - 36.7% and ^{76}Ge - 7.75%) mostly by inelastic scattering, there are several Ge peaks visible in the spectra. For ^{73}Ge , there is one peak coming from this process observed at the energy of 53.44 keV. The peaks of ^{76}Ge caused by the same process are visible at the energies of 562.93 keV and 1108.41 keV. The peaks resulting from inelastic scattering of neutrons on ^{74}Ge are visible at the energies of 595.84 keV, 1204.20 keV, 1463.75 keV, 1489.35 keV, 1756.70 keV and 2402.70 keV. And finally, the ^{70}Ge peak resulting from the same reaction was found at the energy of 1039.51 keV.

The rest of the Ge peaks are caused by (n, γ) reactions, except the

peak of ^{72}Ge at the energy of 691.43 keV, originating in the internal conversion. The neutron capture on ^{74}Ge nuclei led to occurrence of the ^{75}Ge peak at the energy of 139.68 keV. The ^{71}Ge peak at 708.19 keV is visible due to neutron capture on ^{70}Ge . The same process but on ^{76}Ge resulted in three peaks of ^{77}Ge at the energies of 1067.66 keV, 1353.94 keV, and 1446.87 keV. Absorption of neutrons by ^{73}Ge leads to emission of ^{74}Ge γ -line at the energy of 2353.46 keV. The Ge peaks are produced in the germanium crystal, the sensitive part of the detector.

The experimental γ -ray spectra also contain many other peaks produced by neutron interactions with materials used in the setup, especially with shielding materials. The majority belongs to copper and lead peaks, as both materials with large neutron cross sections are the most abundant in the setup.

Copper is used in the crystal holder (close to the Ge crystal), and in the copper cladding of the shield. The observed γ -lines come from inelastic scattering and capture of neutrons on copper and lead nuclei. The

neutron capture prevails for copper isotopes, as it absorbs neutrons much easier than lead thanks to larger cross sections. Gamma-lines of ^{64}Cu excited in neutron capture on ^{63}Cu were observed at the energies of 212.38 keV, 1165.21 keV, 1630.10 keV, 1670.92 keV, 1790.30 keV, 2291.42 keV and 2838.20 keV. Similarly, γ -lines of ^{66}Cu originate in neutron capture on ^{65}Cu nuclei were found at the energies of 89.18 keV, 237.82 keV, 1985.73 keV, 2144.22 keV, 2411.58 keV, 2478.20 keV, 2619.14 keV, and 2806.90 keV. The inelastic scattering led to several peaks from both copper isotopes. The ^{63}Cu peaks are visible at the energies of 955.0 keV, 962.06 keV, 1245.20 keV, 1861.30 keV, 1927.20 keV, 2512.0 keV and 2696.60 keV. The isotope ^{65}Cu gives rise to peaks at the energies of 770.60 keV, 924.50 keV, 978.80 keV, 1261.0 keV, 1832.0 keV and 2862.70 keV.

The bulk of the detector shield is made of lead, and several peaks were observed in the γ -ray spectra. The lead has four stable isotopes with relative abundance of 1.4% (^{204}Pb), 24% (^{206}Pb), 22% (^{207}Pb) and 52% (^{208}Pb). The most intensive is the 2614.51 keV line which is a superposition from the β -decay of ^{208}Tl present in the system as a radioactive impurity, and from inelastic scattering of neutrons on ^{208}Pb nuclei (as discussed in detail in the simulation chapter). Both processes, the neutron inelastic scattering and the β decay excite the same energy level of ^{208}Pb , which is the stable product of the ^{208}Tl β decay. The peaks at the energies of 2103.51 keV and 1592.51 keV are single and double escape peaks, respectively. Lead-208 lines are also visible at the energies of 583.19 keV, 860.56 keV, 1050.90 keV and 2322.65 keV. The ^{208}Pb X-rays are visible at energies of 72.81 keV and 74.97 keV. The 510.74 keV peak is supposed to be hidden in the annihilation peak. Peaks of ^{207}Pb are present in the spectra at the energies of 569.70 keV and 2736.46 keV. Lead-206 has also several γ -lines in the spectra, namely at the energies of 537.47 keV, 803.06 keV, 1620.30 keV and 2682.0 keV. Next, two lines of ^{205}Pb at the energies of 1511.0 keV and 1656.20 keV coming from neutron capture on ^{204}Pb nuclei are present in the spectra, too.

Almost all aluminium γ -rays come from the detector cryostat and the entrance window. Small amounts of aluminium are also present in the germanium crystal and in the iron absorbers as impurity. As expected, one of the main aluminium lines at the energy of 2212.01 keV is visible in the spectra. Its origin is in the third excited state of ^{27}Al and it is induced by inelastic scattering of neutrons on ^{27}Al nuclei. There is one more peak of aluminium at the energy of 2108.24 keV originating in neutron capture on ^{27}Al .

The main sources of tin peaks are in the shielding made of tin layer, and in the tin coating of the iron absorbers. The inelastic scattering was the main induction mechanism of tin γ -rays found in the spectra. Tin element has ten naturally occurring isotopes. Lines of a few of them (with the most abundant isotopes) are visible in the spectra. Tin-116 with abundance of 14.54% is identified by several lines from inelastic scattering: 1421.20 keV, 1476.75 keV, and 2850.30 keV. There is one inelastic scattering line of ^{117}Sn (abundance of 7.68%) in the spectra: 158.56 keV. There is also ^{121}Sn peak excited in neutron capture on ^{120}Sn nuclei at the energy of 966.0 keV.

All iron γ -rays are produced in the iron absorbers, resulting from inelastic scattering of neutrons on iron nuclei, and from the neutron capture. Iron has four stable isotopes, ^{54}Fe , ^{56}Fe , ^{57}Fe , and ^{58}Fe , with abundances of 5.85%, 91.75%, 2.12%, and 0.28%, respectively. The lines from inelastic scattering on ^{56}Fe are visible at 846.76 keV, 1303.4 keV and 1335.40 keV. Similarly, neutron capture excites ^{54}Fe nuclei to the energies of 1129.90 keV, 1153.10 keV. The peaks of ^{58}Fe were not observed. The peaks of ^{55}Fe and ^{57}Fe at the energies of 1917.90 keV and 2202.70 keV are an evidence of neutron capture on ^{54}Fe and ^{56}Fe , respectively. All iron γ -rays are produced in the iron absorbers.

A peak of the neutron capture on hydrogen at the energy of 2224.56 keV is seen in the third spectrum (Fig. 5). The capture takes place on hydrogen present in plastic parts of the setup.

The peak at the energy of 477.61 keV is special. It comes from the ^{10}B (n, α) ^7Li reaction. The inner electrode of the crystal contains boron as a semiconductor dopant and the (n, α) cross section for thermal neutrons

is very high, 3838 b, so that the peak is well visible in the measured background, even if the amount of boron in the setup is very small.

The ^{24}Mg peaks at the energies of 2754.01 keV and 1368.63 keV come from the β decay of ^{24}Na produced in the ^{27}Al (n, α) ^{24}Na reaction in aluminium.

We also searched for proton-induced reactions in the background spectrum. However, as the proton cosmic-ray flux at sea level is below 1% (Bogdanova et al., 2006; Povinac et al., 2008), their contributions to background should be negligible. The proton-induced peaks in ($p, n\gamma$) reactions on Ge nuclei, specifically on ^{72}Ge , ^{73}Ge , ^{74}Ge and ^{76}Ge , as well as in reactions on copper and aluminium (Baginova et al., 2018) were statistically insignificant.

The ^{64}Ni peak (1345.84 keV) witnesses EC transformation of radioactive ^{64}Cu , which was previously formed in neutron capture on ^{63}Cu , the stable isotope of copper.

The two peaks at the energies of 1173.23 keV and 1332.51 keV are de-excitation γ -rays of ^{60}Ni . They come from the β -decay of ^{60}Co produced by activation of the iron absorbers during the previous experiment involving an Am-Be neutron source (Baginova et al., 2018).

Several well visible peaks originating in natural radioactivity are present in the spectra. They come from contamination of the detector, the shield and surrounding materials, such as the laboratory walls and stuffs. Namely, ^{214}Bi resulting from β -decay of ^{214}Pb at energies of 295.22 keV and 351.93 keV and peaks of ^{214}Po coming from subsequent β -decay of ^{214}Bi detected at energies of 609.32 keV, 1120.29 keV and 1764.49 keV. Both of them belong to the ^{238}U decay chain. The peak at 2614.51 keV has double origin: β -decay of ^{208}Tl from the ^{232}Th decay series and de-excitation of ^{208}Pb excited in inelastic neutron scattering. The 1460.80 keV peak comes from the electron-capture decay of ^{40}K to de-exciting ^{40}Ar . Potassium is present as contamination from natural radionuclides in the material surrounding the detector and in the detector itself and it is also present in the iron absorbers as impurity (0.026%). Solutions of potassium-stannate and potassium-hydroxide are used as plating bath for alkali tin plating of metals (Stenfelsa and Lowenheim, 1942).

The 511 keV peak is the annihilation peak coming from annihilation of electron-positron pairs generated by photon interactions with materials of the setup.

The Compton continuum due to the material contamination is considerably lower than the cosmic-ray continuum thanks to the used low-level materials and a high detector relative efficiency. Note that no steep rise of the continuum corresponding to the Compton edge of the 2614.51 keV peak of ^{208}Tl can be observed in our experimental spectrum unlike in the experimental spectrum in (Hung et al., 2017).

5.2. Comparison of Monte Carlo simulations with the experiment

5.2.1. Simulations without the concrete building

Two simulations of the background spectrum were carried out without considering the contamination by natural radionuclides. First, a simulation without the concrete building was carried out and the resulting spectrum was compared with the measured background (Fig. 6.). There is a significant difference between the experimental and simulated spectra in the continuum below 500 keV. The main reason is that penetration of cosmic rays through the building was not in this case taken into account (the effect of the building will be discussed later). Next, contamination lines visible in the experimental spectrum and stemming from natural contamination by ^{40}K , ^{208}Tl , ^{214}Pb , and ^{214}Bi were not coded, so Compton continuum from the corresponding peaks did not contribute to count rates up to 500 keV. Several other differences were observed. The γ -ray emission for a few peaks in the energy range from 450 keV to 1 MeV is higher than in the experimental background spectrum. This effect is visible due to missing concrete shielding. Penetration via massive concrete shield reduces the γ -ray intensity in this energy range.

The triangular shape of Ge peaks coming from summation of the recoil

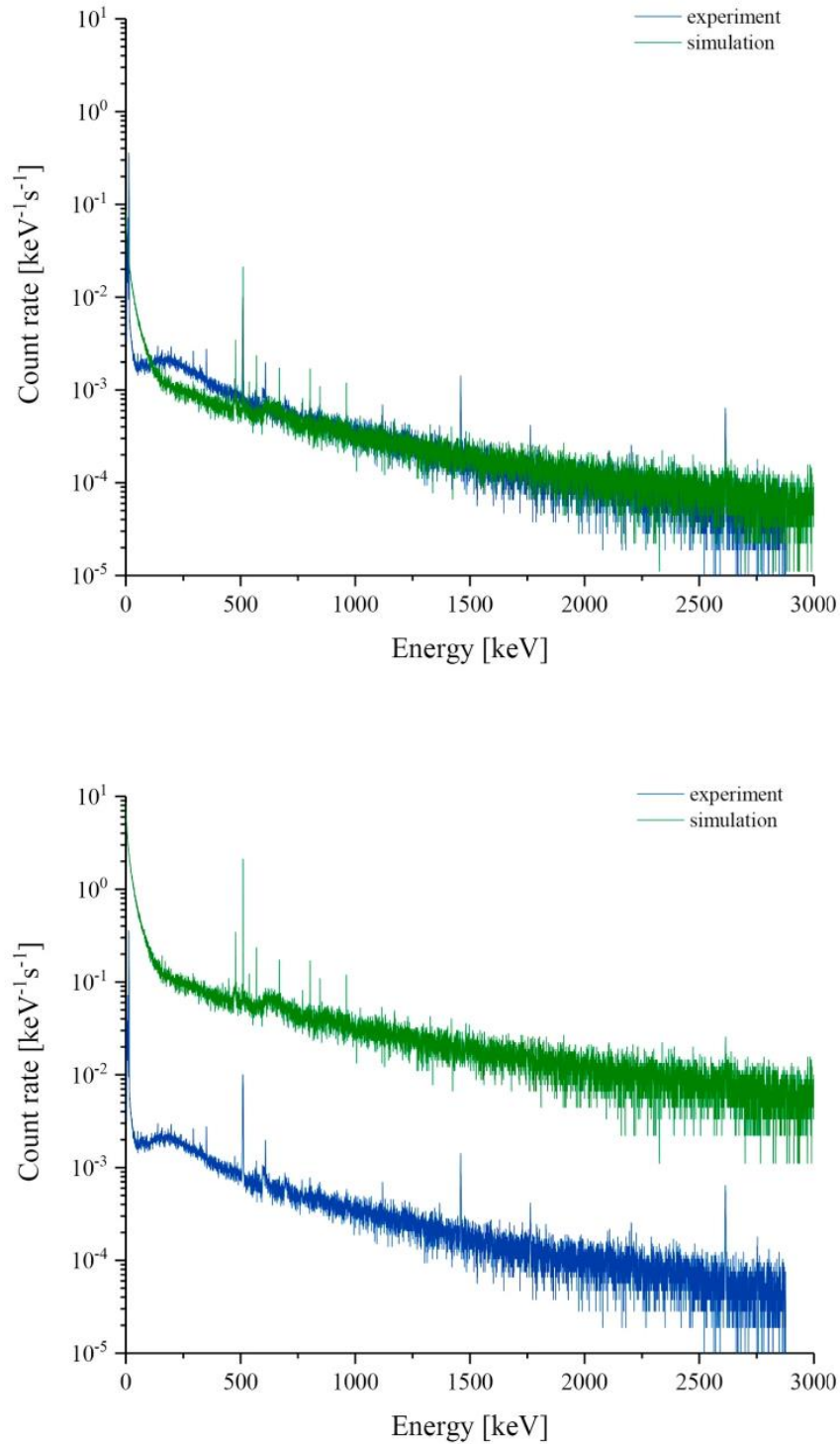


Fig. 6. Comparison of experimental and simulated HPGe background spectra (without the concrete building). The simulated spectrum shown in the bottom figure has been multiplied by 100 for better visibility.

energy in Ge nucleus and the energy of emitted γ -rays, is not simulated correctly by GEANT4, as they are lower, less sharp, and their tails do not fit the real ones. The peak at the energy of 477.61 keV coming from $^{10}\text{B}(n, \alpha)^7\text{Li}$ reaction is overestimated. The count rate of the simulated peak was

approximately 5-times higher than the experimental one. The main reason is that the boron contents in the doped Ge dead layer was not known exactly. As the cross section for boron for this reaction is very high, the simulation could be affected considerably.

Special attention was paid to lead γ -rays in the simulated spectrum (Fig. 7.). The ^{208}Pb peaks known as originating in β -decay of ^{208}Tl , usually present in detector systems as a contaminant, are clearly visible also in the simulated spectrum, although no contamination was assumed. The γ -lines come from the inelastic scattering of neutrons on ^{208}Pb nuclei. The count rates of the main ^{208}Pb peak (2614.51 keV) were compared. It is $0.00048 \pm 0.00014 \text{ s}^{-1}$ for the experimental peak and $0.00024 \pm 0.00007 \text{ s}^{-1}$ for the simulated one. The count rate is higher in the measured than in the simulated background, indicating that there is also a direct contribution from ^{208}Tl decay, as expected. It can be concluded that, approximately 50% of the peak in the measured background spectrum is formed by neutron interactions with ^{208}Pb nuclei. Therefore, as long as lead will be present in the experimental setup, these peaks will be present in the background spectrum, even if the contamination with ^{208}Tl would be eliminated.

The experimental and the simulated spectra were compared by integral count rates for the energy range from 500 keV to 2875 keV where the spectra match each other. The integral count rate measured in the experiment $0.56 \pm 0.03 \text{ s}^{-1}$ was in a very good agreement with the calculated value $0.53 \pm 0.05 \text{ s}^{-1}$. However, omission of the roof shielding in the simulation results in a considerable difference between the measured and simulated spectra below 500 keV. The roof shielding is apparently a very important part of the simulation setup as will be shown in the next Section.

5.2.2. Simulations including the concrete building

Another simulation of background γ -ray spectrum was carried out, this time taking the building into account. The shape of the simulated spectrum replicates the experimental one much better than when the building effect was omitted (Fig. 8.). This time, the typical wide hump in the continuum around 200 keV is predicted well. However, there is still a slight difference in the continuum heights up to 350 keV, probably caused by omission of radionuclide contamination of construction materials in the simulations. The simulated continuum is slightly lower, especially in the part below the ^{214}Bi peaks. The simulated peak of ^7Li at the energy of 477.61 keV is again overestimated, but the count rate of the simulated peak decreased by about a factor of two. The count rates of the ^{208}Pb peaks at the energy of 2614.51 keV were compared again. The experimental one is $0.00048 \pm 0.00014 \text{ s}^{-1}$, while the simulated one is $0.00017 \pm 0.00005 \text{ s}^{-1}$, what means that approximately 35% of the experimental peak originate in inelastic scattering of neutrons on lead

nuclei. The count rate of the simulated peak is lower than in the previous simulation (without the concrete) by 30%, what can be explained by changed neutron spectral fluxes after passing the concrete layer. Due to same reason, the triangular shape of Ge peaks is less visible as it was in the simulation without the concrete layer.

Integral count rates of the experimental and simulated spectra were compared for the energy region from 50 to 2875 keV taking into account the concrete shielding. Below the energy of 50 keV, the count rate is strongly influenced even by small changes in the thicknesses and material composition of various layers. Therefore, it is difficult to achieve quantitative agreement of count rates below this energy. Integral count rate of the measured spectrum $1.26 \pm 0.07 \text{ s}^{-1}$ matches the simulated one of $1.25 \pm 0.13 \text{ s}^{-1}$, indicating a very satisfactory agreement. The numerical difference of less than 1% is rather a random coincidence than a precise result match. It may seem that, in the region above 2000 keV, the simulated count rate is higher than the measured one (Fig. 8.). Therefore, the integral count rates (continuum and peaks) were calculated for both spectra in the energy range from 2000 keV to the end of the measured spectrum at 2875 keV. The obtained count rates were $0.07 \pm 0.005 \text{ s}^{-1}$ for the experimental spectrum and $0.08 \pm 0.009 \text{ s}^{-1}$ for the simulated one (only statistical uncertainties at the 1σ level). The experimental spectrum shows greater statistical fluctuations, which are more pronounced at lower values in the logarithmic y scale.

The measured and simulated results are listed in Table 1 accompanying this paper. The count rates of measured and simulated peaks were compared (Fig. 9.) and it was found that the simulated peaks fit the experimental ones very reasonably. There are only two outliers that cannot be explained by statistical uncertainties visible in the plot, ^7Li (477.61 keV) and ^{208}Pb (2614.51 keV) peaks discussed above. The simulated annihilation peak fits the measured one very well. Very high uncertainties of the rest of the peaks, did not allow us to make their rigorous quantitative comparison. There is tendency to underestimate the simulated peak count rates, what is understandable due to complexity of interactions leading to induction of these peaks. Certain processes cannot be simulated by GEANT4 at all.

No information about radionuclide contamination of different parts of the setup was available, therefore, no rigorous simulation of the background spectrum due to the contamination was possible. Moreover, a large part of the measured count rates (with the exception of ^{40}K), may be caused by presence of radon (^{222}Rn) and thoron (^{220}Rn) in the detector construction and shielding materials, and their decay close to the

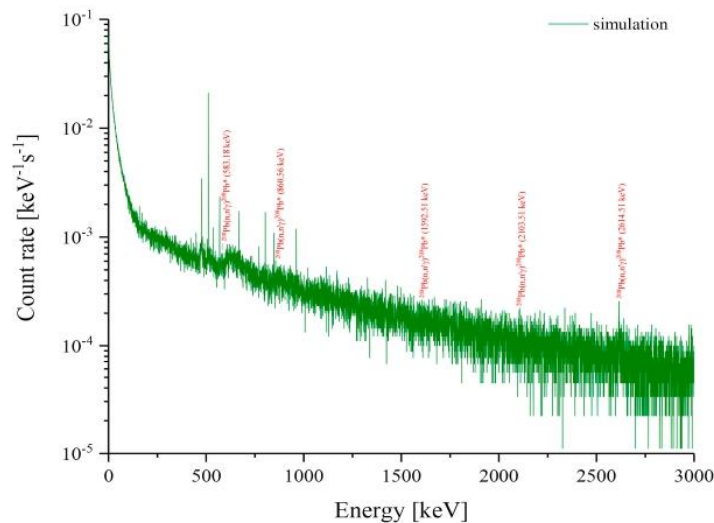


Fig. 7. Simulation with those γ -rays of ^{208}Pb coming from inelastic scattering of neutrons on lead nuclei, which correspond to γ -rays of ^{208}Tl decay if thallium is present in the setup.

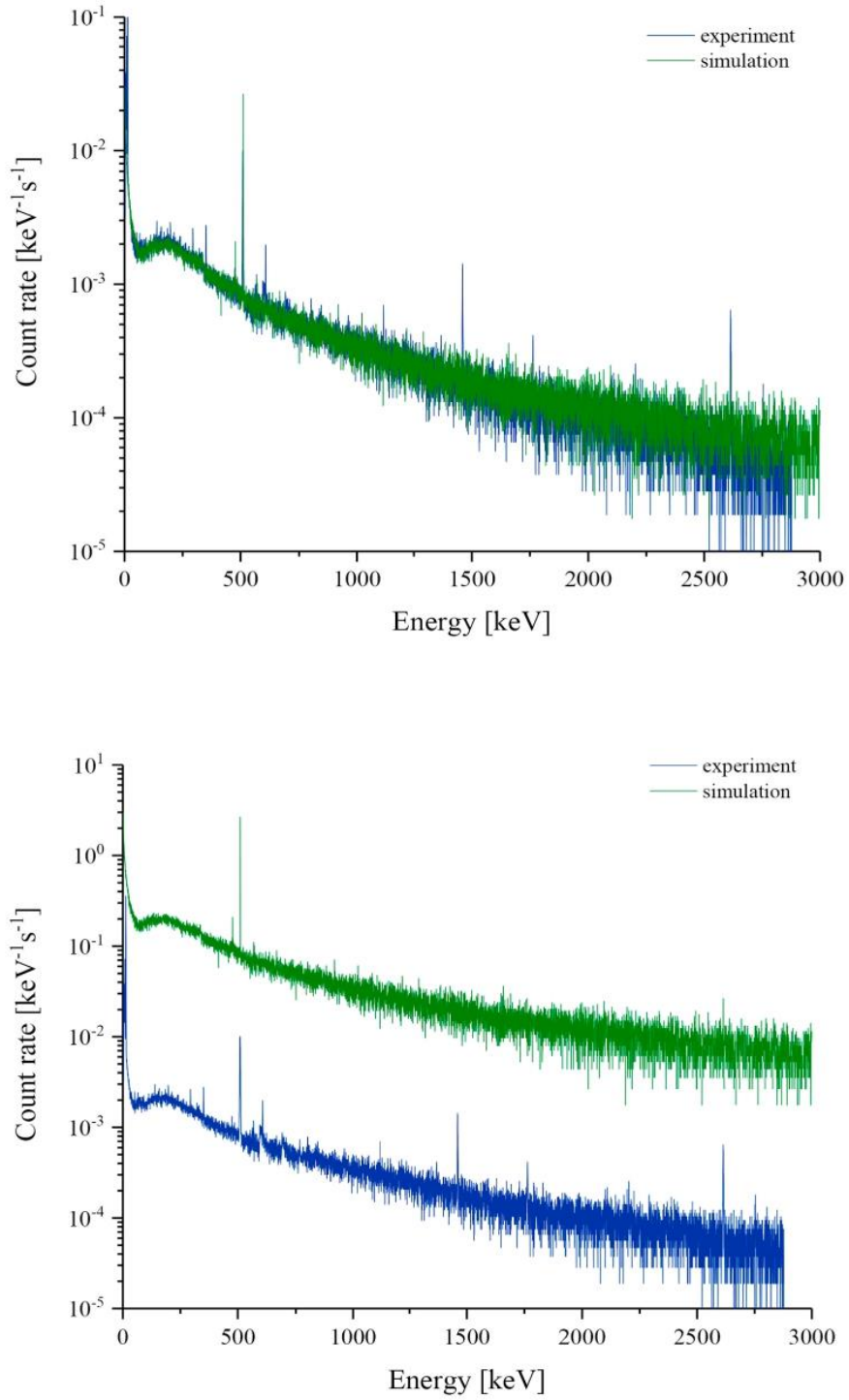


Fig. 8. Comparison of the experimental spectrum and the simulated spectrum when the concrete building was included in the setup. The simulated spectrum shown in the bottom figure has been multiplied by 100 for better visibility.

Table 1

Calculated count rates in measured background γ -ray spectrum and simulated ones with and without the shielding layer of the building (uncertainties are quoted at 1σ).

Energy peaks [keV]	Nuclides and Reactions	Count rates $\times 10^{-5} [s^{-1}]$		
		Experiment	Simulation (without concrete building)	Simulation (with concrete building)
50–2875	Continuum	$(1.26 \pm 0.07) \times 10^5$		$(1.25 \pm 0.13) \times 10^5$
500–2875	Continuum	$(0.56 \pm 0.03) \times 10^5$	$(0.53 \pm 0.06) \times 10^5$	
53.44	$^{73}\text{Ge} (n, n' \gamma)^{73}\text{Ge}^*$	30 ± 13	32 ± 25	26 ± 13
72.81	X-rays of ^{206}Pb	10 ± 6	12 ± 9	12 ± 6
74.97	X-rays of ^{206}Pb	27 ± 13	13 ± 9	20 ± 12
89.18	$^{65}\text{Cu}(n, \gamma)^{65}\text{Cu}^*$	10 ± 6	18 ± 8	10 ± 6
139.68	$^{74}\text{Ge} (n, \gamma)^{75}\text{Ge}^*$	31 ± 14	22 ± 13	27 ± 13
158.56	$^{117}\text{Sn}(n, n' \gamma)^{117}\text{Sn}^*$	14 ± 7	21 ± 12	9 ± 6
212.38	$^{63}\text{Cu}(n, \gamma)^{64}\text{Cu}^*$	35 ± 13	21 ± 16	30 ± 13
237.82	$^{65}\text{Cu}(n, \gamma)^{66}\text{Cu}^*$	39 ± 13	20 ± 10	38 ± 19
295.22	$^{214}\text{Pb}(\beta \text{ decay})^{214}\text{Bi}^*$	101 ± 20	–	–
351.93	$^{214}\text{Pb}(\beta \text{ decay})^{214}\text{Bi}^*$	146 ± 19	–	–
477.61	$^{10}\text{B} (n, \alpha)^7\text{Li}$	22 ± 8	120 ± 12	51 ± 10
511.0	Annihilation	814 ± 46	757 ± 49	943 ± 69
537.47	$^{206}\text{Pb}(n, n' \gamma)^{206}\text{Pb}^*$	15 ± 10	23 ± 9	17 ± 4
562.93	$^{76}\text{Ge} (n, n' \gamma)^{76}\text{Ge}^*$	8 ± 4	4 ± 3	13 ± 7
569.70	$^{207}\text{Pb}(n, n' \gamma)^{207}\text{Pb}^*$	21 ± 9	42 ± 6	15 ± 4
583.19	$^{206}\text{Pb}(n, n' \gamma)^{206}\text{Pb}^*$	12 ± 8	7 ± 4	5 ± 3
595.84	$^{74}\text{Ge} (n, n' \gamma)^{74}\text{Ge}^*$	33 ± 13	18 ± 11	21 ± 11
609.32	$^{214}\text{Bi}(\beta \text{ decay})^{214}\text{Po}^*$	206 ± 23	–	–
691.43	$^{72}\text{Ge} (n, n' \gamma)^{72}\text{Ge}^*$	28 ± 11	12 ± 8	11 ± 7
708.19	$^{70}\text{Ge} (n, \gamma)^{71}\text{Ge}^*$	14 ± 7	10 ± 8	6 ± 3
770.60	$^{65}\text{Cu}(n, n' \gamma)^{65}\text{Cu}^*$	11 ± 7	10 ± 4	13 ± 7
803.06	$^{206}\text{Pb}(n, n' \gamma)^{206}\text{Pb}^*$	29 ± 11	36 ± 6	24 ± 10
846.76	$^{56}\text{Fe} (n, n' \gamma)^{56}\text{Fe}^*$	17 ± 7	9 ± 3	8 ± 3
860.56	$^{206}\text{Pb}(n, n' \gamma)^{206}\text{Pb}^*$	10 ± 6	5 ± 3	7 ± 3
924.50	$^{65}\text{Cu}(n, n' \gamma)^{65}\text{Cu}^*$	7 ± 3	5 ± 3	6 ± 5
955.0	$^{63}\text{Cu}(n, n' \gamma)^{63}\text{Cu}^*$	6 ± 3	11 ± 6	5 ± 3
962.06	$^{63}\text{Cu}(n, n' \gamma)^{63}\text{Cu}^*$	12 ± 7	28 ± 5	15 ± 6
966.0	$^{120}\text{Sn}(n, \gamma)^{121}\text{Sn}^*$	10 ± 5	8 ± 3	5 ± 3
978.80	$^{65}\text{Cu}(n, n' \gamma)^{65}\text{Cu}^*$	8 ± 3	6 ± 3	4 ± 2
1039.51	$^{70}\text{Ge} (n, n' \gamma)^{70}\text{Ge}^*$	13 ± 5	13 ± 8	6 ± 3
1050.90	$^{206}\text{Pb}(n, n' \gamma)^{206}\text{Pb}^*$	6 ± 3	4 ± 2	6 ± 3
1067.66	$^{76}\text{Ge} (n, \gamma)^{77}\text{Ge}^*$	9 ± 5	6 ± 3	5 ± 3
1108.41	$^{76}\text{Ge} (n, n' \gamma)^{76}\text{Ge}^*$	21 ± 5	11 ± 6	10 ± 5
1120.29	$^{214}\text{Bi}(\beta \text{ decay})^{214}\text{Po}^*$	17 ± 7	–	–
1129.90	$^{54}\text{Fe} (n, n' \gamma)^{54}\text{Fe}^*$	16 ± 8	11 ± 6	10 ± 5
1153.10	$^{54}\text{Fe} (n, n' \gamma)^{54}\text{Fe}^*$	6 ± 3	4 ± 2	7 ± 5
1165.21	$^{63}\text{Cu}(n, \gamma)^{64}\text{Cu}^*$	14 ± 5	10 ± 5	11 ± 5
1173.23	$^{60}\text{Co}(\beta \text{ decay})^{60}\text{Ni}^*$	9 ± 5	–	–
1204.20	$^{74}\text{Ge} (n, n' \gamma)^{74}\text{Ge}^*$	10 ± 5	8 ± 5	4 ± 2
1245.20	$^{63}\text{Cu}(n, n' \gamma)^{63}\text{Cu}^*$	4 ± 2	3 ± 2	4 ± 2
1261.0	$^{65}\text{Cu}(n, n' \gamma)^{65}\text{Cu}^*$	13 ± 7	10 ± 5	10 ± 4
1303.40	$^{56}\text{Fe} (n, n' \gamma)^{56}\text{Fe}^*$	18 ± 6	10 ± 5	10 ± 4
1332.51	$^{60}\text{Co}(\beta \text{ decay})^{60}\text{Ni}^*$	14 ± 6	–	–
1335.40	$^{56}\text{Fe} (n, n' \gamma)^{56}\text{Fe}^*$	14 ± 4	8 ± 5	7 ± 4
1345.84	$^{64}\text{Cu}(\epsilon \text{ decay})^{64}\text{Ni}^*$	16 ± 7	7 ± 4	6 ± 2
1353.94	$^{76}\text{Ge} (n, \gamma)^{77}\text{Ge}^*$	11 ± 4	8 ± 5	5 ± 2
1368.63	$^{24}\text{Na} (\beta \text{ decay})^{24}\text{Mg}^*$	13 ± 8	7 ± 5	6 ± 4
1421.20	$^{116}\text{Sn}(n, n' \gamma)^{116}\text{Sn}^*$	10 ± 4	6 ± 4	6 ± 2
1446.87	$^{76}\text{Ge} (n, \gamma)^{77}\text{Ge}^*$	7 ± 4	6 ± 4	6 ± 4
1460.80	$^{40}\text{K} (\beta \text{ decay})^{40}\text{Ar}^*$	115 ± 16	–	–
1463.75	$^{74}\text{Ge} (n, n' \gamma)^{74}\text{Ge}^*$	5 ± 2	9 ± 4	10 ± 4
1476.75	$^{116}\text{Sn}(n, n' \gamma)^{116}\text{Sn}^*$	13 ± 4	6 ± 4	10 ± 4
1489.35	$^{74}\text{Ge} (n, n' \gamma)^{74}\text{Ge}^*$	11 ± 4	5 ± 4	5 ± 2
1511.0	$^{206}\text{Pb}(n, \gamma)^{206}\text{Pb}^*$	9 ± 4	4 ± 2	4 ± 2
1592.51	Single escape peak of 2614.51 keV	12 ± 6	14 ± 7	7 ± 4
1620.30	$^{206}\text{Pb}(n, n' \gamma)^{206}\text{Pb}^*$	6 ± 4	7 ± 4	7 ± 4
1630.10	$^{63}\text{Cu}(n, \gamma)^{64}\text{Cu}^*$	6 ± 4	8 ± 5	4 ± 2
1656.20	$^{206}\text{Pb}(n, \gamma)^{206}\text{Pb}^*$	5 ± 3	6 ± 4	10 ± 4
1756.70	$^{74}\text{Ge} (n, n' \gamma)^{74}\text{Ge}^*$	7 ± 3	9 ± 4	5 ± 2
1764.49	$^{214}\text{Bi}(\beta \text{ decay})^{214}\text{Po}^*$	26 ± 9	–	–
1790.30	$^{63}\text{Cu}(n, \gamma)^{64}\text{Cu}^*$	5 ± 2	4 ± 2	3 ± 3
1832.0	$^{65}\text{Cu}(n, n' \gamma)^{65}\text{Cu}^*$	9 ± 5	9 ± 6	5 ± 3
1861.30	$^{63}\text{Cu}(n, n' \gamma)^{63}\text{Cu}^*$	8 ± 3	10 ± 3	5 ± 3
1917.90	$^{54}\text{Fe} (n, \gamma)^{55}\text{Fe}^*$	6 ± 3	8 ± 4	8 ± 3
1927.20	$^{63}\text{Cu}(n, n' \gamma)^{63}\text{Cu}^*$	8 ± 3	10 ± 4	7 ± 3
1985.73	$^{65}\text{Cu}(n, \gamma)^{66}\text{Cu}^*$	5 ± 2	6 ± 2	4 ± 2
2103.51	Double escape peak of 2614.51 keV	8 ± 3	10 ± 4	6 ± 3
2108.24	$^{27}\text{Al} (n, \gamma)^{28}\text{Al}^*$	4 ± 2	5 ± 2	7 ± 3
2144.22	$^{65}\text{Cu}(n, \gamma)^{66}\text{Cu}^*$	6 ± 3	7 ± 4	4 ± 2
2202.70	$^{56}\text{Fe} (n, \gamma)^{57}\text{Fe}^*$	4 ± 2	5 ± 2	4 ± 2

(continued on next page)

Table 1 (continued)

Energy peaks [keV]	Nuclides and Reactions	Count rates $\times 10^{-5} [s^{-1}]$		
		Experiment	Simulation (without concrete building)	Simulation (with concrete building)
2212.01	$^{27}\text{Al} (n, n'\gamma)^{27}\text{Al}^*$	6 ± 3	8 ± 4	4 ± 1
2224.56	$^1\text{H} (n, \gamma)^2\text{H}$	6 ± 3	7 ± 3	6 ± 3
2291.42	$^{63}\text{Cu} (n, \gamma)^{64}\text{Cu}^*$	8 ± 3	4 ± 2	8 ± 4
2322.65	$^{208}\text{Pb} (n, n'\gamma)^{208}\text{Pb}^*$	6 ± 2	8 ± 3	4 ± 3
2353.46	$^{73}\text{Ge} (n, \gamma)^{74}\text{Ge}^*$	5 ± 3	7 ± 3	4 ± 3
2402.70	$^{74}\text{Ge} (n, n'\gamma)^{74}\text{Ge}^*$	5 ± 2	6 ± 3	5 ± 4
2411.58	$^{65}\text{Cu} (n, \gamma)^{66}\text{Cu}^*$	4 ± 1	4 ± 2	5 ± 3
2478.20	$^{65}\text{Cu} (n, \gamma)^{66}\text{Cu}^*$	4 ± 1	4 ± 2	4 ± 3
2512.0	$^{63}\text{Cu} (n, n'\gamma)^{63}\text{Cu}^*$	4 ± 2	5 ± 3	4 ± 2
2614.51	$^{208}\text{Pb} (n, n'\gamma)^{208}\text{Pb}^*$	48 ± 14	24 ± 7	17 ± 4
2619.14	$^{65}\text{Cu} (n, \gamma)^{66}\text{Cu}^*$	4 ± 2	5 ± 3	5 ± 3
2682.0	$^{208}\text{Pb} (n, n'\gamma)^{208}\text{Pb}^*$	4 ± 2	5 ± 3	2 ± 1
2696.60	$^{63}\text{Cu} (n, n'\gamma)^{63}\text{Cu}^*$	4 ± 2	5 ± 3	4 ± 2
2736.46	$^{207}\text{Pb} (n, n'\gamma)^{207}\text{Pb}^*$	5 ± 2	3 ± 1	3 ± 2
2754.01	$^{24}\text{Na} (\beta \text{ decay})^{24}\text{Mg}^*$	4 ± 3	4 ± 3	3 ± 1
2806.90	$^{65}\text{Cu} (n, \gamma)^{66}\text{Cu}^*$	5 ± 2	7 ± 3	3 ± 1
2838.20	$^{63}\text{Cu} (n, \gamma)^{64}\text{Cu}^*$	4 ± 2	5 ± 3	8 ± 3
2850.30	$^{116}\text{Sn} (n, n'\gamma)^{116}\text{Sn}^*$	4 ± 1	4 ± 1	4 ± 2
2862.70	$^{65}\text{Cu} (n, n'\gamma)^{65}\text{Cu}^*$	3 ± 1	4 ± 1	4 ± 2

Ge detector (Vojtyla, 1995), as the laboratory did not have a ventilation system removing these inert gases and their progeny from the ambient air. The average activities of radon and thoron in the shield may vary with time and their reliable quantification is difficult. Investigation of the effect of material contamination may be a subject of further studies if the material contamination will be known. Other background sources than radioactive contamination dominate the background continuum in systems of this class located in surface laboratory.

The continuum in HPGe background spectrum is formed mainly by muon and neutron interactions. Neutrons interacting with the detector materials, especially with lead, produce many photons contributing to the continuum, while muons contribute via bremsstrahlung of delta electrons. A continuum is, however, not induced only by cosmic ray

particles. Part of it is formed by radioactive contaminants present in the system. Further contributors are, therefore, β -rays originating from decaying radionuclides and Compton scattering coming from interactions of high-energy photons (Povinec, 2007). In particular, commercial lead used for shielding of HPGe detectors is contaminated with ^{210}Pb . In surface laboratories this background component is not distinguishable from the low-energy part of continuum induced mainly by muons (Vojtyla, 1996a).

To estimate the contribution of radioactive contamination to the detector continuum, a number of simulations with ^{230}U , ^{232}Th , and ^{40}K in the setup materials, and ^{222}Rn in air inside the shield cavity were run. The resulting simulation spectra were normalized so that the simulated and the experimental count rates of the contamination peaks agreed

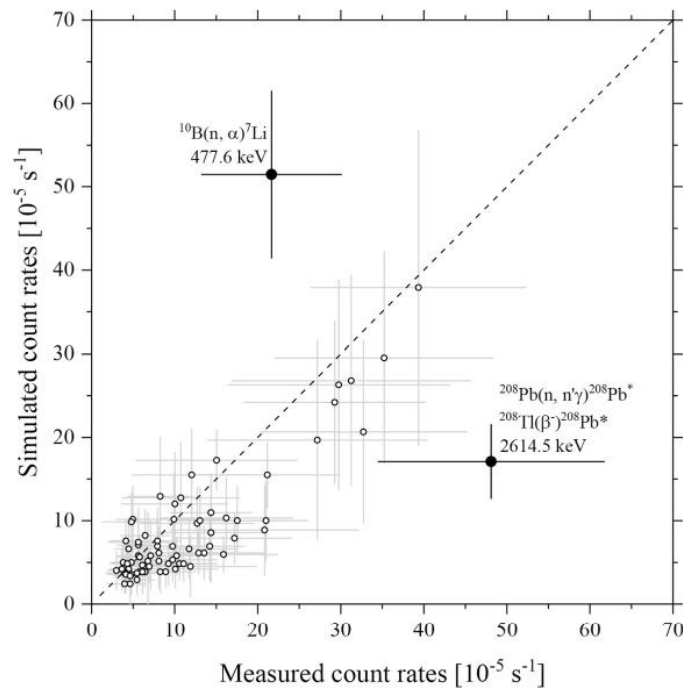


Fig. 9. Comparison of the experimental and simulated peak count rates.

while assuming that 35% of the ^{208}Tl peak at 2614.5 keV was induced by neutrons. It was found that the simulated integral count rate $0.033 \pm 0.006 \text{ s}^{-1}$ (50–2875 keV) due to radioactive contamination of the simulated spectrum made 2.6% of the total experimental integral count rate $1.26 \pm 0.07 \text{ s}^{-1}$. This figure perfectly agrees with the fraction of integral count rate of 2.4% obtained by subtracting the simulated spectrum from the experimental one. Indeed, continua observed in the experimental spectra of low-level HPGe spectrometers operating in surface or shallow laboratories are mostly induced by cosmic rays.

5.2.3. Comparison of the simulated results with published works

Although the GEANT4 code has been originally developed for high energy physics, after many applications in low energy nuclear physics it has proved to be a well-suited code for estimation of neutron fluxes and their interactions with nuclei in surface as well as in underground laboratories (Baginova et al., 2018; Kudryavtsev et al., 2008). The second important input in the simulations is the neutron transport in matter. GEANT4 has been successfully used for neutron tracking in the energy range of interest and in the materials, which were used in the present investigations. The GEANT4 ability to model neutron propagation through matter has been confirmed with cosmic-ray neutrons as well with neutrons from neutron sources (e.g., Ljungvall and Nyberg, 2005; Baginova et al., 2018).

Successful simulations of neutron-induced reactions we need to use accurate correct neutron cross-section data. We already discussed in detail neutron cross-sections we used in this work, and on the basis of our previous experiences (Kudryavtsev et al., 2008; Baginova et al., 2018) we may confirm that the most recent cross-sections were used in the presented calculations.

However, the best way how to validate the model is to compare the simulation products with the experiment, as well as with similar already published results. The simulated results are reliable and they agree with the experimental data (Figs. 8., 9.), as well as with published data.

Several papers have already been dealing with Monte Carlo simulations of background of HPGe detectors operating in surface or shallow underground laboratories (e.g. Vojtyla, 1995, 1996b; Povinec et al., 2008; Breier and Povinec, 2009; Hung et al., 2017).

From the experimental point of view, the γ -lines identified in the experimental background spectrum, which are due to neutron interactions with HPGe detector materials were also seen in previous investigations of neutron-induced γ -ray spectra (Chao, 1993; Vojtyla et al., 1994, Ljungvall and Nyberg, 2005; Jovancevic et al., 2010; Baginova et al., 2018).

The shape of the background γ -ray spectrum was dominated by muon-induced hump with the maximum at energy of 185 keV, similarly as it was observed in previous investigations (Vojtyla et al., 1994, Vojtyla, 1995; Breier and Povinec, 2009; Hung et al., 2017). This background γ -ray spectrum feature is well visible in the experimental (Fig. 3.) as well as in the simulated spectra (Fig. 8.), in agreement with previous measurements and Monte Carlo simulations in the above mentioned works. In (Hung et al., 2017) a SEGe detector with a relative efficiency of 20% was used in an experiment and coded into GEANT4 simulation. The simulated count rate on the top of the hump was about $7.6 \times 10^{-4} \text{ keV}^{-1}\text{s}^{-1}$. After normalization of our value of $2.2 \times 10^{-4} \text{ keV}^{-1}\text{s}^{-1}$ to a 20% detector, one obtains $8.8 \times 10^{-4} \text{ keV}^{-1}\text{s}^{-1}$ indicating a good agreement. In the higher energy part of the continuum at 2000 keV (Hung et al., 2017), got $4.0 \times 10^{-5} \text{ keV}^{-1}\text{s}^{-1}$ to be compared with the value from this work of $1.1 \times 10^{-5} \text{ keV}^{-1}\text{s}^{-1}$. Scaling this value to a 20% detector leads to a spectral count rate of $4.4 \times 10^{-5} \text{ keV}^{-1}\text{s}^{-1}$, which is consistent with the figure from (Hung et al., 2017).

The count rate on the top of the hump in (Vojtyla, 1995) calculated with a 35% HPGe detector is about $1.6 \times 10^{-3} \text{ keV}^{-1}\text{s}^{-1}$ (Fig. 6. in the reference). After normalization to 50% relative efficiency, one obtains $1.5 \times 10^{-3} \text{ keV}^{-1}\text{s}^{-1}$.

In the work (Breier and Povinec, 2009), the cosmic-ray background of an HPGe detector with a relative efficiency of 70% in various shields

Table 2
Comparison of simulated cosmic-ray spectra from the literature.

Size	Reference	(1)	(2)	(3)	(4)
		$\text{keV}^{-1}\text{s}^{-1}$			
20%	Hung et al., 2017	7.6×10^{-4}	8.8×10^{-4}	4.0×10^{-5}	4.4×10^{-5}
35%	Vojtyla et al., 1995	1.6×10^{-3}	1.5×10^{-3}	–	–
50%	This work	2.2×10^{-3}	2.2×10^{-3}	1.1×10^{-4}	1.1×10^{-4}
70%	Breier and Povinec, 2009	1.6×10^{-3}	3.1×10^{-3}	–	–

¹ Spectral count rate on the top of the hump as obtained from the Reference.

² Spectral count rate on the top of the hump from this work normalized to the given relative efficiency.

³ Spectral count rate at 2 MeV as obtained from the Reference.

⁴ Spectral count rate at 2 MeV from this work normalized to the given relative efficiency.

placed on the surface and 10 m. w.e. underground was simulated. The count rate at the maximum of the 200 keV hump shown in Fig. 5. in reference (10 cm lead shield) is about $1.6 \times 10^{-3} \text{ s}^{-1}$. After normalization of our hump count rate to the 70% efficiency one gets $3.1 \times 10^{-3} \text{ keV}^{-1}\text{s}^{-1}$.

Values obtained from different sources are summarized in Table 2. The results in this work agree fairly well with the data from the literature if they are normalized to the relative efficiency of the given detector, except the work (Breier and Povinec, 2009). The simulated shield was made only of lead, while the other simulated shields were lined from the inner side with descending-Z layers (e.g. Sn and Cu, Cd and Cu) (Vojtyla, 1996b). showed that the height of the spectrum hump depended strongly on Z of the innermost shield material – the heavier the material was – the lower was the hump maximum count rate. In the extreme case of a purely lead shield and a purely copper shield, the latter shield provided a count rate 4.5 higher compared with the one of the former shield. The difference in the lining material could explain the lower values reported in (Breier and Povinec, 2009).

The annihilation peak dominated in all experimental and simulated spectra of the above mentioned studies. Nevertheless, the triangular germanium peaks are observable only in our and (Vojtyla et al., 1995) measured background spectra. The visibility of such peaks is highly affected by relative efficiency and resolution of the used HPGe detector, and by a sufficiently long measuring time. In simulated spectra these peaks are not well visible, because GEANT4 is not yet capable to simulate correctly the processes leading to these peaks. The integral count rate of the background simulated in this work of $1.25 \pm 0.13 \text{ s}^{-1}$ is within the range of 0.6–1.6 s^{-1} stated in (Povinec, 2012).

6. Material optimization

In addition to passive cosmic-ray flux reduction and anti-coincidence pulse-rejection techniques, material selection with regard to nuclear interactions is a way of lowering the cosmic-ray induced background.

Besides germanium, copper and lead are the most significant contributors to the neutron background. Copper and lead peaks evidently dominate in all three spectra. All γ -lines produced in neutron interactions with these materials form together a strong source of the neutron background. This source of background is specifically disturbing, because it covers large part of the energy range of HPGe detector and like this, it can easily hide or imitate the searched signal. To find the real signal is extremely important for experiments looking for rare events. For example, the γ -rays coming from neutron inelastic scattering or neutron capture can imitate the signature of the neutrinoless $\beta\beta$ decay (Kudryavtsev et al., 2008). In addition, some of the ^{208}Pb peaks are enhanced by the γ -rays from β -decay of ^{208}Tl . The best way how to avoid such large amount of neutron induced peaks from lead and copper is to

replace them by other types of materials or at least combine them with neutron reducing materials.

Similarly, γ -lines of tin contribute to neutron background. Neutrons interacting with tin parts of the setup, especially with the tin layer of the shield produce many γ -rays. Avoid this contributor is possible by omitting the tin from the setup, especially from the shielding. Shields in deep underground experiments are made mostly of pure lead, so there is no tin present.

Aluminium and iron have a few γ -lines in the background spectrum produced by neutron interactions. They are certainly less significant background components than lead or copper but they contribute to neutron background, too. Aluminium is the most commonly used material for cryostats, entrance windows and sometimes also for crystal holders. Thus, the aluminium peaks will be permanently present in the background spectrum, but reduction of neutron flux can help to minimize them. Iron is usually minimally used as material in the detector setup. There is certain amount of iron in the cooling tube delivering the liquid nitrogen to the detector, but its influence can be eliminated by suitable placing of the shield around the detector, which will shield the tube. Simply, forego the iron peaks is possible by excluding the iron materials from the setup.

The peaks of natural radionuclides coming from contamination of the detector parts, the shield and surrounding form together the γ -ray induced background. To eliminate these peaks is difficult because the radionuclides are present everywhere and they are permanently produced by decay of members of uranium and thorium series. To minimize the influence of γ -rays from natural radionuclides, it is necessary to use ultra-high purity materials for experimental setups and to predict the amount of the contaminants and their activity. The reduction of such peaks is possible using an appropriate shielding, too. Anyway, even in deep underground laboratories is contamination still present.

7. Conclusions

The presented work deals with experimental and theoretical (GEANT4) investigations of background induction mechanisms of a low-level 50% p-type HPGe gamma spectrometer placed in a descending-Z lead shield (Pb-Sn-Cu). The whole system is located on the surface, on the ground floor of a 3-storey building providing around 1 m of concrete bulk shielding. Particular attention is given to clarifying the role of secondary and tertiary cosmic-ray neutrons.

A very good agreement, qualitative as well as quantitative, between the measured and simulated spectra was achieved, confirming that GEANT4 is a suitable detector simulation tool for this type of studies, even if very complex neutron interactions with matter are involved. Nevertheless, triangular peaks, which are characteristic of neutron interactions with Ge crystals, cannot be reproduced correctly at present. The shapes of these peaks reflect particularities of the detection mechanism such as the recoil dynamics and plasma effects in charge collection.

The background continuum in an HPGe system of this class (low-level in a surface building with moderate overhead shielding) is generated mostly by cosmic-ray muons and tertiary cosmic-ray neutrons. The latter are responsible for almost all γ -ray lines of cosmic-ray origin in the background spectrum. The main sources of neutron-induced γ -rays are, except the Ge crystal, lead, copper and tin present in the construction materials of the HPGe detector and in the shield. An extensive list of γ -lines potentially visible in a background spectrum was compiled and the main nuclear reactions generating them were identified. It was found, that the source of the well-known 2614.51 keV peak is not exclusively the β -decay of ^{208}Tl from the ^{232}Th decay series to an excited state of the stable daughter nuclide ^{208}Pb . The inelastic neutron scattering on ^{208}Pb nuclei abundantly present in the lead shield contributes by about 35% to this peak.

Below about 500 keV, the shape of the background continuum predominantly generated by cosmic rays (mainly by muons and neutrons)

in our case depends considerably on the thickness of the overhead concrete bulk shielding associated with the building in which the system is located. Generally, there has been reasonable agreement between the measured and simulated background γ -ray spectra. The final integral counting rates for measured spectrum in the energy range from 50 keV to 2875 keV was $1.26 \pm 0.07 \text{ s}^{-1}$ and for simulated one $1.25 \pm 0.13 \text{ s}^{-1}$, indicating a good agreement with the experiment.

Peaks caused by radioactive contamination of the system were detected and traced to the primordial ^{40}K and a few members of the ^{238}U and ^{232}Th decay series (^{214}Bi , ^{214}Pb , ^{208}Tl). Yet, in the case of the present system, the lack of knowledge of construction material contamination and probable interference of radon and thoron entering the shield cavity did not allow us to investigate this background source theoretically. The issue can be a subject of further studies for detector systems with known contamination placed in rooms with radon and thoron free air.

Although Pb and Cu are very popular materials for construction of low-level HPGe detector systems thanks to their costs and achievable purity, they are not the ideal choice as far as the neutron background is concerned. Interaction cross-sections are large and too many γ -rays are produced in nuclear reactions of various types. Tin should be also avoided as a construction material.

Apparently, no ideal solution is available when dealing with construction materials, however, deeper knowledge of the topic and the tools used in this work are useful in the search for an optimum.

CRedit authorship contribution statement

M. Baginova: Conceptualization, Methodology, Software, Formal analysis, Investigation, Data curation, Writing - original draft. **P. Vojtyla:** Resources, Writing - review & editing. **P.P. Povinec:** Supervision, Writing - review & editing.

Declaration of competing interest

The authors declare that they have no known competing financial interests or personal relationships that could have appeared to influence the work reported in this paper.

Acknowledgments

The authors are thankful to CERN for providing PhD fellowship to Miloslava Baginova. Special thanks to Fabrice Malacrida for his help with the experiment. Support provided by the Slovak Research and Development Agency (APVV-15-0576) is highly acknowledged.

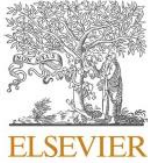
References

- Abdelhameed, A.H., et al., 2019. Geant4-based electromagnetic background model for the CRESST dark matter experiment. *Eur. Phys. J. C* 79, 881.
- Adhikari, G., et al., 2018. Initial performance of the COSINE-100 experiment. *Eur. Phys. J. C* 78, 107.
- Agostinelli, S., et al., 2003. Geant4 – a simulation toolkit. *Nucl. Instrum. Methods Phys. Res.* 506, 250–303.
- Allison, J., et al., 2006. Geant4 developments and applications. *IEEE Trans. Nucl. Sci.* 53, 270–278.
- Allison, J., et al., 2016. Recent developments in Geant4. *Nucl. Instrum. Methods Phys. Res.* 835, 186–225.
- Armengaud, E., et al., 2017. Performance of the EDELWEISS-III experiment for direct dark matter searches. *J. Inst. Met.* 12, P08010.
- Baginova, M., Vojtyla, P., Povinec, P.P., 2018. Investigation of neutron interactions with Ge detectors. *Nucl. Instrum. Methods Phys. Res.* 897, 22–31.
- Bogdanova, L.N., et al., 2006. Cosmic muon flux at shallow depth underground. *Phys. Atom. Nucl.* 69, 1328–1333.
- Breier, R., Povinec, P.P., 2009. Monte Carlo simulation of background characteristics of low-level gamma-spectrometers. *J. Radioanal. Nucl. Chem.* 799–804.
- Chao, J.H., 1993. Neutron-induced gamma-rays in germanium detectors. *Appl. Radiat. Isot.* 44, 605–611.
- Geant4 Collaboration. Introduction to Geant4. available at: <http://geant.cern.ch/> (accessed on June 19th, 2019).
- Greider, P.K.F., 2001. Cosmic Rays at Earth. *Researcher's Reference and Data Book Manual*, first ed. Elsevier, Amsterdam.

- Hung, N.Q., et al., 2017. Investigation of cosmic-ray induced background of Germanium gamma spectrometer using GEANT4 simulation. *Appl. Radiat. Isot.* 121, 87–90.
- Jovancevic, N., et al., 2010. Neutron induced background gamma activity in low-level Ge-spectroscopy systems. *Nucl. Instrum. Methods Phys. Res.* 612, 303–308.
- Kauer, M., The SuperNEMO Collaboration 2008, 2009. Calorimeter R&D for the SuperNEMO double beta decay experiment. *J. Phys.: Conf. Ser.* 160, 012031.
- Kudryavtsev, V.A., et al., 2008. Neutron- and muon-induced background in underground physics experiments. *Europ. Phys. J. A* 36, 171–180.
- Ljungvall, J., Nyberg, J., 2005. A study of fast neutron interactions in high-purity germanium detectors. *Nucl. Instrum. Methods Phys. Res.* 546, 553–573.
- Medhat, M.E., Wang, Y., 2014. Estimation of background spectrum in a shielded HPGe detector using Monte Carlo simulations. *Appl. Radiat. Isot.* 84, 13–18.
- Nuclear Data Center. Japan atomic energy agency (JAEA). available at: <http://www.ndc.jaea.go.jp/jendl/j40/j40.html> (accessed on June 19th, 2019).
- Povinec, P.P., 2007. *Analysis of Environmental Radionuclides*, first ed. Elsevier, Oxford.
- Povinec, P.P., et al., 2008. New isotope technologies in environmental physics. *Acta Phys. Slovaca* 58 (1), 1–154.
- Povinec, P.P., 2012. New gamma-spectrometry technologies for environmental sciences. *J. Analyt. Sci. Tech.* 42–71.
- Shun-Li, N., et al., 2015. Simulation of background reduction and Compton suppression in a low-background HPGe spectrometer at a surface laboratory. *Chin. Phys. C* 39, 086002.
- Sternfelsa, M.M., Lowenheim, F.A., 1942. Tin plating from the potassium stannate bath. *J. Electrochem. Soc.* 82, 77–100.
- Vojtyla, P., et al., 1994. Experimental and simulated cosmic muon induced background of a Ge spectrometer equipped with a top side anticoincidence proportional chamber. *Nucl. Instrum. Methods Phys. Res. B* 86, 380–386.
- Vojtyla, P., 1995. A computer simulation of the cosmic-muon background induction in a Ge γ -spectrometer using GEANT. *Nucl. Instrum. Methods Phys. Res. B* 100, 87–96.
- Vojtyla, P., 1996a. Fast computer simulations of background of low-level Ge γ -spectrometers induced by $^{210}\text{Pb}/^{210}\text{Bi}$ in shielding lead. *Nucl. Instrum. Methods Phys. Res. B* 117, 189–198.
- Vojtyla, P., 1996b. Influence of shield parameters on cosmic-muon induced backgrounds of Ge γ -spectrometers. *Nucl. Instrum. Methods Phys. Res. B* 111, 163–170.
- Ziegler, J.F., 1996. Terrestrial cosmic rays. *IBM J. Res. Dev.* 40 (1), 19–39.

Effect of neutrons on background of HPGe detectors operating deep underground

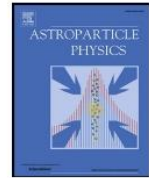
Astroparticle Physics 143 (2022) 102756



Contents lists available at ScienceDirect

Astroparticle Physics

journal homepage: www.elsevier.com/locate/astropartphys



The effect of neutrons on the background of HPGe detectors operating deep underground

M. Baginova^{a,b,*}, P. Vojtyla^a, P.P. Povinec^b

^a CERN, Geneva 1211, Switzerland

^b Faculty of Mathematics, Physics and Informatics, Comenius University, Mlynska dolina F1, 842 48 Bratislava, Slovakia

ARTICLE INFO

Keywords:

Monte Carlo simulation
Neutron induced background
GEANT4
Underground experiments
High-Purity Ge detectors

ABSTRACT

The background of a High Purity Germanium (HPGe) detector measured in a deep underground laboratory was investigated analytically and by Monte Carlo simulations using the GEANT4 toolkit. Contributions of different background sources to the experimental γ -ray background were determined. Namely, contribution of radionuclides in materials of the detector and around the detector, neutrons produced by (α, n) reactions due to presence of radionuclides in rock and concrete and by spontaneous fission of mainly ^{238}U , and finally, cosmic rays with neutron generation. The simulation, including radionuclides in the material, was in a good agreement with the experiment. At the same time, neutron and muon induced spectra were simulated. The radiation coming from the presence of members of the ^{238}U , and ^{232}Th decay series, and ^{40}K in the detector parts and the laboratory walls contribute to the continuum of the experimental spectrum at the level of around 94%. According to simulations, the contribution of muon events to the experimental energy spectrum was below 1% and it was confirmed that muon induced spectra are about three orders of magnitude lower than the experimental one. The comparison of integral count rates of the experimental spectrum with the simulated spectrum induced by neutrons showed that about 6% of the measured background continuum originated from neutron reactions. Fast neutrons contributed more to the background (at around 65%) than thermal neutrons. Despite only a 6% share of neutron contributions in the total γ -ray background, they contributed mainly to the lower continuum of the spectrum up to 250 keV, which is a region of interest for potential low mass weakly interacting massive particle (WIMP) dark matter interactions. In addition, they interact with the detector and the shield by inelastic scattering and induce unwanted γ -rays. Neutron capture, elastic and inelastic scattering were simulated separately as well. It was found that inelastic scattering is the major contributor to the spectrum induced by neutrons. The effect of neutrons on the background of the HPGe detector operating underground, such as Obelix, is manifested mainly by their contribution to the continuum up to 1 MeV, especially in the lower part up to 500 keV. Thus, neutrons are an important background component in deep underground laboratories, too. Possible detector optimization is also discussed.

1. Introduction

Underground experiments looking for rare events such as searching for dark matter and rare α and β decays or detection of low energy neutrino interactions are important experiments of today. These experiments are based on the detection of rare signals, therefore the main research tools are detectors with large sensitive volumes, e.g. HPGe detectors with big germanium crystals [1]. These detectors are used also for material screening [2]. Shielding against particles coming from muon interactions and γ -rays coming from decay of natural

radionuclides is a key issue for such detectors. Signals produced by neutrons interacting in a low-background experiment are particularly troublesome as they may imitate or mask the very signals that are being searched for [3]. In deep underground laboratories, cosmic rays are represented only by their hard component, thus only cosmic-ray muons and neutrinos are present here, as only they are able to penetrate to this depth. Neutrons are produced in interactions of muons with the experimental setup and the surroundings, and may contribute to the background. Another source of neutrons deep underground is spontaneous fission of natural radionuclides (such as ^{232}Th and ^{238}U) and (α, n)

* Corresponding author at: Dr. Miloslava Baginova, CERN, Geneva 1211, Switzerland; Comenius University, Faculty of Mathematics Physics and Informatics, Mlynska dolina F1, 84248 Bratislava, Slovakia

E-mail address: miloslava.baginova@cern.ch (M. Baginova).

<https://doi.org/10.1016/j.astropartphys.2022.102756>

Received 22 January 2020; Received in revised form 12 May 2022; Accepted 4 July 2022

Available online 6 July 2022

0927-6505/© 2022 The Author(s). Published by Elsevier B.V. This is an open access article under the CC BY license (<http://creativecommons.org/licenses/by/4.0/>).

reactions [4]. Therefore, the investigation of neutron induced backgrounds in deep underground laboratories is crucial for low background experiments.

Existing background studies in underground experiments deal therefore also with the neutron influence on the expected results. They are mainly focused on investigation of neutron fluxes from different underground sources and on the neutron energy spectra, when neutrons are originating from natural radioactivity (e.g. [5, 6]). An important part of the low energy neutron background comes from natural radioactivity. The main contributors are uranium and thorium decay chains via (α, n) reactions and, to a smaller extent, spontaneous fission. The background from fast neutrons is induced by interactions of cosmic-ray muons with detectors and their shielding. The neutron induced spectrum formed by muon interactions in deep underground laboratories can range up to several GeV [5]. Several Monte Carlo simulations of neutron energy spectra caused by uranium and thorium decay chains were carried out in materials considered as potential neutron sources, with the aim to estimate the event rate invoked by neutrons. Contributions of spontaneous fission and (α, n) reactions were estimated in [6].

A thorough analysis of background spectra measured in a deep underground laboratory can bring valuable information about neutron induced background of HPGe detectors and help to identify all background components. Such a study would be beneficial for underground experiments looking for rare nuclear processes.

The aim of this study has been to investigate the neutron background in the Obelix HPGe detector operating in the Modane deep underground laboratory. The background energy spectrum of the HPGe detector was studied and compared with Monte Carlo simulations carried out by the GEANT4 simulation code for better understanding of neutron contributions to the detector background.

2. Cosmic rays deep underground

Cosmic rays in deep underground laboratories are represented by muons and neutrinos, the only particles which are able to penetrate so deeply. All other types of particles are eliminated during their travel underground by interactions with matter, absorption, ionization or nuclear processes. The muon flux decreases exponentially with increasing depth. To know the intensity of muons in deep underground laboratories is very important for the background estimation of planned and running experiments looking for rare events.

Muons penetrating underground lose their energy by ionization, atomic excitation, pair production, bremsstrahlung and photo-nuclear interactions. The total energy loss of muons can be expressed as [7]

$$-\frac{dE}{dx} = a(E) + b(E)E, \quad (1)$$

where E is the energy [GeV], the $a(E)$ [GeV (m w.e.)⁻¹] represents the energy loss due to ionization and atomic excitation, and $b(E)$ [(m w.e.)⁻¹] is the sum of the losses caused by bremsstrahlung, pair production and photo-nuclear interactions. At shallow depths, the ionization dominates, while at deep depths the other electromagnetic processes take over. The energy loss by bremsstrahlung, specifically dominant at high energies, induces fluctuations of the depth-intensity relation. On average, the vertical flux at an energy E at depth X [m w.e.] can be expressed as [7]

$$j(E, X) = B e^{-bX\gamma} \left(E + \frac{a}{b} (1 - e^{-bX}) \right)^{-(\gamma+1)}, \quad (2)$$

where γ is the spectral index of the muon flux at sea level and $B = \frac{1}{b}(Aa)^{-\gamma}$. A is the normalization constant of the muon spectrum at sea level. The first part of the equation gives information about the attenuation of the high energy muon flux and the second part, enclosed in parentheses, specifies the shape of the energy spectrum underground.

The average energy of muons at depth X can be calculated by the

following equation [7]

$$E_{ave} = \left(\frac{a}{b(\gamma-1)} \right) (1 - e^{-bX}). \quad (3)$$

Atmospheric muons, mostly coming from the decay of secondary pions and kaons, are the most abundant muons down to the depth of 8 km w.e. (water equivalent). At deeper depths, the neutrino induced muons gain significance and beyond a depth of about 13 km w.e. they dominate [7]. Only low energy muons manifest an azimuthal dependence down to the sea level because of the geomagnetic field but this dependence ceases in deeper depths [7].

Neutrinos are particles with very small cross sections, which depend on their energy. At very low energies the cross section increases logarithmically. At several MeV it is 10^{-44} cm² and increases linearly. Above 1 GeV, the cross section is 10^{-38} cm² and increases further linearly. In addition, neutrinos have no charge and they interact only through the weak subatomic force and gravity. Therefore, the neutrinos at the energy less than 100 TeV pass through the Earth almost without interaction. The neutrino flux is not significantly different underground in comparison with the flux at sea level.

3. Modane underground laboratory

The deepest European underground laboratory hosting experiments related to rare nuclear processes and decays is the Modane underground laboratory (Laboratoire Souterrain de Modane, LSM). It hosts experiments such as EDELWEISS for direct detection of dark matter particles and SuperNEMO for neutrinoless double-beta decay. The laboratory is located in Auvergne-Rhône-Alpes region under the Cottian Alps mountains. It is situated in the middle of the 12.6 km long Fréjus road tunnel connecting France and Italy at 1700 m under the Fréjus Peak, equivalent to a depth of 4800 m w.e. Thanks to this depth, LSM is very well shielded against cosmic rays, therefore the muon flux there is very low (4.73 ± 0.09) m⁻²d⁻¹ [8]. The flux was measured through a horizontal plane [9].

Natural radionuclides such as ⁴⁰K and members of the ²³⁸U and ²³²Th decay series are present in the laboratory walls consisting of Fréjus rock and concrete, in surrounding materials and, in construction parts of the detectors. The concentrations of ²³⁸U in the rock and in the concrete are (11.8 ± 6) Bq kg⁻¹ and (10.2 ± 5) Bq kg⁻¹. The concentrations of ²³²Th in the rock and in the concrete are (22.8 ± 7) Bq kg⁻¹ and (6.7 ± 2) Bq kg⁻¹, respectively. The concentration of ⁴⁰K is (182 ± 4) Bq kg⁻¹ in rock and (91 ± 3) Bq kg⁻¹ in concrete [8]. Further, the LSM operates a ventilation system removing the inert and noble gases Radon (²²²Rn) and Thoron (²²⁰Rn), and so reduces also their progenies in the ambient air to negligible levels. The γ -ray flux in LSM is relatively very high (5.4 ± 0.4) $\times 10^3$ m⁻²d⁻¹ (measured in the power supply room) when compared with the muon flux, and therefore it significantly contributes to the background. However, most of the detectors operating in LSM are located in the detector hall, where the count rate of measured γ -rays is higher almost by about a factor of 3 than in the mentioned power supply room [10].

Another source of background in the LSM laboratory are neutrons. The measured neutron flux in LSM is (1381 ± 860) m⁻²d⁻¹ for neutron energies above 2 MeV [11] and (1382 ± 864) m⁻²d⁻¹ for thermal neutrons [12] measured before the installation of large experiments. After these installations, the flux of thermal neutrons was measured again and it was found that it increased to (3084 ± 280) m⁻²d⁻¹ [13]. However, the flux of thermal neutrons may vary as much as by a factor of 3, depending on the location. A table of thermal neutron fluxes for different locations at LSM is given in [14]. The flux of thermal neutrons in the detector hall is (3888 ± 432) m⁻²d⁻¹. Fast neutrons in LSM are produced by (α, n) reactions of alpha particles emitted by members of the ²³⁸U and ²³²Th decay series on light elements such as C, O, Mg, Na, Al, Si and Fe, present mainly in the walls, and by spontaneous fission of

natural radionuclides, present mostly in the walls, especially of ^{238}U . The (α, n) reactions contribute to the fast neutron flux by $1930 \text{ y}^{-1}\text{kg}^{-1}$, while spontaneous fission adds $470 \text{ y}^{-1}\text{kg}^{-1}$ [12]. Neutrons originating in muon interactions with walls contribute to fast neutron flux by $(2.3 \pm 0.5) \times 10^{-5} \text{ y}^{-1}\text{kg}^{-1}$, while neutrons resulting from muon interactions with the lead shield of the detector by $(3.2 \pm 0.2) \times 10^{-4} \text{ y}^{-1}\text{kg}^{-1}$ [12]. We can conclude that, neutrons from (α, n) reactions are the major contributor to the total fast neutron flux in LSM, while the contribution from muon-induced neutrons is minimal.

4. HPGe detector

Several HPGe detectors with large germanium crystals are located in the detector hall in LSM. One of them is the detector called Obelix, primarily used for radiopurity measurements and for investigations of rare decays [15]. Obelix is a p-type coaxial HPGe detector (Canberra) with a relative efficiency of 160%, which is the efficiency relative to a ^{60}Co source (using the 1332 keV peak) measured with a NaI(Tl) detector at a distance of 25 cm from the detector. The volume of the crystal is 600 cm^3 , which corresponds to about 3 kg of ultra-pure germanium. The crystal is placed in a thermoplastic foil, embedded in the crystal holder made of an Al-Si alloy (4% of Si) and enclosed in aluminium U-type cryostat made of the same alloy. The cryostat is connected with a cooled Field Effect Transistor (FET). The entrance window of the end-cap is made using the same material as the crystal holder. The thickness of the entrance window is 1.6 mm. The distance between the entrance window and the crystal is 4 mm. The end cap is fixed to the bottom part of the cryostat by an O-ring made of synthetic rubber. The detector is placed in ultra-low level shield consisting of (from outside to inside) radiopure normal lead with a thickness of 20 cm and a roman low-activity lead with a thickness of 12 cm. The lead shield is secured by a stainless steel frame. All screws in the detector are made from leadless brass. The energy resolution of the detector is 1.2 keV at 122.06 keV γ -rays of ^{57}Co and 2 keV at 1332.40 keV γ -rays of ^{60}Co . The detector can be operated either with 8192 channels or 16384 channels ADCs. A detailed view of the detector parts is shown in Fig. 1b.

The detector parts were produced from ultra-pure materials with the aim to reduce the concentration of natural radionuclides to a minimum. Al-Si alloy contains cosmogenic ^{26}Al and it also contains ^{226}Ra , ^{228}Ra , ^{228}Th and ^{40}K . Radionuclides ^{226}Ra , ^{228}Ra , ^{228}Th and ^{40}K are present in other construction parts of the detector, such as leadless brass, O-ring and FET, as well. Even if the brass is classified as leadless, it still contains ^{210}Pb at measurable levels. The concentration of these radionuclides in the O-ring is high, but the O-ring is small and it is placed far enough from the crystal. The FET is one of the most radioactive parts of the detector and it contributes to the detector background. In order, to reduce the background from the FET, a disk made of roman lead with a thickness of 10 mm is placed at the bottom part of the crystal holder. The radioactivity concentration in this lead is minimal. Normal lead contains a high concentration of ^{210}Pb in comparison with roman lead. Besides ^{210}Pb , roman lead contains also ^{226}Ra and ^{228}Ra . All values of the various radionuclide concentrations are listed in Table 1 and were taken from [15].

5. Detector background

5.1. Experiment

5.1.1. Experimental background spectrum

In order to determine neutron contributions to the Obelix background energy spectrum measured in the Modane underground laboratory, investigations of impacts of cosmic ray interactions with the HPGe detector materials, as well as influence of present radionuclides on the resulting background were carried out. The experimental background spectrum was analysed and reproduced using a Monte Carlo simulation.

Table 1

Concentration of radionuclides in the detector parts [15].

	^{207}Bi	^{26}Al	^{226}Ra	^{228}Ra	^{228}Th	^{40}K	^{210}Pb
	mBq kg $^{-1}$						
Al-Si alloy		$0.4^{+0.2}_{-0.1}$	0.3 ± 0.2	< 0.11	1.4 ± 0.2	$1.1^{+0.2}_{-0.1}$	
Leadless brass			4.9 ± 1.3	< 5	< 3	< 40	< 100
O-ring			910 ± 80	320 ± 70	350 ± 30	1360 ± 400	
Normal lead							20000
Roman lead			< 0.3	< 0.3			< 60
FET	mBq						
	1.7 ± 0.7		1.6 ± 0.2	2.9 ± 0.6	< 0.5	< 5	

The background spectrum of the Obelix HPGe detector was measured in LSM in September 2011. The detector has been in non-stop use and the background was measured only occasionally. Therefore, it was difficult to measure the background spectrum for time sufficiently long for evaluation. Thus, the 2011 spectrum of 34.2 days reported in [15, 16] was used for analysis. The background measurement was carried out with a full installation of the Obelix detector including the lead shielding. The geometry of the Obelix detector, as it was implemented in the GEANT4 simulation code, is shown in Fig. 1a. and 1b.

The signal was processed by a Canberra preamplifier PSC761 and a spectroscopy Canberra Amplifier 2022 connected to the detector, and it was digitized by a channel Canberra ADC Multiport II. The energy spectrum was measured in the energy range from 40 to 3000 keV with 8192 channels and analysed using the Canberra GENIE 2000 software.

5.1.2. Peak analysis

Gamma lines in the measured background spectrum were analysed. Lines with net count rates above the detection limit at the 95% C.L. were identified (Fig. 2) and evaluated. Because many measures were taken to reduce the detector background, the count rates are extremely low and peaks are often very hardly distinguishable from the continuum.

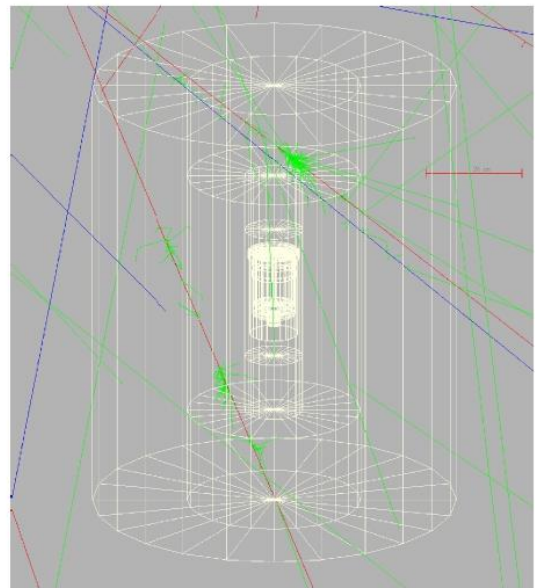


Fig. 1a. The geometry of the Obelix detector simulated in GEANT4 with several muon interactions (trajectories of positive particles are blue, of negative particles are red and of neutral particles are green).

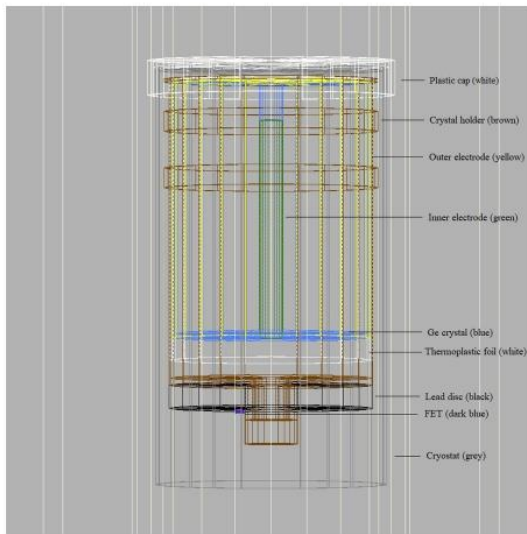


Fig. 1b. Detailed view of the detector parts. Blue, yellow and green parts together show the whole crystal volume.

Nevertheless, a number of lines were identified. Gamma-lines coming from neutron interactions are marked with red colour and those resulting from decay of natural radionuclides are marked in brown. Very short-lived radionuclides (half-lives less than 1 ms), usually excited states, are marked with the asterisk character. Nuclear data are taken from NuDat 2.8 [17].

Contribution of radionuclides dominates in the energy spectrum, as seen by the presence of peaks from the daughter isotopes of ^{238}U , ^{232}Th decay series and by ^{40}K . Natural radionuclides are present in the detector construction materials, the shield and its surroundings, especially in the walls.

The ^{208}Pb peaks coming from β decay of ^{208}Tl are visible at energies

of 583.19 keV and 2614.51 keV. However, they are convolved with the γ -rays resulting from inelastic neutron scattering on ^{208}Pb nuclei. In addition, ^{208}Pb X-rays are visible at the energies of 72.81 keV and 74.97 keV (Fig. 3 left), while the second line (74.97 keV) should include also X-rays from daughter nuclides of ^{214}Pb and ^{212}Pb decays. Contribution from ^{206}Pb X-rays through the ^{210}Pb decay chain should be present as well.

The presence of ^{40}K is detected via the ^{40}Ar peak at the energy of 1460.80 keV coming from the electron-capture decay of the parent nuclide.

The 84.21 keV peak (Fig. 3 left) has two contributions from the decays of ^{208}Tl (X-ray doublet) and ^{228}Th (γ -ray). The source of the peak around 143 keV is cosmogenic ^{57}Co . The electron-capture decay of ^{57}Co leads to the formation of ^{57}Fe peak at the energy of 122.06 keV, which is, in this case, summed with a ^{57}Co 14.41 keV γ -rays and one of the two abundant Co X-rays with the energies of 6.39 keV and 6.40 keV [16]. The result is a narrow doublet with an energy of 142.87 keV.

Daughter nuclides of ^{232}Th series are observable at different energies. The peak of ^{212}Bi at the energy of 238.63 keV is produced by β decay of ^{212}Pb . Peaks of ^{228}Th induced by β decay of ^{228}Ac are seen at the energies of 911.2 keV, 968.97 keV and 1588.2 keV. There is one more γ -line of ^{228}Th at an energy of 1677.67 keV combined with ^{212}Po and ^{214}Po peaks at energies of 1679.7 keV and 1684.01 keV originating in β decay of ^{212}Bi and ^{214}Bi .

Daughter nuclides of ^{238}U series are represented by the ^{214}Bi peak resulting from β decay of ^{214}Pb is visible at the energy of 351.93 keV, while peaks of ^{214}Po coming from subsequent β decay of ^{214}Bi were detected at the energies of 609.32 keV, 1120.29 keV, 1509.21 keV and 1764.49 keV. Both nuclides belong to the ^{238}U decay series.

Several short-lived radionuclides are present in the spectrum. The ^{54}Cr γ -line produced by electron-capture decay of cosmogenic ^{54}Mn and summed with emitted X-rays is observable at the energy of 840.25 keV. The β decay of ^{65}Zn gives rise to the peak of ^{65}Cu combined with X-rays emitted during the decay [16] at an energy of 1124.54 keV (Fig. 3 right). The peak of ^{22}Ne at an energy of 1274.54 keV resulting from β decay of cosmogenic ^{22}Na is also present in the spectrum as well as a peak of ^{26}Mg at an energy of 1808.65 keV coming from electron-capture decay of

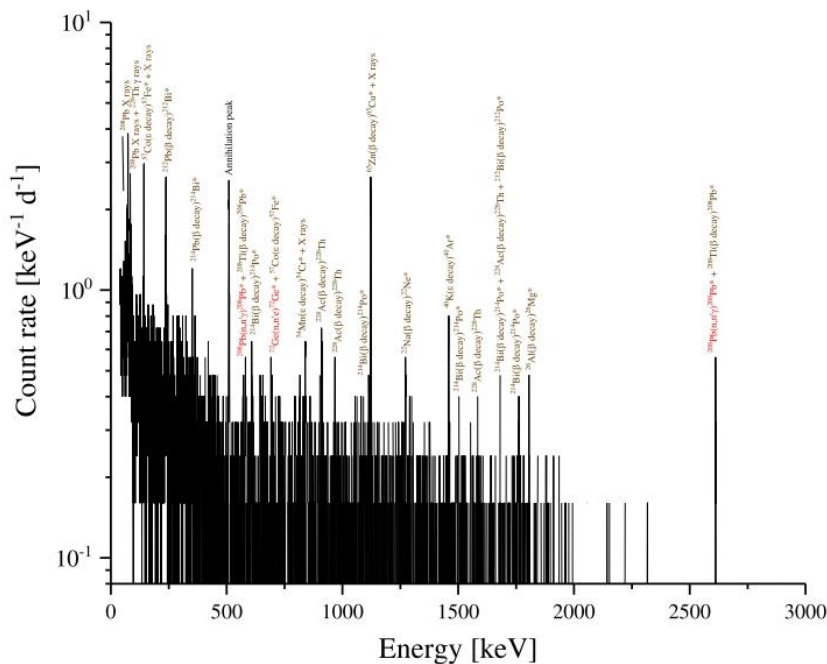


Fig. 2. Experimental HPGe detector background spectrum for the energy range from 0-3 MeV.

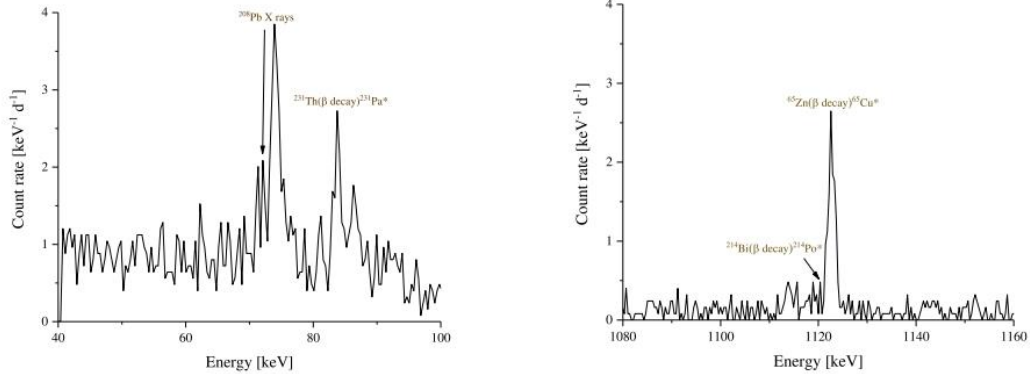


Fig. 3. Experimental HPGe detector background spectrum in linear scale for energy ranges from 40–100 and 1080–1160 keV

cosmogenic ^{26}Al . All these cosmogenic radionuclides were produced in detector materials during the construction processes, before the HPGe detector was located underground. ^{57}Co , ^{54}Mn and ^{65}Zn were present in the crystal.

One more peak is visible in the spectrum at an energy of 691.43 keV. This peak belongs to ^{72}Ge and it is evidence of neutron contribution to the background spectrum (produced on the surface and underground as well). The peak is produced by the internal conversion process. However, the peak is interfered with ^{57}Fe γ -rays at an energy of 692.41 keV emitted during electron-capture decay of ^{57}Co .

The 511 keV peak is the peak coming from annihilation of electron-positron pairs generated by photon interactions with the detector and shielding. It has also contributions from ^{208}Tl , ^{40}K , ^{22}Na and ^{26}Al decays.

5.2. Monte Carlo simulations

For the simulation of the Obelix detector background, the Monte Carlo simulation code GEANT4 was used. It was specially developed for modelling of physics events and provides wide spectrum of tools for simulations of particle transportation via matter. GEANT4 is equally suitable for simulations at high energies as at low energies. It contains all relevant physics processes and corresponding cross sections organized in individual data files [18–21].

The complete geometry of the Obelix detector was coded in GEANT4 including the massive lead shield. The detector was placed into a box with dimensions of $14 \times 5 \times 3 \text{ m}^3$ representing the detector hall in LSM and the rock and concrete around were modelled as layers 60 cm and 10 cm thick, respectively. The thickness of walls was considered as sufficient, because already 30 cm of Fréjus rock decreases the neutron energy below 1 MeV, below which the chance to emerge from the wall is negligible [12]. The compositions of rock and concrete are shown in Table 2 and were taken from [12], except the density of the Fréjus rock, which was taken from [7]. The rock density of 2.65 g cm^{-3} stated in [12] is typical for standard rock, while the real density of Fréjus rock is higher.

Muons have the ability to penetrate deep underground. The muon vertical energy spectrum in LSM (Fig. 4) was calculated from equation (2), taking into account the muon total energy loss given in equation (1). The fluxes of positive and negative muons were calculated from the charge ratio reported in [22]. The values of the energy loss parameters

($a = 0.217 \text{ GeV (m w.e.)}^{-1}$, $b = 4.24 \times 10^{-4} \text{ (m w.e.)}^{-1}$) in Fréjus rock were taken from [7]. The spectral index γ of muon flux at sea level and the normalization constant A were taken from [23]. The average muon energy ($E_{\text{ave}} = 250 \text{ GeV}$) was calculated from equation (3). The total muon flux of $4.73 \text{ m}^{-2} \text{ d}^{-1}$ as measured in the laboratory was taken into account. This flux does not include muon multiplicities. The cosmic-ray particle source was modelled as a plane ($14 \times 5 \text{ m}^2$) placed above the laboratory.

The contribution of radionuclides present in the detector parts and walls described above was also simulated using GEANT4. RadioactiveDecay 4.3.2 data file was used for simulation of decay modes and individual decays of radionuclides in selected volumes were processed by the grdm command. Geant4 Radioactive Decay Module (grdm) is a particle generator able to simulate the decay of radioactive nuclei.

Neutron processes were treated by G4NEUTRONXS 1.4 and G4NDL 4.5 data files, and γ -ray processes by G4EMLOW 6.5 data file. G4NEUTRONXS 1.4 is preferably used for elements with natural composition, as it contains evaluated neutron cross-sections on natural composition of elements, while G4NDL 4.5 is more suitable for thermal neutron cross sections on individual isotopes.

One of the most suitable GEANT4 physics list for underground or low background experiments, as well as for neutron penetration studies is SHIELDING 2.1. It brings the best collection of electromagnetic and hadronic physics processes needed for underground installations. Therefore, this physics list was used for simulation of particle interactions with Obelix detector.

5.3. Comparison of Monte Carlo simulations with experimental spectrum

The Monte Carlo simulation of the experimental background energy spectrum was carried out including the concentration of radionuclides in the detector parts and the laboratory walls given in Table 1 and 2. The concentration level of cosmogenic radionuclides (except of ^{26}Al) was not known, therefore it was not coded into the simulation (i.e. ^{22}Na , ^{54}Mn , ^{57}Co and ^{65}Zn).

The experimental spectrum was compared with the simulated one (Fig. 5). Integral count rates were calculated in the energy range from 40 keV to 3000 keV. The value of the integral count rate for the experimental spectrum was $345 \pm 18 \text{ d}^{-1}$ and $320 \pm 31 \text{ d}^{-1}$ for the simulated one. The simulation reproduces the main features of the measured

Table 2
Composition of Fréjus rock and concrete in LSM [5, 10].

	ρ [g cm^{-3}]	Abundance of elements [%]												
		H	C	O	Na	Mg	Al	Si	P	K	Ca	Ti	Mn	Fe
Fréjus rock	2.74	1.02	6.10	48.61	0.45	0.84	2.65	6.96	0.07	0.21	30.6	0.07	0.03	1.96
Concrete	2.40	1.25	7.46	48.99	0.01	0.78	0.58	2.71	0.07	0.02	36.81	0.10	0.01	0.52

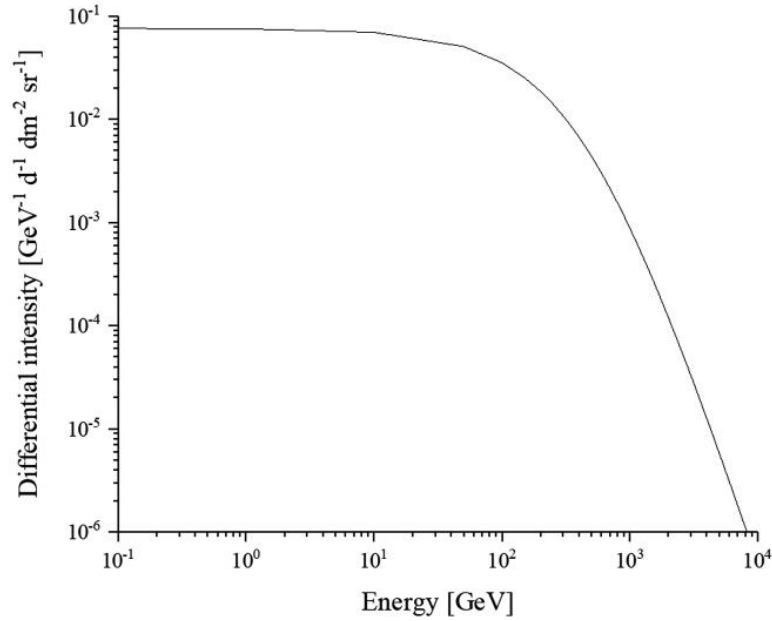


Fig. 4. Calculated muon vertical energy spectrum in LSM.

spectrum fairly well, considering the poor statistics of the experimental spectrum and missing peaks from cosmogenic radionuclides. We can conclude, that the simulation is in a good agreement with the experiment. The count rates of individual peaks were compared, too. The count rates of the simulated peaks agree with the experimental ones well, except for the 84.21 keV peak of double origin (see above). However, the difference is still within a factor of two. All measured and simulated results are listed in Table 3.

Muons are survivors of the cosmic-rays underground, therefore background spectra induced only by muons were simulated. The muon flux in LSM is very low, therefore muons only make a small contribution to the detector background in LSM. Simulation of muon background with a live time of 34.2 days was carried out and subsequently, the contribution of muon events to the experimental spectrum was calculated. It was found, that only $0.20 \pm 0.02 \text{ d}^{-1}$ of them deposited energy in the detector, which is much less than 1% of the total count rate $345 \pm 18 \text{ d}^{-1}$. Therefore, the role of muons in the background energy spectrum of the HPGe detector measured underground is negligible. Nevertheless, if the background induced by radionuclides would be suppressed, then it would gain significance, especially for experiments looking for rare processes. In order to investigate and demonstrate the contribution of muons to the long-time measured spectrum, the next simulation of background induced by muons were carried out with the number of events corresponding to measuring time of 220 years (Fig. 6). The long measuring time was chosen in order to show a relevant energy spectrum induced by muon interactions with a sufficient number of counts due to the very low muon flux. The simulated spectrum was analysed and it was found, that besides the annihilation peak, also neutron induced peaks are rising from the continuum. Peaks were identified and explained also using information from the previously measured background energy spectrum [24]. Although the statistics are still very low, these peaks indicate, that muon induced neutrons indeed contribute to the spectrum. We can see rising ^{206}Pb peaks at energies of 583.19 keV and 2614.51 keV, as well as indication of ^{74}Ge and ^{72}Ge peaks at energies of 595.84 keV and 691.43 keV, respectively. It means, that neutron induced peaks from cosmic-rays contribute to the total background but might be visible

only in spectra measured over a long time. Hence, peaks originating in neutron interactions with the lead shield also contribute to the total count rate of ^{206}Pb peaks coming from ^{206}Tl decay. The measured spectrum was compared with the simulated muon-induced spectrum (Fig. 7). It was confirmed, that the simulated spectrum is about three orders of magnitude lower than the experimental one as it was stated in [16].

Since neutrons from (α, n) reactions and spontaneous fission form a critical background source in underground laboratories, their effect on the Obelix detector was simulated as the next step. Neutron fluxes in LSM reported in [11] and [12] were used for simulations. A total energy spectrum induced by neutrons was simulated (Fig. 8), as well as individual contributions from thermal and fast neutrons (Fig. 9) for measuring times 34.2 and 900 days. The integral count rate of the total spectrum induced by neutrons with a live time of 34.2 days was compared with the count rate of the experimental spectrum (Fig. 10). The simulated one was $19 \pm 2 \text{ d}^{-1}$ and the experimental one of $345 \pm 18 \text{ d}^{-1}$, which indicates, that about 6% of the measured background continuum is formed by neutron interactions. A comparison of the integral count rates of spectra induced by thermal and fast neutrons with the total spectrum showed that fast neutrons contribute to the total spectrum of neutrons more than thermal neutrons. The integral count rate of the spectrum induced by fast neutrons was $12.5 \pm 1.3 \text{ d}^{-1}$, indicating that about 65% of the total spectrum ($19 \pm 2 \text{ d}^{-1}$) was invoked by fast neutrons. Thermal neutrons typically give rise to a boron peak at the energy of 477.61 keV coming from $^{10}\text{B}(n, \alpha)^7\text{Li}$ reaction due to boron present in the contact layer of the crystal, while fast neutrons significantly contribute to the continuum up to 250 keV, and induce lead and germanium peaks coming from inelastic scattering of neutrons on Pb and Ge nuclei. Rising ^{206}Pb , ^{207}Pb and ^{208}Pb peaks are visible in the spectrum induced by fast neutrons in Fig. 9 at the energies of 803.06 keV, 569.70 and 1770.23 keV, and 2614.51 keV, respectively. A peak of ^{72}Ge at the energy of 691.43 keV is indicated as well. The contribution of fast neutrons up to 250 keV energy region is important for dark matter particle search in the low mass range of WIMPs ($<1 \text{ GeV}$), and γ -rays resulting from neutron interactions can imitate signatures of such events

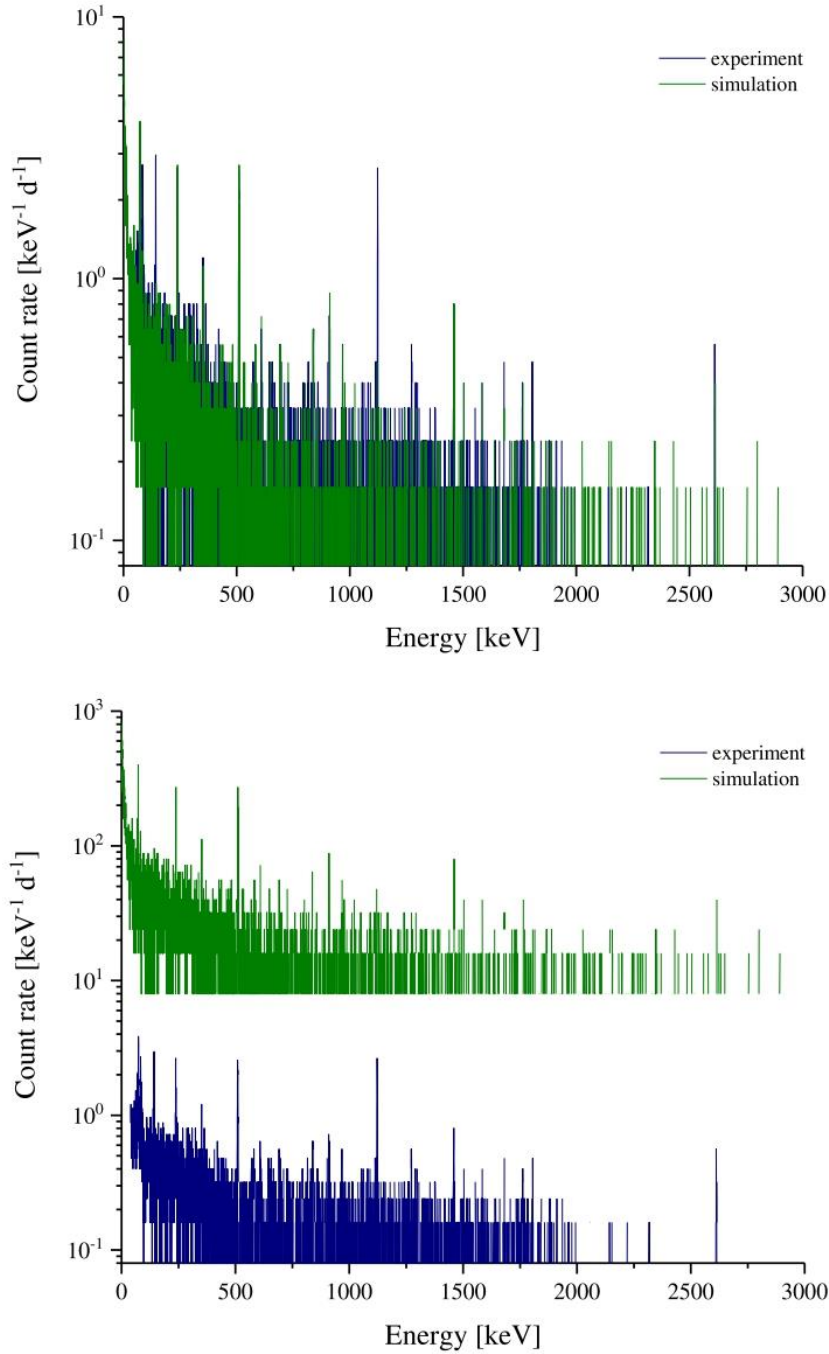


Fig. 5. Comparison of experimental and simulated background spectra. The simulated spectrum includes contributions from muons, neutrons and natural radionuclides. The simulation shown in the bottom figure has been multiplied by 100 for better visibility.

[3]. The boron peak clearly dominates in the spectra induced by thermal neutrons. The inner electrode of the detector is made of boron and the ^{10}B cross section for thermal neutrons is very high, especially for (n, α) reaction, therefore the boron peak is well visible in these spectra. Similarly, ^{10}B , ^{72}Ge and ^{208}Pb peaks are also visible in the total spectra induced by neutrons. In addition, a peak due to inelastic scattering of neutrons on ^{74}Ge nuclei is seen there as well. The statistics are again very low, therefore only the boron peak is identified reliably. The rest of the peaks were predicted based on the information from the measured

energy spectrum induced by a neutron source [4].

All neutron induced peaks contribute to the total measured background, too. Some of them are visible in the experimental background, such as ^{72}Ge or ^{208}Pb . Lead is the most abundant material in the setup, therefore the manifestation of neutron interactions with lead is preferentially visible in the spectra. Consequently, peaks resulting from ^{208}Tl decay are convolved with ^{208}Pb peaks coming from neutron interactions. For the ^{72}Ge peak, there is an interference with a ^{57}Fe γ -rays coming from electron-capture decay of ^{57}Co . Nevertheless, contribution

Table 3
Measured and simulated count rates.

Energy peaks [keV]	Nuclides and Reactions	Count rates [d ⁻¹]	
		Experiment	Simulation
40-3000	Continuum	345 ± 18	320 ± 31
72.81	X-rays of ²⁰⁸ Pb	0.3 ± 0.1	0.3 ± 0.1
74.97	X-rays of ²⁰⁸ Pb + X-rays of ²¹² Pb and ²¹⁴ Pb	3.0 ± 0.6	2.5 ± 0.4
84.21	X-rays of ²⁰⁸ Pb + γ -rays of ²²⁸ Th	2.8 ± 0.6	1.2 ± 0.3
142.87	⁵⁷ Co(ϵ decay) ⁵⁷ Fe*	3.1 ± 0.5	-
238.63	²¹² Pb(β decay) ²¹² Bi*	1.6 ± 0.3	1.4 ± 0.2
351.93	²¹⁴ Pb(β decay) ²¹⁴ Bi*	0.6 ± 0.3	0.6 ± 0.2
511.0	Annihilation	2.5 ± 0.6	2.3 ± 0.4
583.19	²⁰⁸ Pb(n, n' γ) ²⁰⁸ Pb* + ²⁰⁹ Tl(β decay) ²⁰⁹ Pb*	0.3 ± 0.1	0.3 ± 0.1
609.32	²¹⁴ Bi(β decay) ²¹⁴ Po*	0.5 ± 0.2	0.5 ± 0.1
691.43	⁷² Ge(n, n'e) ⁷² Ge* + ⁵⁷ Co(ϵ decay) ⁵⁷ Fe*	0.2 ± 0.1	0.2 ± 0.1
840.25	⁵⁴ Mn(ϵ decay) ⁵⁴ Cr* + X-rays	0.2 ± 0.1	-
911.40	²²⁸ Ac(β decay) ²²⁸ Th	0.8 ± 0.2	0.7 ± 0.2
968.97	²²⁸ Ac(β decay) ²²⁸ Th	0.5 ± 0.1	0.4 ± 0.1
1120.29	²¹⁴ Bi(β decay) ²¹⁴ Po*	0.3 ± 0.1	0.3 ± 0.1
1124.54	⁶⁵ Zn(β decay) ⁶⁵ Cu* + X-rays	3.0 ± 0.5	-
1274.54	²² Na(β decay) ²² Ne*	0.6 ± 0.2	-
1460.80	⁴⁰ K(β decay) ⁴⁰ Ar*	1.1 ± 0.3	1.1 ± 0.2
1509.21	²¹⁴ Bi(β decay) ²¹⁴ Po*	0.2 ± 0.1	0.2 ± 0.1
1588.20	²²⁸ Ac(β decay) ²²⁸ Th	0.2 ± 0.1	0.2 ± 0.1
1677.10	²¹⁴ Bi(β decay) ²¹⁴ Po* + ²²⁸ Ac(β decay) ²²⁸ Th + ²¹² Bi(β decay) ²¹² Po*	0.3 ± 0.1	0.3 ± 0.1
1764.49	²¹⁴ Bi(β decay) ²¹⁴ Po*	0.3 ± 0.1	0.3 ± 0.1
1808.65	²⁶ Al(β decay) ²⁶ Mg*	0.3 ± 0.1	-
2614.51	²⁰⁸ Pb(n, n' γ) ²⁰⁸ Pb* + ²⁰⁹ Tl(β decay) ²⁰⁹ Pb*	0.3 ± 0.1	0.3 ± 0.1

of neutron induced γ -rays to the total count rate of these peaks is only about 2%.

5.4. Neutrons and their effect

The continuum of background spectrum obtained underground with the Obelix γ -ray spectrometer is formed mainly by contribution of

radionuclides and only a small part can be assigned to neutron interactions. Concentration of the natural radionuclides in the detector parts and the laboratory walls forms almost 94% of the continuum, which raises a question of the importance of radiopure material usage. The contribution from muons is much less than 1% and is therefore negligible. Nevertheless, neutrons are still an important background component even if their contribution to the continuum is only about 6%. In order to further investigate the effect of neutrons on the background spectrum of the Obelix detector, simulations of individual physics processes of neutron interactions were carried out. Neutron capture, elastic and inelastic scattering were simulated separately (Fig. 11.). Simulations were carried out for a measuring time of 900 days, as the total neutron induced spectrum. It was found that inelastic scattering is the major contributor to the spectrum induced by neutrons. The second most frequent process was neutron capture. Elastic scattering occurred infrequently. In comparison with inelastic scattering, it is about 70% less. Neutron capture is about 30% less occurring than inelastic scattering. Inelastic scattering significantly contributes to the lower continuum of the spectrum induced by neutrons up to 500 keV and contributes less to the part up to 1 MeV. Neutron capture contributes to the total neutron induced energy spectrum almost evenly. Elastic scattering contributes only to the first part of the total neutron induced energy spectrum up to 300 keV. We can conclude, that the effect of neutrons on the background of the HPGe detector operating underground, such as the Obelix, is manifested mainly by their contribution to the continuum up to 1 MeV, and especially below 500 keV.

Investigation of neutron production in the lead shield was carried out as well. Simulations of neutron interactions with the lead shield were carried out with the generation of secondary particles in the shield and without. Simulations showed that particles generated in the shield contribute only about 1% to the total count rate of the resulting spectrum. It indicates that neutrons coming from outside of the detector are more important than neutrons generated inside the lead shield.

6. Detector optimization

The major contributor to the Obelix detector background is the

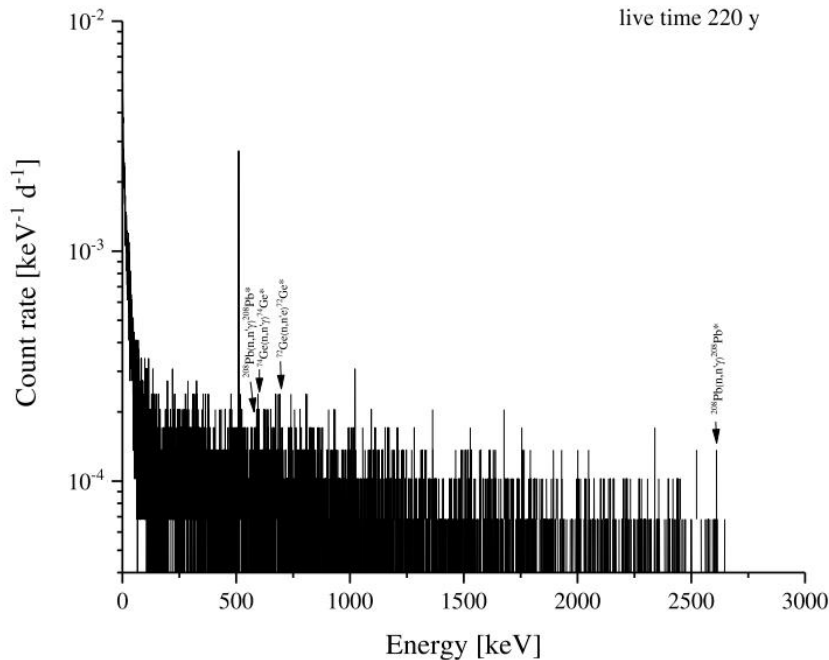


Fig. 6. Simulated muon induced background energy spectra corresponding to the live times of 220 years.

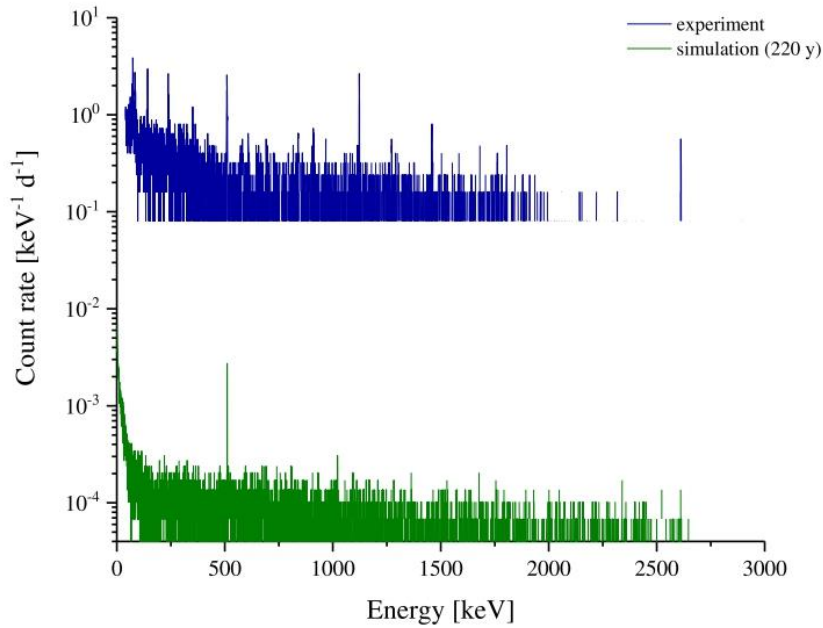


Fig. 7. Comparison of experimental and simulated muon energy spectra corresponding to the live time of 220 years.

concentration of radionuclides present in the detector construction parts and laboratory walls. The most abundant are the daughter products of the ^{238}U , ^{232}Th decay series and ^{40}K . It is not possible to avoid the radiation of radionuclides in the laboratory walls consisting mainly of Fréjus rock, present everywhere in LSM. The concentration of radionuclides in the detector construction materials should be further minimised by using even more radiopure materials. Significant reduction of long-lived radionuclides in these materials is a key issue. As ^{238}U , ^{232}Th and ^{40}K are present everywhere, it is advised to process the materials and assemble the detector parts in a place with a very low level of these radionuclides, as these radionuclides come to the detector parts from primary materials and the assembly rooms can be very clean. Special attention should be paid to electronics, as the FET was one of the most radioactive parts.

Neutrons gain significance especially through interactions with materials having large neutron cross sections, such as lead and copper. Although, the neutron flux in LSM is low, its contribution to the background spectrum is crucial for experiments looking for rare processes. Fast neutrons significantly contribute to the continuum up to 250 keV and can influence the search for low mass WIMPs expected to occur in this energy region. Whereas the main contributor to the total neutron flux in LSM are (α, n) reactions occurring in walls, the most effective way of suppression is an antineutron shielding. The composition of the detector shield is a rather complicated issue. It is difficult to select appropriate materials for suppression of γ -rays from natural radionuclides and cosmic-rays together with neutrons effectively. It is unlikely that an ideal solution exists, so a compromise must be found, for which computer simulations are a useful tool. So a commonly used lead shield is indeed an effective γ -ray suppressor, but is not suitable against neutrons. On the contrary, neutrons interact with lead easily and so produce many γ -rays inside the shield, resulting from neutron capture or inelastic scattering [4]. Therefore, an optimal shield design would require further investigation, and will be the subject of the next study. Similarly, copper material used in the detector as a construction part, is a source of additional γ -rays emitted during neutron interactions. The most efficient way how to avoid the creation of neutron induced γ -rays from lead and copper, is to replace them by other types of materials or at least combine them with effective neutron suppressing materials [25].

Several parts of the detector, such as the cryostats, entrance windows or the crystal holder are made of aluminium. Fast neutrons interact with aluminium and produce γ -lines usually visible in the background spectrum [4]. Thus, aluminium is also a potential background source. Nevertheless, the amount of aluminium material in the Obelix detector is much smaller than the amount of lead, and the neutron flux is low, therefore there is no sign of such peaks in the experimental spectrum.

The muon flux is very low in LSM, however, after suppressing the other background components, it would make sense also to reduce the muon-induced part. The usual technique deploys plastic scintillator sheets all around the main lead shield. In combination with other neutron reducing materials, it could effectively eliminate events from muon-induced neutrons, too.

7. Conclusions

The present study deals with the investigation of a background spectrum of a 160% relative efficiency HPGe detector located in the deep underground laboratory in Modane (4800 m w.e.). Special attention was paid to the neutron induced background and to the contribution of the radionuclides in the detector parts to the measured background. The experimental spectrum was reproduced by a GEANT4 simulation with good agreement. Simulations of cosmic-ray and neutron induced spectra were carried out, too. It was found that the contribution of muon events to the experimental spectrum is much less than 1%, and it was confirmed that the muon induced spectra are about three orders of magnitude lower than the experimental ones.

The contribution of radionuclides to the background measured underground is dominating. Almost 94% of the continuum of the experimental spectrum is formed by radiation coming from members of the ^{238}U , ^{232}Th decay series and ^{40}K . Hence, even more radiopure materials should be manufactured to decrease the detector background significantly.

The detector background induced by neutrons coming mainly from (α, n) reactions and fission reactions due to Uranium and Thorium present in the Fréjus rock and wall concrete in LSM was investigated by Monte Carlo simulations. The total neutron invoked energy spectrum as well as individual contributions from thermal and fast neutrons were

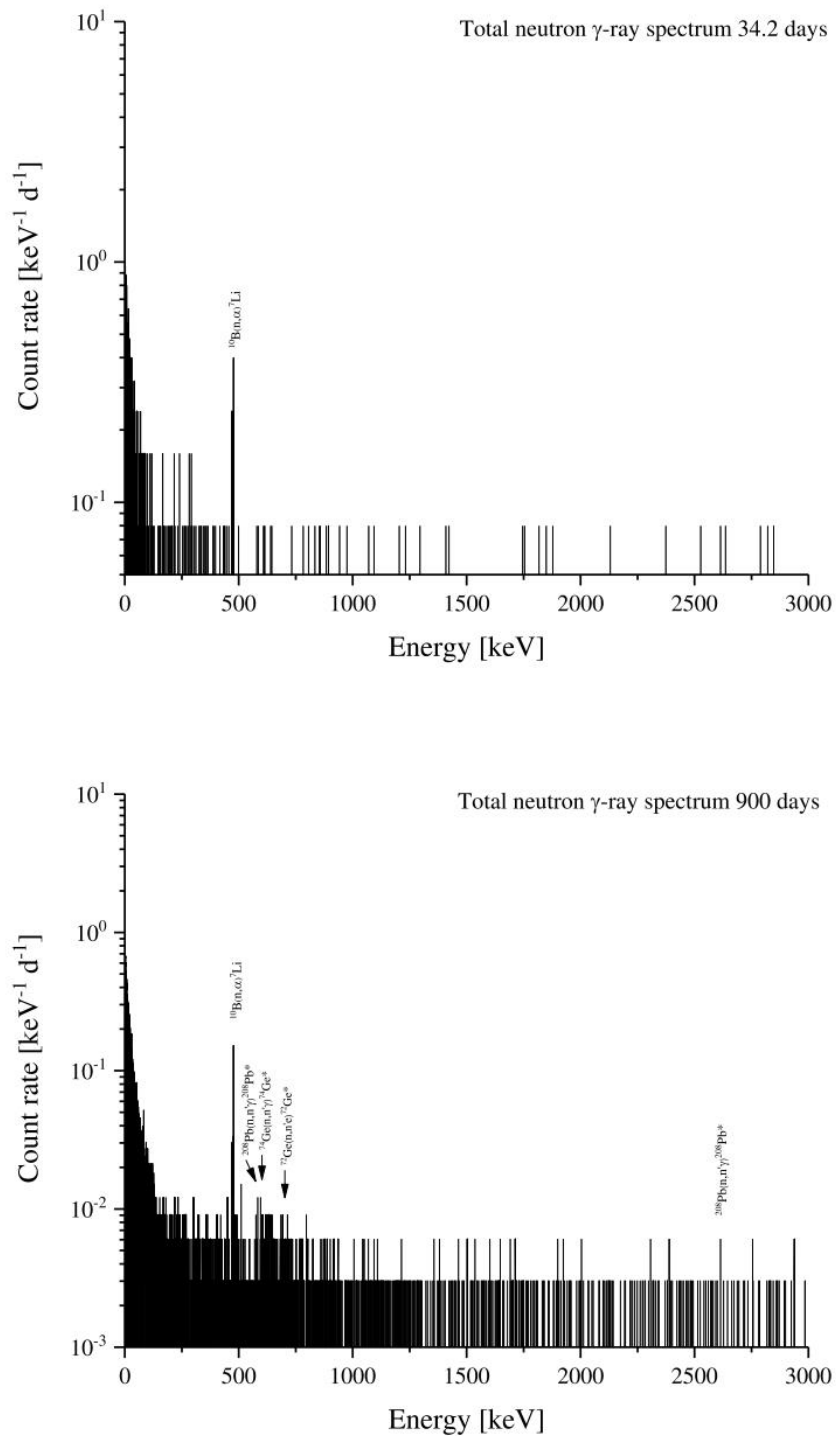


Fig. 8. Simulated total neutron induced background of the Obelix detector for live times corresponding to 34.2 and 900 days.

simulated. The comparison of integral count rates of the experimental spectrum and the simulated total neutron invoked energy spectrum showed that only about 6% of the measured background continuum is formed by interactions of neutrons. Fast neutrons contribute to the total spectrum induced by neutrons more than thermal neutrons, specifically about 65% of the total spectrum was induced by them. Furthermore,

they contribute mainly to the lower continuum up to 250 keV, which is the region of interest for potential low mass WIMPs occurrence and events resulting from neutron interactions can imitate the searched signals. This gives this background source more importance. In addition, neutron interactions with the detector materials, especially with lead, copper and germanium, induce unwanted γ -rays contributing to the

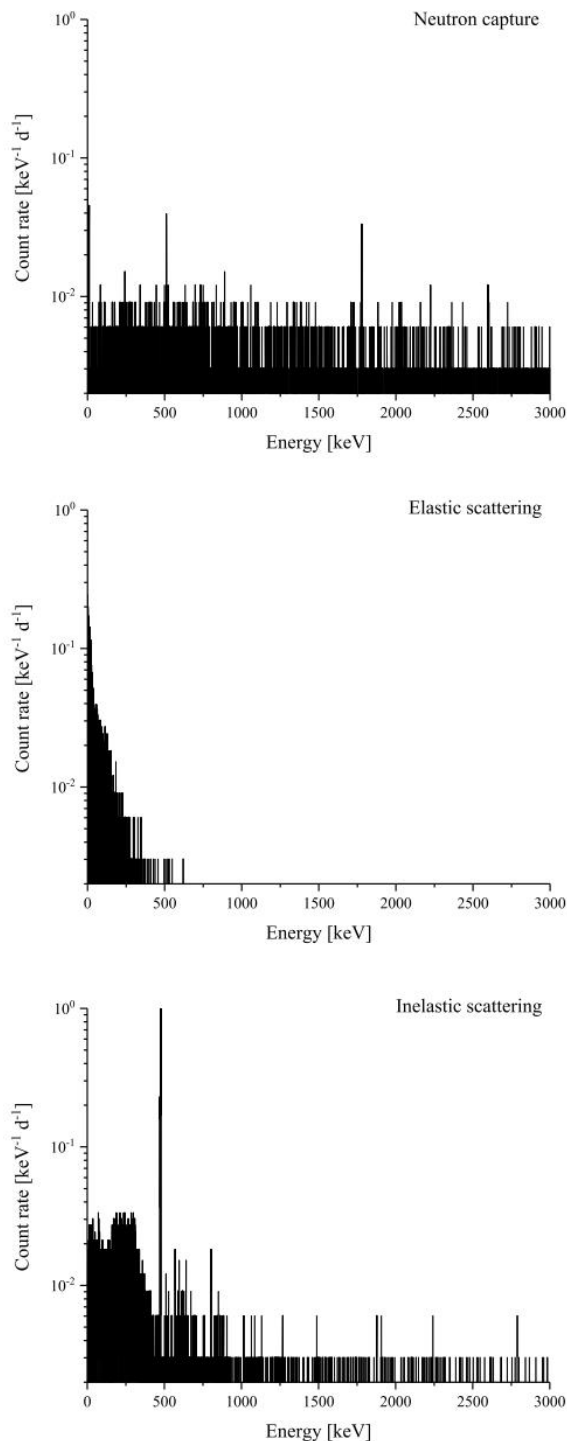


Fig. 11. Simulations of neutron capture, elastic and inelastic scattering for measuring time of 900 days.

background spectrum. Peaks resulting from ^{206}Tl decay are superimposed with ^{208}Pb peaks coming from inelastic neutron scattering. Similarly, the ^{57}Fe γ -rays at an energy of 692.41 keV coming from the electron-capture decay of ^{57}Co are combined with γ -rays of ^{72}Ge originating in neutron interactions with the germanium crystal.

Nevertheless, the contribution of neutron induced γ -rays to the total count rates of these peaks is only about 2%. Neutron capture, elastic and inelastic scattering were simulated separately as well. It was found that inelastic scattering is the major contributor to the spectrum induced by neutrons. The effect of neutrons on the background of the HPGe detector operating underground, such as the Obelix, is manifested mainly by their contribution to the continuum up to 1 MeV, especially in the lower part up to 500 keV. Simulations of neutron interactions in the lead shield showed, that particles generated in the shield contribute only about 1% to the total count rate of the resulting spectrum.

In general, we can conclude that the background continuum of the Obelix detector obtained underground is generated mostly by concentration of radionuclides and only a small part is formed by neutron interactions. Contribution of muons is minimal and thus, negligible.

Lead and copper are very common materials used in the construction of low-level HPGe spectrometers, mainly due to their relatively low cost and high achievable radiopurity; however, they are not the best choice for underground experiments where neutron induced backgrounds play an important role. Their neutron cross-sections are large and many γ -rays are generated in neutron capture and inelastic scattering, which affects the measured spectrum. The most efficient way of avoiding the creation of neutron induced γ -rays from lead and copper, is to replace them by other types of materials or at least combine them with effective neutron suppressing materials. Another way of neutron background suppression is the use of neutron absorbing layers covering the walls and floor of the detector room. Further study of this subject is necessary.

Declaration of Competing Interest

The authors declare that they have no known competing financial interests or personal relationships that could have appeared to influence the work reported in this paper.

Acknowledgments

The authors are thankful to CERN for provided PhD fellowship to Miloslava Baginova. Special thanks to Dr. Pia Loaiza and the staff of the Modane underground laboratory for information about the detector and provided background spectra. Support provided by the Slovak Research and Development Agency (project no. 15-0576) is highly acknowledged.

References

- [1] P. Belli, et al., Experimental searches for rare alpha and beta decays, *Eur. Phys. J. A* 55 (2019) 140.
- [2] M. Laubenstein, Screening of materials with high purity germanium detectors at the Laboratori Nazionali del Gran Sasso, *Int. J. Mod. Phys. A* 32 (30) (2017), 1743002. No.
- [3] V.A. Kudryavtsev, L. Pandola, V. Tomasello, Neutron- and muon-induced background in underground physics experiments, *Eur. Phys. J. A* 36 (2008) 171–180.
- [4] M. Baginova, P. Vojtyla, P.P. Povinec, Investigation of neutron interactions with Ge detectors, *Nucl. Instrum. Methods Phys. Res. A* 897 (2018) 22–31.
- [5] N. Jovancevic, M. Krmar, D. Mrda, J. Slivka, I. Bikit, Neutron induced background gamma activity in low-level Ge-spectroscopy systems, *Nucl. Instrum. Methods Phys. Res. A* 612 (2010) 303–308.
- [6] J.H. Chao, Neutron-induced gamma-rays in germanium detectors, *Appl. Radiat. Isot.* 44 (1993) 605–611.
- [7] P.K.F. Greider, *Cosmic Rays at Earth, Researcher's Reference and Data Book Manual*, 1st ed., Elsevier, Amsterdam, 2001.
- [8] C. Berger, et al., Experimental study of muon bundles observed in the Fréjus detector, *Phys. Rev. D* 40 (1989) 2163–2171.
- [9] B. Schmidt, et al., Muon-induced background in the EDELWEISS dark matter search, *Astropart. Phys.* 44 (2013) 28–39.
- [10] D. Malczewski, J. Kisiel, J. Dorda, Gamma background measurements in the Laboratoire Souterrain de Modane, *J. Radioanal. Nucl. Chem.* (2012) 751–756.
- [11] V. Chazal, et al., Neutron background measurements in the underground laboratory of Modane, *Astropart. Phys.* 9 (1998) 163–172.
- [12] G. Chardin, G. Gerbier, in: *Proceedings of the 4th Int. Workshop on Identification of Dark Matter*, World Scientific, Singapore, 2003.
- [13] K. Eitel, Measurements of neutron fluxes in the LSM underground laboratory, *J. Phys. Conf. Ser.* 375 (2012), 012016.

- [14] S. Rozov, et al., Monitoring of the thermal neutron flux in the LSM underground laboratory, *J. Phys. G: Nucl. Phys.* (2010). Preprint arXiv:1001.4383.
- [15] V.B. Brudanin, et al., The Low-Background HPGe Γ -Spectrometer OBELIX for the investigation of the Double Beta Decay to Excited States, *J. Appl. Phys.* 9 (2017) 22–29.
- [16] R. Breier, et al., Environmental radionuclides as contaminants of HPGe gamma-ray spectrometers: Monte Carlo simulations for Modane underground laboratory, *J. Env. Radioact.* (2018) 134–140, 190–191.
- [17] L.A. Sonzogni, National Nuclear Data Center, Brookhaven National Laboratory, available at <https://www.nndc.bnl.gov/nudat2/> (accessed 20 October 2020).
- [18] GEANT4 Collaboration, Introduction to Geant4, available at <http://geant.cern.ch/> (accessed on June 19th, 2019).
- [19] S. Agostinelli, et al., Geant4 - a simulation toolkit, *Nucl. Instrum. Methods Phys. Res. A* 506 (2003) 250–303.
- [20] J. Allison, et al., Geant4 developments and applications, *IEEE Trans. Nucl. Sci.* 53 (2006) 270–278.
- [21] J. Allison, et al., Recent developments in Geant4, *Nucl. Instrum. Methods Phys. Res. A* 835 (2016) 186–225.
- [22] H.M. Kluck, Measurement of the Cosmic-Induced Neutron Yield at the Modane Underground Laboratory, Springer, Berlin, 2015.
- [23] M. Aglietta, et al., Muon “depth-intensity” relation measured by the LVD underground experiment and cosmic-ray muon spectrum at sea level, *Phys. Rev. D* 58 (1998), 092005.
- [24] M. Baginova, P. Vojtyla, P.P. Povinec, The neutron component of background of an HPGe detector operating in a surface laboratory, *Appl. Radiat. Isot.* 166 (2020), 109422.
- [25] G. Heusser, et al., GIOVE: a new detector setup for high sensitivity germanium spectroscopy at shallow depth, *Eur. Phys. J. C* 75 (2015) 531.